4 15

JUN 27 1961

MASTER

EXTERNAL TRANSMITTAL AUTHORIZED

ORNL
Central Files Number
61-3-9, Appendices

146

THORIUM BREEDER REACTOR EVALUATION. PART I. FUEL YIELD AND FUEL CYCLE COSTS IN FIVE THERMAL BREEDERS. APPENDICES

L. G. Alexander
W. L. Carter
R. H. Chapman
B. W. Kinyon
J. W. Miller
R. Van Winkle

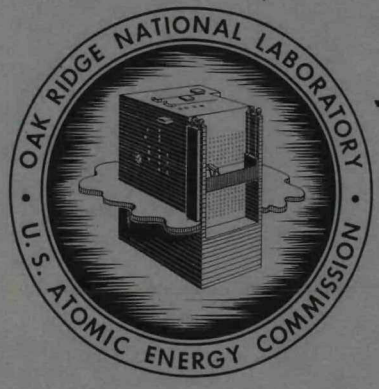

NOTICE

This document contains information of a preliminary nature and was prepared primarily for internal use at the Oak Ridge National Laboratory. It is subject to revision or correction and therefore does not represent a final report. The information is not to be abstracted, reprinted or otherwise given public dissemination without the approval of the ORNL patent branch, Legal and Information Control Department.

OAK RIDGE NATIONAL LABORATORY
operated by
UNION CARBIDE CORPORATION
for the
U.S. ATOMIC ENERGY COMMISSION

DISCLAIMER

Portions of this document may be illegible in electronic image products. Images are produced from the best available original document.

LEGAL NOTICE

This report was prepared as an account of Government sponsored work. Neither the United States, nor the Commission, nor any person acting on behalf of the Commission:

A. Makes any warranty or representation, expressed or implied, with respect to the accuracy, completeness, or usefulness of the information contained in this report, or that the use of any information, apparatus, method, or process disclosed in this report may not infringe privately owned rights; or

B. Assumes any liabilities with respect to the use of, or for damages resulting from the use of any information, apparatus, method, or process disclosed in this report.

As used in the above, "person acting on behalf of the Commission" includes any employee or contractor of the Commission, or employee of such contractor, to the extent that such employee or contractor of the Commission, or employee of such contractor prepares, disseminates, or provides access to, any information pursuant to his employment or contract with the Commission, or his employment with such contractor.

ORNL
Central Files Number
61-3-9
Copy No. _____

REACTOR DIVISION

THORIUM BREEDER REACTOR EVALUATION. PART I. FUEL YIELD AND FUEL CYCLE COSTS IN FIVE THERMAL BREEDERS. APPENDICES

L. G. Alexander
W. L. Carter
R. H. Chapman
B. W. Kinyon
J. W. Miller
R. Van Winkle

DATE ISSUED

MAY 2 4 1961

OAK RIDGE NATIONAL LABORATORY
Oak Ridge, Tennessee
operated by
UNION CARBIDE CORPORATION
for the
U.S. ATOMIC ENERGY COMMISSION

THORIUM BREEDER REACTOR EVALUATION. PART I. FUEL YIELD AND FUEL CYCLE COSTS IN FIVE THERMAL BREEDERS. APPENDICES

L. G. Alexander
W. L. Carter
R. H. Chapman
B. W. Kinyon
J. W. Miller
R. Van Winkle

ABSTRACT

The performances of aqueous-homogeneous (AHBR), molten-salt (MSBR), liquid-bismuth (LBBR), gas-cooled graphite-moderated (GCBR), and deuterium-moderated gas-cooled (DGBR) breeder reactors were evaluated in respect to fuel yield, fuel cycle costs, and development status. A net electrical plant capability of 1000 Mwe was selected, and the fuel and fertile streams were processed continuously on-site.

The maximum annual fuel yields were 16, 7, 4, 4, and 4.5%/yr respectively at a fuel cycle cost of 1.5 mills/kwhr. The minimum estimated fuel cycle costs were 0.9, 0.6, 1.0, 1.2, and 1.3 mills/kwhr at fuel yields of 7, 1, 1, 2, and 3%/yr. At a fuel yield of 4%/yr, the costs were 0.9, 0.9, 1.5, 1.5, and 1.3 mills/kwhr. Only the AHBR and the MSBR are capable of achieving fuel yields substantially in excess of 4%/yr, and therefore, in view of the uncertainties in nuclear data and efficiencies of processing methods, only these two can be listed with confidence as being able to satisfy the main criterion of the AEC long-range thorium breeder program; viz, a doubling time of 25 years or less.

The development effort required to bring the various concepts to the stage where a prototype station could be designed was estimated to be least for the AHBR, somewhat more for the MSBR, and several times as much for the other systems.

The AHBR was judged to rank first in regard to nuclear capability, fuel cycle potential, and status of development.

APPENDIX A

Power Removal from Thermal Breeder Reactors

APPENDIX A

Power Removal from Thermal Breeder Reactors

The design of the power removal system is of prime importance in thermal breeder reactors. To be suitable for use in an expanding nuclear power economy, a breeder reactor should be capable of producing excess fuel at the rate of 4%/yr or more. In order to accomplish this, the ratio of thermal power to fuel isotope inventory must be high. Referring to Eq. 3.1, Section 3, and taking, for reference, a breeding gain, G, of 0.1, a consumption ratio, R, of 1.1, a plant utilization factor, F, of 0.8, it is found that a thermal specific power, (P_e/EI) of not less than 1.2 Mwt/kg is required to achieve a fuel yield of 4%/yr.

The inventory, I, is coupled to the thermal power, P_e/E, in both fluid fuel and solid fuel reactors. In fluid fuel reactors, the volume of the external portion of the fuel circuit increases with increasing power output since pipes, pumps, and heat exchangers must all be made larger. In solid fuel reactors, increasing the power (at constant percentage burnup of fuel) increases the rate of processing of fuel and thereby increases the inventory in the processing plant (for a given holdup time). Further, the thermal system in a solid fuel reactor must be compatible with the mechanical and nuclear design.

The power density and associated capital costs in three fluid fuel reactors (AHBR, MSBR, LBBR) were studied in detail by Spiewak and Parsly (11). Section 1 below is an extract from their report. The power removal from gas-cooled solid-fuel reactors was studied by Kinyon and Chapman. Their work is presented in Section 2.

1. Power Removal from Fluid Fuel Reactors*

This memorandum contains opinions regarding the external holdup and associated capital costs for the power removal circuits of a number of 1000 Mwe breeder stations. These quantities were estimated at two levels of conservatism, corresponding to typical first and second generation plants.

Prepared by I. Spiewak and L. F. Parsly

It was hoped, at first, to evaluate the holdup of fuel and blanket materials of the reactors as a function of pumping power. However, the uncertainties in design of heat exchangers, surge volumes, pumps and piping (from the standpoint of minimum holdup) were so great as to completely overshadow any possible benefits obtainable from increased pumping power.

Therefore, following discussions with persons who had worked on the fluid fuel reactors and the reading of many reports, ground rules were established for designing power components for the three reactor systems on a comparable basis. The first generation plants were designed to use current technology as far as possible, with attention devoted to minimizing holdup only where conservative practices could be retained. The second generation plants assumed that some technological improvements were made (note that no new scientific or technological breakthroughs were assumed), which permitted equipment designs with lower holdup and cost.

1.1 Design of AHBR Plants

The first generation AHBR station is assumed to contain 7 reactors, each of which supplies steam to a 148 Mw turbogenerator. The net output of the station is 1000 Mwe when all 7 reactors are operating at design conditions. In the second generation plant, it is assumed that five reactor vessels will supply the required amount of steam for the production of 1000 Mwe.

First Generation AHBR Plant. - The overall layout approximates that of the TBR study (110). Fuel solution leaves the reactor vessel at 290°C in a vertical pipe 25.3 in. inside diameter. The stream splits into two parallel circuits contained in 17.9 in. inside diameter pipe, each circuit containing one 19,550 gpm pump and a steam generator. Steam is generated in the shell of the generators at 400 psia saturated. Fuel leaving the steam generators enters the reactor vessel in a double-intake volute at 245°C. The piping system is believed to be adequate from the standpoint of thermal expansion, which was reviewed thoroughly by Korsmeyer et al in the TBR design (110). The blanket circuit, which consists of D_2O, is similar to the fuel circuit, except that 18-in. pipe is used throughout. Design pressure is 2000 psi. Design temperature is 650°F.

The circulating pumps are of canned-rotor type similar to those used in PWR plants. Basic pump materials and design are similar to present pumps, and the size is comparable. Special features are: a) Cast Zircaloy hydraulic parts now commercially available at prices comparable to machined stainless steel, b) aluminum oxide hydrodynamic bearings, c) a special shaft seal to minimize motor irradiation, and d) a special seal-weld adaptable to remote machining and welding. It is expected that AHBR pumps will be about 30% more expensive than PWR pumps.

The fuel steam generators are of U-tube and shell type with natural circulation risers and downcomers from separate steam drums (111, 112). Shell side design pressure is 1200 psi. In principle, such steam generators are standard in PWR plants. Special features are: a) Composite tubing of stainless steel-carbon steel to eliminate stress corrosion cracking problems, b) unusually high quality control standards to reduce failures to the vanishing point, and c) provision for in-place tube plugging in a manner resembling the Pennsylvania Advanced Reactor philosophy (113, 114). Blanket steam generators are straight through bent-tube type.

The piping is cast 347 or other cast stainless steel. Elbows are forged or mitred. The piping holdup was assumed to be that of the TBR design, corrected for 25 ft/sec in the present study compared to the earlier 32, corrected for the relative flow rates (39,100 gpm vs 24,000) and a 20% contingency.

The pressurizer contains a D_2O vapor space generated from purge-D_2O. Uranium is excluded from the surge volume by purge in a manner similar to that used in the HRE-2.

Steam goes from the steam generator to a 400 psi saturated turbo-generator plant.

Second Generation AHBR Reactor Plant. - The second generation plant is similar to the first-generation plant with the following modifications:

a) The equipment is closely coupled, as shown in Fig. 5.1.1. A single pump is directly above the reactor vessel with a pipe-line gas separator between them. The pump contains a double-discharge volute.

b) Instead of using internal recombination for the radiolytic gases produced in the core, $D_2 + 1/2\ O_2$ with some steam is removed in the gas separator and recombined in a high pressure sub-system. The heat of reaction is used to superheat the steam leaving the main steam generators. The amount of the reactor's heat transmitted in the superheater is 3-4%.

c) The heat exchangers contain 3/8-in. tubes instead of 1/2-in. tubes, which increase the difficulty of fabrication and repair to the high standards needed. Less fouling is assumed than in the first generation plant.

Enumeration of AHBR Technical Problems and Design Uncertainties. - Known problems which affect the feasibility of the aqueous heat removal system are the following:

a) The 347 stainless steel system must be designed to minimize stress corrosion cracking. Failure of main pipe-lines and components in AHR service from this cause has not created serious difficulties to date. However, it might be desirable to switch to a more crack-resistant alloy such as cast CD4MCu stainless steel.

b) The heat exchanger tubes are subject to fouling by corrosion-fission products. In the HRE-2, the scale coefficients of the fuel steam generator has leveled out at about 2400 Btu/hr-ft^2 ^oF. There is at present no good method to predict the amount of fouling as related to chemical plant operation and other process variables. Some progress was made by Chemical Technology and Reactor Divisions in developing descaling methods, but additional experience is needed to demonstrate that the scale can be controlled at a reasonable level.

c) The consequences of failed heat exchanger tubes must be overcome in an economic fashion. This implies that failures will be infrequent (none have occurred to date in the HRE-2), that a leak will be contained adequately and economically (the HRE-2 has a steam stop valve which has been tested only on nonradioactive steam to date), and that tubes can be repaired (the

c) Continued
Pennsylvania Advanced Reactor personnel showed the feasibility of this, but a radioactive heat exchanger has not been repaired).

Some uncertainties which may affect the cost or holdup of the systems are the following:

a) Development of maintenance equipment and procedures is needed in order to support a proposed plant layout and design. Some information on this has been gained by the HRE-2 program, the MSR program, the Pennsylvania Advanced Reactor program and equipment vendors.

b) Detailed design and stress analyses are needed to support holdup volume estimates.

c) Detailed component design requires further experimental development and demonstration. For example, flow tests are needed to define the pressurizer-piping geometry for minimum holdup. Large alumina bearings, and seals need to be developed for pumps. Numerous other minor difficulties can influence component cost and holdup. No equipment problems which may be unsolvable are known.

d) The permissible fluid velocity in the external piping, which influences the cost and holdup of the piping, was assumed to be 25 ft/sec. This is a conservative specification based on corrosion tests in in-pile and out-of-pile loops. It is believed likely that the velocities can be increased.

Heat Exchangers for AHBR Plants. - As discussed in the body of the memorandum, the first generation plant was based on a U-tube design with 1/2-in. tubes and the second generation plant on a straight-tube design with 3/8-in. tubes.

The AHBR heat exchangers were designed in accordance with procedures developed by A. L. Gaines (110, 120) for the TBR study. Inside film coefficients are calculated by the Dittus-Boelter equation (121).

Boiling-film coefficients are calculated from the relation $h = \alpha_o \Delta T^{\beta}$, α_o and β being temperature-dependent constants.

The equation

$$\Delta T \alpha_o^{1/(\beta+1)} \phi^{-1/(\beta+1)} - \alpha_o^{1/(\beta+1)} \left[\frac{D_o}{D_i h_i} + \frac{D_o}{D_i h_s} + \frac{D_o}{D_w h_w} \right] \phi^{\beta/(\beta+1)} = 1 \quad \text{(A-1)}$$

is used to determine terminal heat fluxes ϕ_1 and ϕ_2 and

$$\text{area} = wC_p \left[\frac{D_o}{D_i h_i} + \frac{D_o}{D_i h_s} + \frac{D_o}{D_w h_w} \right] \ln \frac{\phi_1}{\phi_2} + \frac{wC_p}{\beta} \frac{1}{\alpha_o^{1/(\beta+1)}} \left[\frac{1}{\phi_2^{\beta/(\beta+1)}} - \frac{1}{\phi_1^{\beta/(\beta+1)}} \right] \quad \text{(A-2)}$$

is used to calculate the required surface.

Fouling factors used in the first generation design were based on HRE-2 experience. For the second generation plants it was assumed that in-place descaling procedures would be developed and that fouling factors could be reduced accordingly.

It was assumed that the tubes could be laid out on a triangular pitch of 1.25 tube diameter. Thus the first generation plant with 1/2-in. tubes uses 5/8-in. pitch and the second generation plant with 3/8-in. tubes uses 1/2-in. pitch. Similar assumptions were made for the LBBR and MSBR plants. It is recognized that increased tube pitch may be necessary to meet the requirements for high performance tube-to-tubesheet attachments. (The HRE-2 exchanger has 3/8-in. tubes on 5/8-in. triangular pitch.) If this proves necessary, the diameter of the shell must increase and thicker shells, heads and tubesheets will be required. Holdup will be increased due to the larger head diameter and to the slight increase in tube length required with thicker tubesheets.

The first generation exchanger is visualized as a U-tube design; the second as a straight-tube design with some sort of offset bends to take care of thermal expansion. For both plants, the heat exchanger shells are carbon steel, the tubes are carbon steel-stainless steel composite, tubesheets and heads are stainless clad carbon steel.

In the second generation AHBR plant, 4.18% of the energy produced is recovered by recombining the radiolytic gases produced in the core circuit at a relatively high temperature and using the steam so produced to superheat the steam going to the generators.

The superheater must necessarily be designed for low pressure drop on both the shell and tube sides. The design selected is a conventional shell and tube exchanger, using 1/2-in x 0.035 in. wall tubes. Superheated steam from the recombiner enters the tube side at 879°F and a mixture of saturated steam and condensate leaves at 596°F. The uncondensed steam is recirculated through the recombiner and acts as a diluent for the D_2 and O_2 being recombined. A jet pump, using the D_2-O_2-D_2O vapor mixture being let down to the recombiner as motive fluid, provides the power for recirculating the D_2O vapor. Saturated steam at 448.5°F and 415 psia enters the shell and steam leaves at 407.8 psia and 500°F.

1.2 Design of MSBR Plants

The MSBR station is assumed to contain 2 reactors, each of which supplies steam to a single 526 Mw turbogenerator. The net output of the station is 1000 Mw when both reactors are operating at design conditions.

First Generation MSBR Reactor Plant. - The entire fuel circulating system is a very compact arrangement contained within the reactor vessel (26), shown in Fig. 5.2.1. Fuel salt leaves the core at 1300°F and flows up 15 ft into the pump suction, which discharges fluid directly into the intermediate heat exchanger head. The tubes of the heat exchanger, containing fuel, spiral down at a 45° angle in an annulus surrounding the pump suction line. The discharge header empties into the core at 1125°F. Surge volume is provided in the pump, which is a sump type.

The blanket circuit was not laid out in detail, but the principle is the same as that of the fuel circuit.

The intermediate coolant is LiF-BeF_2 at a pressure slightly above fuel pressure. This coolant has the great advantage of complete compatibility with both core and blanket fluids so that small heat exchanger leaks

are tolerable. It is also reasonably compatible with water (compared to sodium-water compatibility). Its disadvantages are high cost, and high melting point.

The design pressure of salt components used in this study was 250 psi.

The fuel salt circulating pumps are sump-type (10, 42). The motor is a conventional water-cooled type with a pressure can around it, containing inert helium gas. Beryllium shielding is provided to limit radiation damage to motor insulation. Pumps are bayonet-mounted into the primary reactor shield for easy maintenance (10). Either pump or stator may be replaced, but the casing is permanently installed. The pump size and design is not unusual for liquid metal pump suppliers, and much successful small pump operation is cited by the Reactor Division. Fission product gases are removed in the pump sump. A special feature of the pump is a lower sleeve bearing operating in salt.

The intermediate heat exchanger requires considerable additional design and development work. This is a removable unit just above the reactor core physically, about 15 ft long and 6 ft in diameter. Coolant salt flows in the shell, but no practical means of baffling the shell fluid has been proposed. Using more optimistic design assumptions than used in the present study, Kinyon proposed a more compact unit (26). The unit is made entirely of INOR.

The coolant salt leaves the reactor vessel, enters a pump room, passes through pumps similar to the reactor fuel pump but without shielding, goes to steam generator-superheaters and reheaters, another pump and back to the reactor. The layout is similar to that proposed by Thomas (22), for the Liquid Metal Thorium Breeder Reactor.

The only special item in the coolant salt system is the steam generator-superheater proposed by B. Kinyon. This features bayonet tubes in which steam passes through an annulus in which it is superheated and gives up heat to boiling water in a second internal annulus. The cost of this type of unit is believed to be competitive with other high temperature

liquid metal-to-water heat exchangers, and it is believed that the Kinyon design might be superior from the stress standpoint. A boiler recirculating pump is needed to recycle water.

Steam is sent through a plant similar, in all respects except size, to the TVA John Sevier Plant (19). The condenser cooling water is assumed to be available at 63°F (typical of northern U.S.) compared to 72°F in Tennessee.

Second Generation MSBR Plant. - The second generation plant is similar to the first generation plant with the following modifications:

a) Sodium is used as intermediate coolant. It is realized that sodium is incompatible with fuel salt and water, but if heat exchangers don't leak, incompatibility is immaterial. The sodium viscosity and thermal conductivity insure adequate performance of a compact intermediate heat exchanger. Sodium, has a low melting point. Sodium is cheap. On the other hand, sodium has well known disadvantages.

b) Material selection is changed to conform to sodium practice. Composite tubing is needed in some cases.

Enumeration of MSBR Technical Problems and Design Uncertainties. - Known problems which affect the feasibility of the MSBR heat removal system are:

a) The design of liquid-metal (and presumably molten salt) steam generator-superheaters is very difficult because of mechanical problems (116, 117). There is no strikingly successful industrial experience in the field. On the other hand, MSBR will get the benefit of technological improvements made in the SGR and fast breeder 10-year programs of the USAEC.

b) The fuel and blanket pumps and heat exchangers will be required to operate reliably for long periods of time in the temperature range where creep is important. Some replacements will need to be executed, possibly of parts which have changed slightly in dimensions. Long-term operating experience with equipment run at 1300°F is needed to show whether this is a serious problem.

c) In the second generation plant using sodium coolant, the consequences of failed heat exchanger tubes must be overcome in an economic fashion. This implies that sodium-steam and sodium-salt interchange can be controlled, and that heat exchangers can be repaired or replaced afterward. This problem is present to a much lesser degree in the first generation plant using a salt coolant.

d) It is presumed, on the basis of several in-pile experiments, that the INOR pipe and tubing will not corrode rapidly in contact with radioactive fuel.

Some uncertainties which may affect the cost or holdup of the systems are the following:

a) Development of maintenance equipment and procedures is needed in order to support a proposed plant layout and design. The feasibility of some types of operations has been demonstrated at the Remote Maintenance Facility, the HRE-2 and by the Pennsylvania Advanced Reactor Program. The maintenance will have to be done without introducing excessive oxygen contamination.

b) Detailed design and stress analyses are needed to support holdup volume estimates.

c) Detail component design requires further experimental investigation. The amount of work needed in this area is much larger than in the corresponding AHBR area. For example, it is difficult to predict the heat transfer coefficients on the shell side of the fuel-to-intermediate coolant heat exchanger without additional model tests in an unbaffled spiral geometry with a high-viscosity (molten-salt) coolant. A sweep-gas system for the circulating-pump motor should be developed to prevent radiation damage by fission products. The dead fuel volume needed to disengage fission-gas bubbles from the fuel salt cannot be accurately predicted. Although the present pump seals and bearings are considered adequate for use in the pumps

c) (Continued)
of a small experimental reactor, improved parts are needed to provide the service life presumed for a power breeder. No equipment problems which may be unsolvable are known.

d) Insoluble materials are introduced into the fuel stream by some fission products, as a result of chromium leaching from INOR and from oxygen contamination. It is believed that the fouling of heat transfer surfaces by such materials will be unimportant, on the basis of loop tests.

e) To prevent cavitation of the fuel circulating pump, a suction pressure of 100 psi is required (118). This requirement might be relaxed as a result of experimental investigation, or the pump could be redesigned (with more holdup and cost) to reduce the net positive suction head.

f) The thermal conductivity of INOR at the temperature of the intermediate heat exchanger may be about 35% below that assumed in this study. The fuel holdup of the first generation plant might thereby be increased 8%, and the heat exchanger area increased 10%.

g) In the first generation plant, the holdup of coolant salt might be reduced considerably by detail design and development of the steam generators.

h) The INOR costs may be lower than estimated here.

Heat Exchangers for MSBR Plants. - For both the first and second-generation plants, the core heat exchangers are considered to be annular, mounted directly above the reactor core. The circulating pump suction line is placed at the center of the annulus and the pump discharge flows down through the heat exchanger tubes back to the reactor. For the first generation plant, the coolant is $LiF-BeF_2$; for the second generation plant, it is sodium. Tubes are 3/8-in. for both plants.

For both plants, a modification of an arrangement proposed by B. W. Kinyon in which the tubes are formed into 45° spirals, wound right hand and left hand in alternate rows, is used. The modification consists of providing straight end sections to permit radial flow distribution. Shell inlet and outlet connections are presumed to be made through the outer shell wall near the ends of the tube bundle.

Emphasis has been placed on minimizing the holdup, particularly in the first generation exchanger. An optimization has been made with respect to core inlet temperature, leaving the core outlet temperature and the coolant temperatures fixed. This shows that the optimum fuel exit temperature is very close to 1125°F. Investigation of tube side velocity and tube diameter indicates that the holdup decreases as the former increases and the latter decreases; it was arbitrarily decided to limit velocity to 20 ft/sec and diameter to 3/8-in.

Thermal Design of Intermediate Heat Exchanger. - The following data were used in the thermal design of the intermediate heat exchanger:

(1) Fuel (inside) film coefficients - For Reynolds numbers below 12,000, empirical data obtained by Amos et al (122) are used. Above 12,000 the Dittus-Boelter equation applies.

(2) Shell-side film coefficients - For the first generation plant, it is assumed that the Dittus-Boelter equation will apply, with the constant increased from 0.023 to 0.046. This is based on the presumption that the alternating spiral tube layout will provide enhanced turbulence. Experimental verification of the assumption is required.

It was also assumed that the spiral-tube sections only would be effective in heat transfer and that all radial flow would occur in the straight-tube end sections. The first of these assumptions obviously cannot be correct, but a calculation which takes the end section heat transfer into account would require far more time than is available for the present study. It would require row-by-row treatment of the radial flow end sections and of the axial flow in the channels between the bent tubes. The second assumption appears not to be greatly in error - a row-by-row calculation based on this assumption indicates axial velocities in adjacent channels differ by 0.1 ft/sec at most and pressure differences will therefore be fairly small.

For the sodium-cooled case, shell coefficients are based on the equation (123)

$$Nu = 0.19\,(D_e')^{0.6}\left(\frac{D_t G_e}{\mu}\right)^{0.6}\left(\frac{C_p \mu}{k}\right)^{1/3} \qquad (A\text{-}3)$$

Fouling Factors for Intermediate Heat Exchanger. - A fouling factor of 0.0001 has been assumed for both the first and second-generation plant heat exchangers. Although it has been argued that no oxide film or other deposit which would interfere with heat transfer will be present in the molten fluoride system, development of a thin (approx. 0.0002 in.) film on a hot INOR-8 surface exposed to fuel salt number 130 in a forced-convection system has been reported (124). Until experimental proof to the contrary is obtained, it seems prudent to assume that any such deposit is likely to represent an increased heat transfer resistance. Also, fission or corrosion products produced in a reactor may foul the heat transfer surface.

Mechanical Design of Intermediate Heat Exchanger. - The basic exchanger design used for the MSBR practically dictates the arrangement of the tubes in concentric circles. For the salt-cooled exchanger, the 3/8-in. tubes are placed on 1/2-in. radial pitch, since this appears to be the minimum which normally would be employed. A circumferential pitch of 5/8-in. is used, largely dictated by the necessity of providing some clearance between the bent tubes. This gives 0.093 in. clearance in the bent section.

The straight-tube end sections were assumed to be 12-in. long. This is not necessarily optimum but does appear to give reasonably good radial flow distribution.

Shell and tube wall thicknesses were calculated from the formulas given in the ASME Boiler Construction Code, Section VIII, Unfired Pressure Vessels. A design temperature of 1200°F was used, and it was assumed that the internal annulus would be thermally shielded from the core outlet fluid. Tube sheet thicknesses were calculated in accordance with the TEMA formula for Class R heat exchangers with U-tubes. It was again assumed that tube-to-tubesheet joint design requirements would not influence the tube spacing

and that no reduction in allowable stresses would be required to allow for the effects of hydraulic noise or thermal shocks. For this type reactor, an increase in tube spacing to satisfy joint design requirements would produce a far more severe penalty than for the AHBR, since it would lead to lower shell-side film coefficients and therefore increased tube length.

The shell-side fluid flow calculations also indicated that the annuli between the inner and outer tube rows and the shells must be kept quite narrow by baffling or by designing the shell so that its inside diameter opposite the bent tube section is less than at the ends. This applies particularly to the annulus between the outer tube row and the outer shell, since if this annulus is not restricted, 15-20% of the flow will go through it and essentially bypass the exchanger.

Design of Steam Generators for MSBR. - The steam generators were designed as proposed by B. Kinyon. The tube size was selected to be 1.032 in. inside diameter. Based on several steam flows per tube investigated by Kinyon, 900 lb of steam per hour per tube was selected to give a reasonable combination of tube side pressure drop (100 psi) and length (at constant enthalpy change).

Each tube contains (a) an annulus through which steam is flowing, receiving heat from the secondary coolant and giving heat up to (b) a second annulus through which water is pumped at high pressure so that it boils. The water and steam leaving this annulus, at 50% quality, pass through (c) a small steam separator. The water is discharged through (d) a central tube to a water chest. The water is pumped by a boiler recirculating pump from the water chest to annulus (b).

The bayonet tubes are collected in several headers, (a) the superheated steam header, (b) the water inlet header and (c) the water chest or water outlet header.

Steam coefficients were computed from the usual Dittus-Boelter equation. The outside film coefficients were for baffled shells.

Design of Reheater for MSBR. - The reheaters were entirely conventional shell-and-tube exchangers selected such that the steam pressure drop was 40 psi, from 400 psia in to 360 psia out. This was the same drop used in the TVA John Sevier plant reheaters.

1.3 Design of LBBR Plants

The LBBR station is assumed to contain 2 reactors, each of which supplies steam to a single 529 Mw turbogenerator. The net output of the station is 1000 Mw when both reactors are operating at design conditions.

First Generation LBBR Reactor Plant. - The plant layout (Fig. 5.3.1) is essentially that proposed by Thomas (22). Bismuth containing 22 g U-233 + U-235 per liter leaves the core at 1300°F and immediately passes up through the tantalum intermediate exchanger. The reactor surge volume, at 1000°F, is just above the heat exchanger exit. From this plenum liquid enters the propeller pump. A single pump is assumed, but the holdup volume would be independent of the number of pumps in parallel. The pump discharges directly into an annular plenum leading to the reactor.

The blanket circuit is essentially the same. The blanket fluid is a slurry of ThO_2 in bismuth, containing 1025 g Th/liter and U-233 + Pa-233 per liter.

The intermediate coolant is sodium.

Design pressure for this system is 400 psi which is the sum of the pump head developed, the net positive suction head to prevent cavitation and the elevation head.

The bismuth pumps are similar in design to large liquid metal pumps used elsewhere. It is not known whether pumps this big have actually been built. However, as indicated above, for purposes of the present study the number of Bi pumps is immaterial except from the standpoint of cost. Pumps are bayonet-mounted into the primary reactor shield for easy maintenance. Either pump or stator may be replaced, but the casing is permanently installed. Shielding of the pump-motor from radiation is installed.

The intermediate heat exchanger requires the conversion of tantalum from a meterial used in small quantities to one used in multi-ton assemblies. The design, outlined by Thomas (22), is straightforward except (a) to make the unit compact, the 1/2-in. tubes are swaged down to 3/8-in. in the tubesheet, (b) because of the close tube spacing, high sodium pumping power is probably needed to remove the heat uniformly, (c) in order to reduce the thickness and thereby the cost of the tubesheet, the sodium in the shell is kept at a higher pressure than that of the bismuth in the tubes.

The sodium leaves the reactor vessel and enters the pump and steam generator rooms as proposed by Thomas. The steam is generated at the same conditions as used in the MSR plant, 1800 psi and 1050°F.

The only difficult equipment problem in this part of the system is the steam generator-superheater. Of all available designs which were reviewed, the most practical appeared to be one proposed by Alco (15) for generating 70 Mw of 2200 psi steam. The Alco design was modified to double its capacity, at an operating pressure of 1800 psi. The unit consists of bayonet tubes in the steam-generator section and straight-through tubes in the superheater section. Sodium flows through the shell of both sections, leaving the steam generator at 725°F. The sodium is mixed with 1175°F fluid to gain an average temperature of 900°F at the entrance to the reactor vessel. This technique is used to minimize thermal stresses in the steam generator and in the intermediate heat exchanger.

Second Generation LBBR Reactor. - The second generation plant used somewhat more optimistic costs for tantalum, and used slightly more optimistic fuel heat exchanger design parameters. The heat exchanger tubes were reduced from 1/2-in. OD to 3/8-in.

Enumeration of LBBR Technical Problems and Design Uncertainties. - Known problems affecting the feasibility of the LMFR heat removal system are:

(a) Problems similar to those cited for the MSR in Sections 5.2.2 and 5.2.5 except that preliminary tests indicate that tantalum creep will not be important at 1300°F or below (119).

(b) Satisfactory circulation of the blanket slurry in a system of appropriate complexity remains to be demonstrated.

(c) The possible interaction of slurry particles and fission gases may lead to difficulties with foaming.

(d) The feasibility of use of tantalum in large pieces requires demonstration.

The design uncertainties a, b, c, d, and e listed under the MSBR in Section 1.2 apply also to the LBBR.

Thermal Design of Intermediate Heat Exchanger. - The design closely follows the proposal in BAW-1171. Straight 1/2-in. OD tubes, swaged down to 3/8-in. OD where they pass through the tubesheets, are used. Tubesheets are made the same thickness as the cylindrical shell.

This mechanical design is based on the premise that the intermediate coolant pressure will be maintained higher than the fuel pressure and that the tubes can therefore be assumed to act as staybolts to support the tubesheets. This is common practice in fire-tube steam boilers and is permitted under the ASME Boiler Construction Code, Section I, Power Boilers. We have accepted the above premise with some reservations, since the tube side pressure will be substantially greater than atmospheric and it seems unreasonable to rule out an accident which could result in depressuring the shell. Accepting the assumption decreases the tubesheet thickness compared to that required by TEMA Class "R" standards by a factor of the order of 5.

Static axial pressure and thermal stresses in the tubes and shell have been investigated and do not exceed allowable values. As in the case of the MSBR, the presence of significant hydraulic noise and thermal transients must be recognized. Such factors might well cause a reduction in allowable stresses where a component is designed for long-term life.

Although tantalum apparently is not corroded measurably by bismuth-uranium solutions, significant corrosion by liquid sodium has been reported (127). Corrosion rates were reported as 0.1 mpy in oxygen-free sodium and 3 mpy in sodium containing approximately 40 ppm O_2 at 1200°F. Based on this information, a 3-mil corrosion allowance was provided in establishing the tube wall thickness.

Tube side film coefficients were calculated from

$$Nu = 0.625\ (Re\ Pr)^{0.4}$$

Shell side coefficients were calculated from

$$Nu = 0.19\ (D_e')^{0.6} \left(\frac{D_t G_e}{\mu} \right)^{0.6} \left(\frac{C_p \mu}{k} \right)^{1/3}$$

1.4 Results

Results obtained by Spiewak and Parsly (11) were reported under the headings:

1 Comparison of Fuel Heat Exchangers
2 Comparison of Blanket Heat Exchangers
3 Comparison of Steam Generators-Superheaters
4 Comparison of Reheaters
5 Cost of Heat Exchangers, $\$10^6$
6 Pump Cost and Size Summary
7 Summary of Piping Assumed
8 Station Cost of Spare Equipment for Reactor Cooling System
9 Expected Life of Power Components
10 Turbo-Generator Plant Summary
11 AHBR Breakdown of External Holdup Containing U, Basis 1 Reactor
12 MSBR Breakdown of External Holdup Containing U, Basis 1 Reactor
13 LBBR Breakdown of External Holdup Containing U, Basis 1 Reactor
14 Station Summary of Holdup in Heat Removal System
15 Summary - Cost of Heat Removal and Turbogenerator Equipment

For the purposes of this study, items 11, 12, and 13 were extracted and are presented in Tables A.1.1, A.1.2, and A.1.3.

Table A.1.1 AHBR Breakdown of External Holdup Basis 1 Reactor
Core Power: 588 Mwt

	1st Generation	2nd Generation
Holdup of fuel, (ft^3):		
Heat Exchangers	132	164
Pump	47.0	46.2
Main Circuit Piping	175	158
I-Xe Removal System	11.1	--
Underflow Pot of Clones, etc.	3.5	5.7
Feed and Letdown Line	0.3	1.0
Dump Tanks	0	3.5
Total	368.9	378.4
Power Density in External Fuel Circuit, Mwt/ft^3	1.59	1.55

Table A.1.2 MSBR Breakdown of External Holdup Basis 1 Reactor
Core Power: 1070

	1st Generation	2nd Generation
Holdup of Fuel, (ft^3):		
Pipe, Core to Pump	50.6	25.3
Pump	18.0	16.0
Heat Exchanger Tubes	98.5	49.3
Heat Exchanger Heads	30	30
Surge Volume	20	20
Total	217.1	140.6
Power Density in External Fuel Circuit, Mwt/ft^3	4.9	7.6

Table A.1.3 LBBR Breakdown of External Holdup Basis 1 Reactor
Core Power: 933 Mwt

	1st Generation	2nd Generation
Holdup of Fuel, (ft^3):		
Heat Exchanger Inlet Plenum	20	10
Tubes	123	85
Annulus Between Heat Exchanger and Vessel	20	10
Surge Volume	74	74
Pump and Piping	89	75
Pump Discharge Plenum	25	25
Total	351	279
Power Density in External Fuel Circuit, Mwt/ft^3	2.66	3.35

2. Power Removal from Solid-Fuel, Gas-Cooled Reactors

In the analysis of heat removal from gas-cooled reactors, the selection of the independent variables is a matter of convenience and purpose -- that is, the expressions may be thrown into forms containing explicitly those parameters over which the designer has control or with respect to which he desires to correlate and interpret the performance of the system. Examples of the first sort are the length and diameter of the core; of the second sort the ratio of pump-work to reactor heat. The treatment is rather straightforward, once the approach has been chosen, and a number of analyses have been published of various systems. That presented here was tailored to the purposes of this study, but closely parallels that of Carlsmith (50), and is generically related to that of Ozisik and Korsmeyer (88, 89).

2.1 Working Equations

Power Equation. - The rate of removal of heat from a reactor may be expressed by the equation(a)

$$Q = wC_p\,(T_2 - T_1)\,(C.F.) \qquad (A\text{-}4)$$

where Q is the heat rate in Mwt, w is the coolant flow rate in lb/sec, C_p is the heat capacity of the coolant in Btu/lb ^{o}R, T_2 and T_1 are coolant outlet and inlet temperatures respectively in ^{o}R, and C.F. represents appropriate conversion factors.

The flow rate may be eliminated by relating it to the maximum velocity of the coolant.

$$w = \rho_1\, u_1\, F_1\, \pi\, d^2/4R_3 \qquad (A\text{-}5)$$

where ρ_1 is the coolant density at the inlet in lb/ft^3, u_1 the inlet velocity in the central channel in ft/sec, F_1 is the fraction of core volume occupied by gas passages, d is the diameter of the core in ft, and R_3 is the ratio of maximum to radial average power density in the core, and is introduced because only the central channel will operate at maximum velocity, other channels being orificed to regulate the flow in proportion to the heat release rate in those channels.

(a) A table of nomenclature is given in Table A.2.1.

Table A.2.1. Table of Nomenclature for Eqs. A-1 Through A-25

A	total heat transfer area of fuel plates, ft^2
a	width of fuel plate, ft
b	lattice spacing of fuel plates, ft
C_p	heat capacity, Btu/lb ^oF
C.F.	conversion factor (units determined by equation in which used)
D	diameter, ft
D_i	inside diameter, ft
D_o	Outside diameter, ft
D_t	tube diameter, ft
D_e	equivalent diameter of gas passage, ft
D_e'	equivalent diameter of shell, ft
D_v	inside diameter of pressure vessel, ft
d	diameter of cylindrical core, ft
E	Young's modulus, psi
E_w	weld efficiency
F_1	fraction of core volume occupied by gas passages
F_2	fraction of core volume occupied by fuel plates
f	friction factor
G_e	mass flow rate in shell, lb/hr ft^2
g_c	conversion factor = 32.2 ft lb (mass)/sec^2 lb (force)
h	film heat transfer coefficient, Btu/hr ft^2 ^oF
h_i	inside film heat transfer coefficient, Btu/hr ft^2 ^oF
h_s	scale heat transfer coefficient, Btu/hr ft^2 ^oF
h_w	wall heat transfer coefficient, Btu/hr ft^2 ^oF
k	thermal conductivity, Btu ft/hr ft^2 ^oF
k_2	thermal conductivity of fuel plate, Btu ft/hr ft^2 ^oF
L	length of gas passage in core, ft
Nu	Nusselt number
n	number of fuel plates per fuel element
P	pressure, psi
Pr	Prandtl number
Q	heat removal rate, Mwt
q	surface heat flux, Btu/hr ft^2

Table A.2.1 (Continued)

Re	Reynolds number
R_o	gas constant (units determined by equation in which used)
R_1	ratio defined by Eq. A-7
R_2	ratio of pressure drop across core to total pressure drop in circuit
R_3	ratio of maximum to radial power density in core
R_4	ratio of maximum to average axial power density in core
S	thermal stress in fuel plate, psi
$S_{v,max}$	maximum allowable stress in pressure vessel, psi
T	temperature, ^oF
T_1	inlet gas temperature, ^oF
T_2	outlet gas temperature, ^oF
$\Delta T_{1,max}$	maximum temperature difference across gas film, ^oF
$\Delta T_{2,max}$	temperature rise in fuel plate, ^oF
t_1	gas passage thickness, in.
t_2	fuel plate thickness, in.
$t_{2,min}$	minimum fuel plate thickness, in.
t_v	thickness of pressure vessel wall, ft
u	velocity, ft/sec
$\bar{u}$	average velocity, ft/sec
W_p	pump work, hp
w	mass flow rate, lb/hr
α	coefficient of cubical expansion, $in^3/in^3\ ^oF$
α_o	temperature dependent constant used in calculating boiling film coefficient
β	temperature dependent constant used in calculating boiling film coefficient
μ	coefficient of viscosity, lb/ft hr
ν_p	Poisson ratio
ρ	density, lb/ft^3
$\bar{\rho}$	average density, lb/ft^3
ϕ_1	heat flux at inlet of heat exchanger, Btu/hr ft^2
ϕ_2	heat flux at outlet of heat exchanger, Btu/hr ft^2

The velocity may be eliminated by introducing the pressure drop around the coolant circuit.

$$R_2 \Delta P = \frac{fL}{D_e} \frac{\bar{\rho} u^2}{2g_c} \quad (C.F.) \tag{A-6}$$

where R_2=ratio of pressure drop across core to total circuit pressure drop, ΔP is the pressure drop in psi, f is the friction factor, L is the length of the gas passages in the core in ft, D_e is the "equilivant" diameter of the gas passages in inches, and g_c is a conversion factor equal to 32.2 ft lb of mass/sec^2 lb of force.

By definition, let

$$R_1 = (W_p/Q) \ (C.F.) \tag{A-7}$$

where W_p is the pump work in horsepower. The pump work and the pressure drop may both be eliminated by relating them back to the flow rate.

$$W_p = \frac{w \Delta P}{\rho_t} \quad (C.F.) \tag{A-8}$$

The equivalent diameter for the geometry illustrated in Fig. 5.4.1 is approximately twice the distance between adjacent fuel plates. Since the ratio of the fraction of volume of core occupied by gas passages to the fraction occupied by fuel plates is equal to the ratio of thickness of gas passages to thickness of the plates, the equivalent diameter may be expressed as

$$D_e = 2t_1 = 2t_2 F_1/F_2 \tag{A-9}$$

where t_1 is the gas passage thickness, t_2 the fuel plate thickness in inches, and F_2 is the fraction of core volume occupied by fuel plates.

The gas densities are eliminated by means of the gas law.

$$\bar{\rho} = \frac{P}{R_o (T_1 + T_2)/2} \qquad \text{(A-10)}$$

where P is the pressure, in psi, R_o is the gas constant in appropriate units. Equations A-4 through A-10 may be combined to eliminate w, u, ΔP, D_e, etc.

$$Q = \frac{Pd^2 [C_p(T_2-T_1)]^{\frac{3}{2}}}{T_1 \left[1 + \frac{T_1}{T_2}\right]^{\frac{1}{2}}} \left[\frac{R_1 R_2 F_1^3 t_2}{R_3^2 f F_2 L}\right]^{\frac{1}{2}} \quad \text{(C.F.)} \qquad \text{(A-11)}$$

where all constants have been thrown into the conversion factor. In Sec. 2.3, the coupling between P and pressure vessel diameter is given.

Pressure Drop Equation. - Similarly, the pressure drop across the reactor core may be expressed as

$$\Delta P = \frac{P R_1 C_p (T_2 - T_1)}{T_1} \quad \text{(C.F.)} \quad . \qquad \text{(A-12)}$$

Gas Film Temperature Rise Equation. - The maximum temperature difference across the gas film is given by

$$\Delta T_{1,max} = \frac{q}{h} = \frac{Q R_3 R_4}{h A} \qquad \text{(A-13)}$$

where q is the surface heat flux in Btu/hr ft^2, R_4 is the ratio of maximum to axial average power density in the core, A is the total heat transfer area, and h is the gas-film conductance coefficient. Denoting by "a" the width of a fuel plate and by "b" the lattice spacing for a square array of fuel elements,

$$A = 2naL\left[\frac{\pi d^2/4}{b^2}\right] \qquad \text{(A-14)}$$

where n is the number of fuel plates per element. The ratio $\frac{na}{b^2}$ may be eliminated by utilizing the definition of F_2, the fraction of core volume occupied by fuel plates.

$$F_2 = nat_2/b^2 \tag{A-15}$$

Substituting into Eq. A-14 above, and thence into Eq. A-13 gives

$$\Delta T_{1,max} = \frac{2QLt_2}{\pi h F_2 d^2} \tag{A-16}$$

The film conductance is obtained by means of the well-known relation

$$h = (0.023k/D_e)\ Re^{0.8}\ Pr^{0.4} \tag{A-17}$$

where k is the thermal conductivity of the gas, Pr is the Prandtl modulus, and Re is the Reynolds modulus.

$$Re = D_e u\rho/\mu \tag{A-18}$$

where μ is the viscosity of the coolant. Substituting for D_e from Eq. A-9, $u\rho$ from Eq. A-5, and w from Eq. A-4 gives

$$Re = 3\ R_3 Qt_2/\pi\ \mu C_p(T_2-T_1)F_2 d^2 \quad \text{(C.F.)} \tag{A-19}$$

Fuel Plate Temperature Rise Equation. - The temperature rise in a fuel plate cooled on both sides and in which heat is uniformly generated throughout is given by

$$\Delta T_{2,max} = qt_2/4k_2 = QR_3R_4t_2/4k_2A \tag{A-20}$$

where q is the surface heat flux in Btu/hr ft^2 ^oF, and k_2 is the thermal conductivity of the material of the plate.

Substituting for A from Eq. A-14, and making use of Eq. A-15,

$$\Delta T_{2,max} = \frac{QR_3R_4t_2^2}{2\pi k_2 F_2 L d^2} \tag{A-21}$$

Thermal Stress Equation. - The thermal stress is related to the temperature rise in an internally heated plate by

$$S = \frac{2\alpha E}{3(1-\nu_p)} \quad \Delta T_{2,max} \tag{A-22}$$

where α is the coefficient of cubical expansion, ν_p is Poisson's ratio, E is Young's modulus, and S is the stress in psi.

If now, the thermal stress approaches the permissible stress, and the fuel plate thickness, t_2, approaches an allowable lower limit, then an upper limit is imposed on $T_{1,max}$. Combining Eqs. A-21 and A-20 gives

$$S_{max} = \frac{2\alpha E}{3(1-\nu_p)} \quad \frac{QR_3R_4t_{2,min}^2}{2\pi k_2 F_2 L D^2} \quad . \tag{A-23}$$

This equation establishes a limit on F_2L, which may be put into Eq. A-11 to get a stress limited power equation.

The pressure may be eliminated by means of the equation for hoop stress in the pressure vessel. (See Sec. 2.3 for a discussion of design limitations.)

$$P = \frac{2S_{v,max}E_w t_v}{D_v + 1.2\ t_v} \simeq \frac{2S_{v,max}E_w t_v}{D_v} \tag{A-24}$$

where $S_{v,max}$ is the maximum allowable stress in the pressure vessel wall, t_v is the thickness of the wall, and D_v is the inside diameter of the vessel.

The result of these substitutions is

$$Q^{\frac{3}{2}} = \frac{2S_{v,max}t_v E_w d \left[C_p(T_2-T_1)\right]^{\frac{3}{2}}}{D\ T_1 \left[1 - \frac{T_1}{T_2}\right]^{1/2}} \left[\frac{3\pi R_1 R_2 F_1^3 (1-\nu_p)k_2}{R_3^3 f\alpha E R_4 t_{2,min} S_{max}}\right]^{\frac{1}{2}} \quad \text{(C.F.)} \tag{A-25}$$

Either L or F_2 may be fixed independently, but not both, since Eq. A-23 must be satisfied.

2.2 Selection of Values

Graphite Properties. - The physical properties of graphite depend on the type of graphite, grain direction, the temperature, and the neutron flux-temperature history. For this study, the properties of ATJ graphite are used, considering the effect of temperature variation, but neglecting the neutron flux-temperature effect, except in the case of thermal conductivity. It is proposed that the fuel plates would be impregnated with a solution of uranyl nitrate followed by heat treatment that results in the formation of UO_2. This should not materially alter the material properties.

The effect of irradiation at the temperatures being considered here (800 to 1800°F) has had little study to date, but indications are that most effects will be annealed as they occur. Tensile strength and Young's modulus both increase under irradiation, and are nearly compensating (125, p. 6.10). Thermal conductivity is most affected by irradiation at lower temperatures, with the effect decreasing with increasing temperature (125, p. 6.15).

Allowable Stress and Factor of Safety. - One-half of the stress pattern due to cooling the two sides of a plate having uniform internal heat generation is similar to that for flexural stress, having maximum tension at the surface and progressing through zero to compressive stress at the center. Thus, it appears that the allowable thermal stress can be based on flexural strength of the graphite, rather than on the tensile strength, which is about half as great. However, tests (126) on a 1/8 in. thick graphite strip electrically heated and gas-cooled on both surfaces indicated that fracture occurred when the calculated stress amounted to only half the tensile stress required for rupture. Based on these results, the allowable stress is taken to be the tensile value with a factor of safety of two. Because of the spread of tensile strength tests, it would be necessary to have close inspection and perhaps some screening test to insure good quality fuel plates.

Tensile strength increases with increasing temperature, and is higher with the grain than across the grain. If the fuel plates are molded to nearly finished thickness, all directions of thermal tensile stress at the surface will be with the grain. Fig. A.2.1 shows the assumed tensile strength as a function of temperature. Flexural strength

UNCLASSIFIED
ORNL-LR-DWG 55919

FIG. A.2.1

SOME PROPERTIES OF ATJ GRAPHITE
AS A FUNCTION OF TEMPERATURE

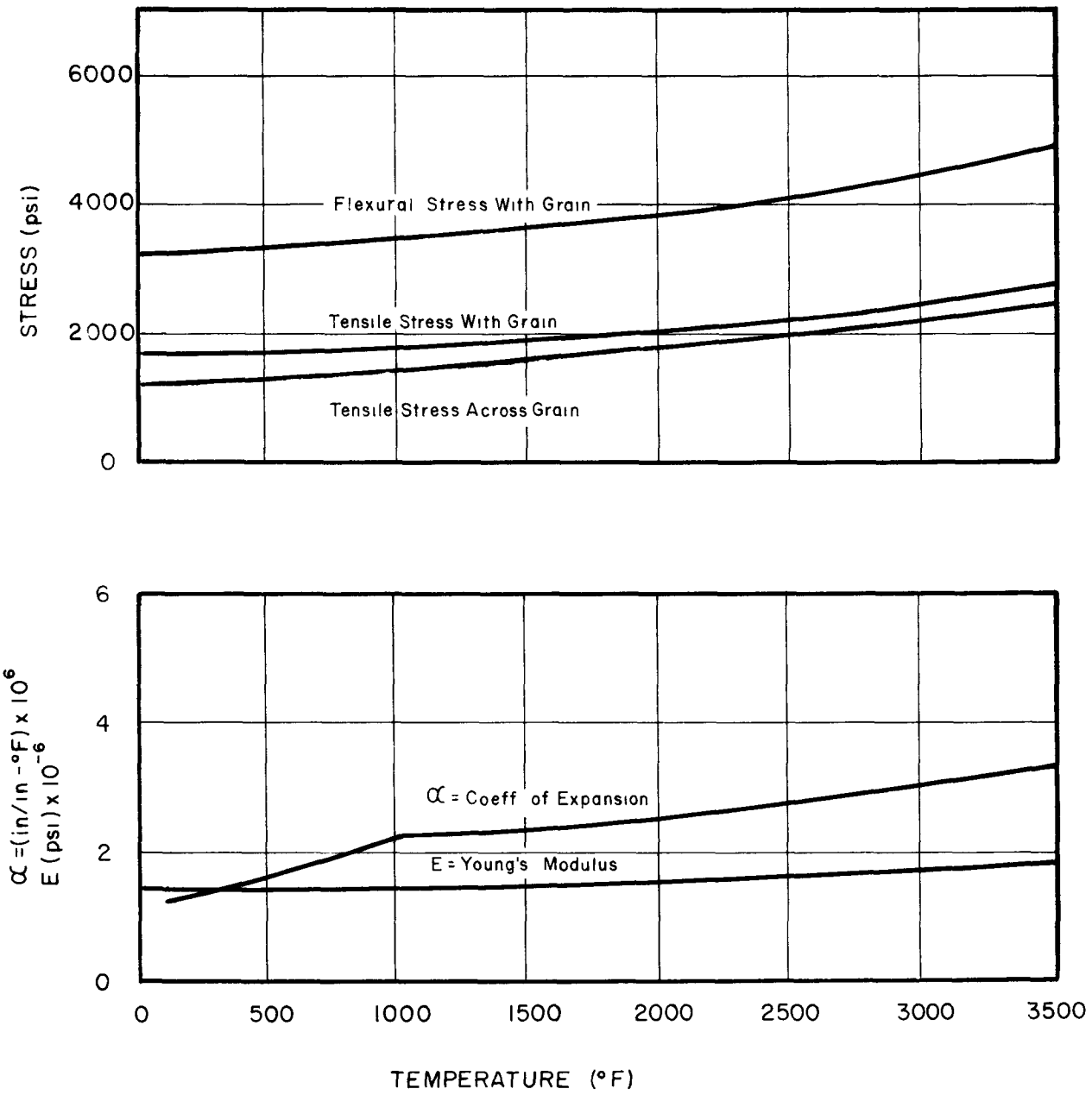

and tensile strength across the grain are shown, for comparison. The temperature dependent curves drawn were adjusted to conform with room temperature values taken from Tables 5A.02.01 and 5A.02.01 in reference 125.

Young's Modulus. - The values for Young's modulus, like the tensile strength, increase with temperature and are higher with the grain than across the grain. The assumed curve, Fig. A.2.2 was drawn by using the tabulated value at room temperature (Ref. 125, Table 5A.07.01 and Fig. 5A.01.01-.02) to locate a typical temperature dependent curve.

Poisson's Ratio. - This is taken as 0.25. Values from 0.20 to 0.30 are reported.

Coefficient of Thermal Expansion. - For calculation of thermal stress, the coefficient of thermal expansion at the temperature is needed. Values plotted in Fig. A.2.1 were calculated from the mean coefficient at room temperature to the final temperature listed in Table 5b.02.03 of reference 125.

Thermal Conductivity. - Thermal conductivity in a direction across the grain, which is smaller than that in a direction with the grain, is used to determine the temperature difference between the center and the surface of the fuel plates. In Fig. A.2.2 are plotted three curves from the thermal conductivity of ATJ graphite, representing the published work of two investigations (128, 129). As the lower set seems more consistent with other work, a value of 17.5 Btu/hr-ft-^{o}F was selected, and reduced to 15 Btu/hr-ft-^{o}F to allow for the effect of radiation.

Plate Thickness. - Plates as thin as 0.1 in. can be fabricated and handled.

Gas Coolant Temperature. - A recent study by W. B. Cottrell, et al (62) optimized the power extraction system and gas temperatures for a similar reactor. Although the gas pressure level considered here is much higher than used in the study (300 psig), and other factors are different, the temperature conditions there chosen are used here. These are 525^{o}F gas temperature at reactor entrance and 1500^{o}F at exit, giving 975^{o}F temperature rise.

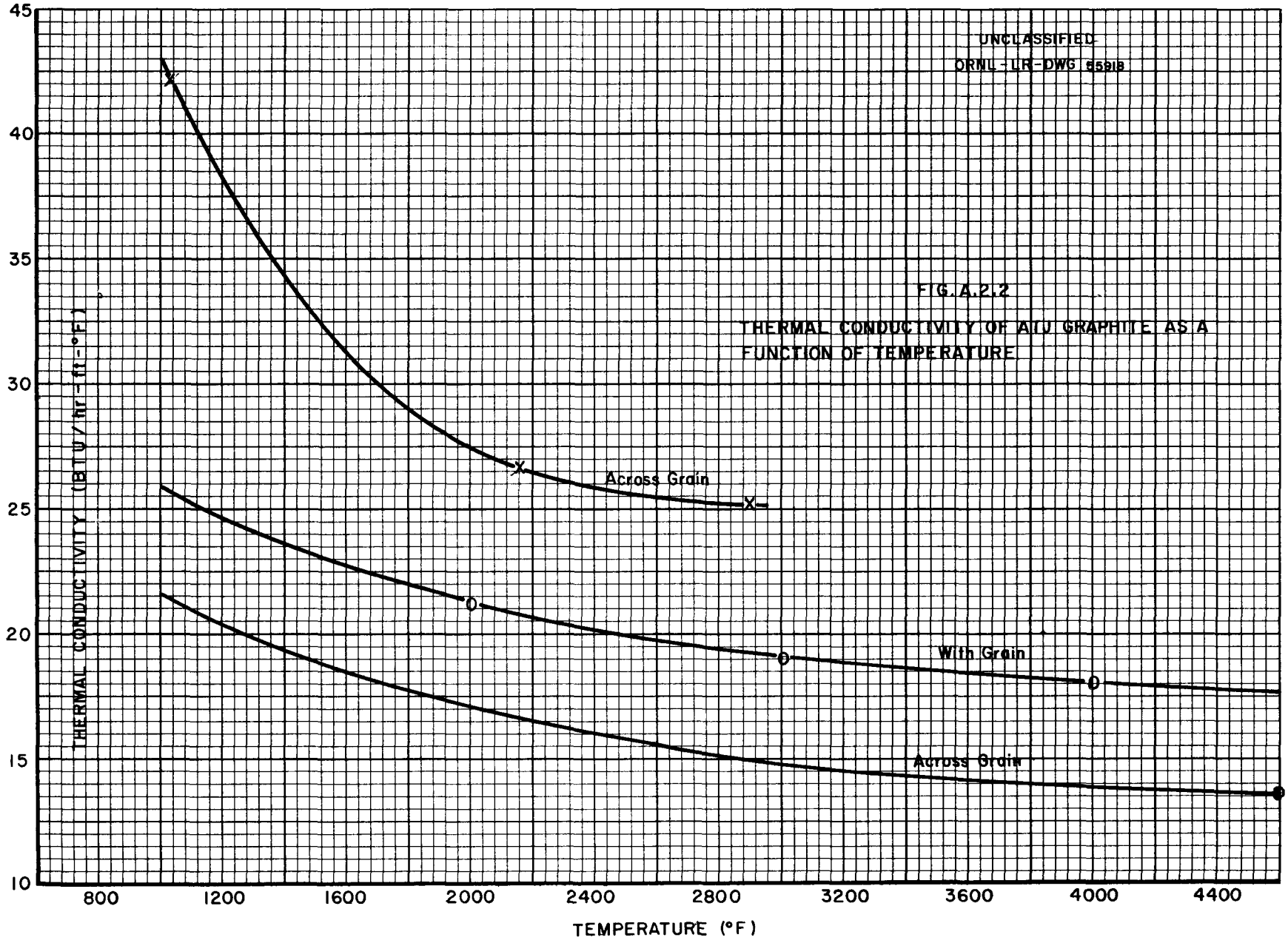

FIG. A.2.2
THERMAL CONDUCTIVITY OF ATJ GRAPHITE AS A FUNCTION OF TEMPERATURE

Gas Coolant Loop Parameters. - The fraction, R_2, of the total circuit pressure drop of the gas coolant across the core ranges from 0.5 to 0.9 for different reactors. For this study it was taken to be 0.75.

The ratio, R_1, of work (Mwe) used in pumping coolant gas to the heat removed (Mwt) from the reactor probably would optimize at a higher value for a breeder reactor than for a lower conversion ratio reactor designed for economic power production. As a base, a value of 0.025 was selected. This allows about 6.25% of the gross electrical output for coolant pumping. For the balance of plant operation, 3-1/2% of gross electrical generation was allowed.

For converting from the Mwe to the work input into the gas, 93.5% motor efficiency and 80% blower efficiency are used, giving a combined efficiency of 74.6%. This gives 1 hp into the gas for 1 kw of pumping power.

The temperature rise through the core is used for determining the gas flow, and the pumping is presumed to be done at the reactor entrance temperature. Actually the gas would enter the pump at a lower temperature with pump inefficiency causing the temperature rise. This adds slightly to the heat input to the steam and the electrical generation therefrom, but was disregarded in the calculations.

The friction factor, f, must account for contraction and expansion losses between fuel elements as well as the straight-run friction. The method and data presented by LeTourneau and Grimble (51) were used to compute a typical number, and a constant value of 0.025 was adopted to allow for uncertainties and for setting the fuel plates at an angle to reduce streaming of neutrons in the core.

2.3 Vessel Thickness Limitations on Coolant Pressure

It was shown above (Eq. A-11) that the core power removal is proportional to the coolant pressure; hence, it is desirable to operate the reactor with the coolant pressure as high as possible. The thickness of the reactor containment vessel is the limiting factor in determining the operating pressure.

In general, practical design limitations exist on diameter, thickness, and/or weight for shop and field fabricated reactor vessels. For shop fabricated vessels plate forming equipment capabilities limit thicknesses to about 10 to 12 in., and shop crane capabilities limit the largest component to be handled to about 250 tons. The outside diameter is limited to about 13 ft if the vessel is shipped by rail and to about 18 ft if the vessel is shipped by water. (The limitation on diameter for water transportation is imposed by capability of shop stress-relieving facilities.) For field fabricated vessels, current technology imposes a thickness limitation of about 4 in. because of limitations on field facilities. There are no weight limitations, within the range of interest, on field fabricated vessels.

For this study it has been assumed that shop fabricating facilities can be erected at the plant site for manufacture of large size units. In this manner the weight and, to some extent, diameter limitations on shop fabrication and thickness limitations on field fabricated units are removed. It it is further assumed that the reactor vessel plates can be rolled at a shop and shipped to the plant site where temporary shop facilities are available for assembly and stress relief of the complete unit, then the limitations on the vessel design are a thickness of 4 in., a diameter of 20 ft, and no weight limitation.

The reactor vessel design must comply with all of the rules and procedures of the ASME Boiler and Pressure Vessel Code, Section VIII (140), and to the specific interpretations of the code for nuclear reactor vessels, in particular Code Case 1234. An interpretation of Code Case 1234 limits the sum of the thermal stress, σ_t, and the pressure stress, σ_p, to 1.5 times the allowable stress, σ_a, provided the pressure stress is no greater than the allowable stress. In effect this interpretation states that the vessel thickness can be determined from pressure considerations alone provided that

the thermal stress is limited to not more than one-half the allowable stress. The problem at hand is to determine the thermal shield thickness necessary to reduce the heat generation in the vessel wall to a value such that the resulting thermal stress is one-half the allowable stress. Once this shield thickness is determined and the other dimensions are known from the nuclear calculations, the vessel diameter and allowable pressure can be obtained. For these calculations it is assumed that the coolant gas flow is routed so that the reactor vessel operates at an average temperature of 600°F.

Pressure-Diameter-Thickness Relationship. - The Unfired Pressure Vessel Code gives the following equation for determining the allowable pressure:

$$p = \frac{\sigma_a E_w t_v}{R_v + 0.6 t_v} \qquad \text{(A-26)}$$

where the symbols for this equation and subsequent equations are defined in Table A.2.1. The term E_w applies to fully radiographed and stress relieved weld joints and is given a value of 0.95. The allowable stress, σ_a, is assigned a value of 17,500 psi at 600°F. The vessel wall thickness, t_v, is an independent variable and can be assigned any value up to the assumed limiting value of 10 in. Before the coolant gas pressure, p, can be found, it is necessary to determine the inside radius, R_v. Presumably nuclear and other calculations have fixed the radii of the core and blanket; it is therefore necessary to determine the thickness of the thermal shield in order to fix R_v.

Thermal Stress Calculation. - Timoshenko and Goodier (141) give the general equation for the tangential thermal stress in hollow cylinders for any steady state temperature distribution, T(r), as:

$$\sigma_t(r) = \frac{\alpha E}{1-\nu} \frac{1}{r^2} \frac{r^2+a^2}{b^2-a^2} \int_a^b T(r)rdr + \int_a^r T(r)rdr - T(r)r^2 \qquad \text{(A-27)}$$

Table A.2.1. Nomenclature

NOTE: Any consistent set of dimensions may be used.

a = inside radius of cylinder, ft

b = outside radius of cylinder, ft

E = modulus of elasticity, psi

E_w = weld joint efficiency

$F(mt_v) = 1 - (1 - e^{-mt_v})\left(\frac{2 + mt_v}{2mt_v}\right)$, dimensionless

G_o = heat generation rate at inside surface of first thermal shield, $\frac{\text{Btu}}{\text{ft}^3\text{-hr}}$

G_v = heat generation rate at inside surface of pressure vessel, $\frac{\text{Btu}}{\text{ft}^3\text{-hr}}$

k = thermal conductivity of vessel material, $\frac{\text{Btu}}{\text{hr-ft-}^\circ\text{F}}$

L = thickness of slab, ft

m = heat generation attenuation coefficient, ft^{-1}

p = coolant pressure, psi

q''' = volumetric heat source, $\frac{\text{Btu}}{\text{ft}^3\ \text{hr}}$

R_v = inside radius of pressure vessel, ft

r = radius of any point in vessel wall, ft

T = temperature at any point in slab, $^\circ$F

$\bar{T}$ = average temperature of vessel wall, $^\circ$F

$T(r)$ = temperature at any point in vessel wall, $^\circ$F

t_{1s} = thickness of first thermal shield, ft

t_{2s} = thickness of second thermal shield, ft

t_{ns} = thickness of n^{th} thermal shield, ft

t_s = total thickness of thermal shield, ft

t_v = thickness of vessel wall, ft

x = distance from face of slab, ft

Table A.2.1. (Continued)

α = thermal coefficient of expansion, $\frac{\text{in.}}{\text{in. } ^{o}\text{F}}$

ν = Poisson's ratio, dimensionless

σ_a = allowable stress, psi

σ_p = tangential pressure stress, psi

σ_t = tangential thermal stress, psi

$\sigma_{t,max}$ = maximum tensile thermal stress, psi

It is assumed that the material properties are not a function of temperature. The combined thermal and pressure stress will have its maximum value at the point where the thermal stress is maximum, since the pressure stress distribution is assumed to be uniform across the vessel wall thickness. It can be shown that the maximum tangential thermal stress is at the point where the temperature is lowest, that is to say at the surfaces. It can also be shown that the maximum tangential thermal stress has its minimum value when both surfaces are at the same temperature.

For a given temperature distribution, $T(r)$, in a hollow cylinder, the average temperature, $\overline{T}$, is given as:

$$\overline{T} = \frac{2}{b^2-a^2} \int_a^b T(r)\, r\, dr \qquad \text{(A-28)}$$

Letting r = a, in Eq. A-28, it is seen that

$$\sigma_t(a) = \frac{\alpha E}{1-\nu}\left[(\overline{T} - T(a))\right], \qquad \text{(A-29)}$$

and for r = b

$$\sigma_t(b) = \frac{\alpha E}{1-\nu}\left[(\overline{T} - T(b))\right] . \qquad \text{(A-30)}$$

In a homogeneous material, a change from one uniform temperature to another uniform temperature results in zero thermal stress. In the case of a non-uniform temperature distribution across the vessel wall, the thermal stress can be conveniently calculated by assuming the surface temperature to be zero as a datum, and interpreting the average temperature as the difference between the true average temperature and the true surface temperature.

Therefore, for the case of $T(a) = T(b) = 0$, and where $\overline{T}$ is the average temperature of the non-uniform distribution above the datum,

$$\sigma_t(a) = \sigma_t(b) = \sigma_{t,max} = \frac{\alpha E}{1-\nu}\,\overline{T} \quad . \qquad \text{(A-31)}$$

It should be pointed out that the proper value of the thermal coefficient, α, as used in Eq. A-31 is the instantaneous value at the true average temperature and not the mean value in going from room temperature to the average temperature. This latter value is the one usually reported in the literature. In the absence of data on the instantaneous value, the mean value in going from a temperature slightly below the average to a temperature slightly above the average is sufficient. This mean can be calculated from data usually available.

For simplicity and ease of calculation, the radial temperature distribution, $T(r)$, in the vessel wall is taken the same as that for a flat plate. This is a reasonable approximation when the ratio of radius to thickness is large and permits a direct solution for the thermal shield thickness, whereas an iterative solution is necessary if the temperature distribution is based on cylindrical geometry.

The general equation for steady state heat conduction in a slab with an internal heat source is given (142) as:

$$\frac{d^2T}{dx^2} = - \frac{q'''}{k} \qquad \text{(A-32)}$$

where the symbols are defined in Table 2.3.1. Assuming that the heat generation expression is given by:

$$q''' = G_o \, e^{-mx} \qquad \text{(A-33)}$$

then

$$\frac{d^2T}{dx^2} = - \frac{G_o \, e^{-mx}}{k} \qquad \text{(A-34)}$$

Using the boundary conditions of $x = 0$, $T = 0$, and $x = L$, $T = 0$, the temperature distribution is given as:

$$T = \frac{G_o}{km^2} \left[1 - (1 - e^{-mL}) \frac{x}{L} - e^{-mx} \right], \qquad \text{(A-35)}$$

and the average temperature is given as:

$$\bar{T} = \frac{G_o}{km^2} \left[1 - (1 - e^{-mL})(\frac{2 + mL}{2mL}) \right] . \qquad (A-36)$$

Substituting this expression for the average temperature into Eq. A.31 and letting $L = t_v$ and $G_o = G_v$, gives the maximum tensile thermal stress in the vessel wall as:

$$\sigma_{t,max} = \frac{\alpha E}{1-\nu} \frac{G_v}{km^2} \left[1 - (1 - e^{-mt_v})(\frac{2 + mt_v}{2mt_v}) \right] , \qquad (A-37)$$

Let

$$F(mt_v) = 1 - (1 - e^{-mt_v})(\frac{2 + mt_v}{2mt_v}) , \qquad (A-38)$$

then Eq. A-37 may be written as:

$$\sigma_{t,max} = \frac{\alpha E}{1-\nu} \frac{G_v}{km^2} F(mt_v) . \qquad (A-39)$$

As an aid in the solution of the problem, a plot of $F(mt_v)$ versus mt_v is given in Fig. A.2.3. Since $\sigma_{t,max}$ is taken as 0.5 σ_a and m is known from the heat generation expression, one can choose a value for t_v and then calculate from Eq. A-39, the value of G_v which gives the permissible thermal stress in the vessel wall.

Thermal Shield Thickness. - Neglecting the energy absorption of the coolant in the thermal shield coolant passages, G_v is related to the heat generation rate at the face of the first thermal shield, G_o, by Eq. A-33 as:

$$G_v = G_o e^{-mt_s} \qquad (A-40)$$

where

$$t_s = t_{1s} + t_{2s} = t_{3s} + \cdots \qquad (A-41)$$

UNCLASSIFIED
ORNL-LR-DWG 56026

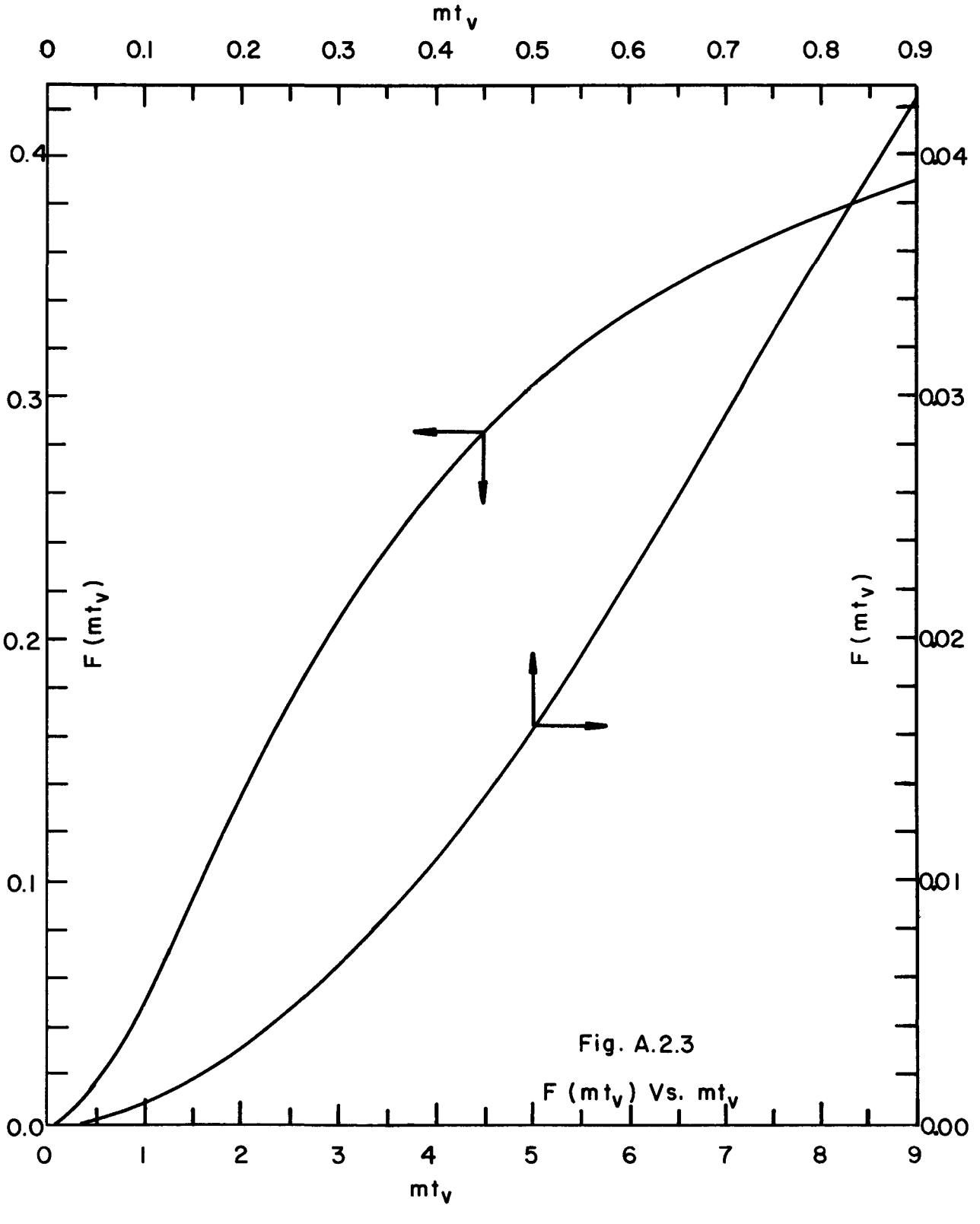

Fig. A.2.3

F (mt_v) Vs. mt_v

Since G_o and m are known from Eq. A-33 and G_v is calculated by use of Eq. A-39, the total shield thickness may be calculated by use of Eq. A-41.

Before the radius of the pressure vessel can be fixed, one must decide how the thermal shield should be divided. The criteria used here is to make the thickness such that the maximum tensile stress in the thermal shields is equal to or less than 1-1/2 times the allowable stress. Fig. A.2.3 and Eq. A-40 can be used to obtain the various shell thicknesses by working the problem in reverse.

Once the thermal shield is divided, the coolant passages fixed, and the various dimensions of the core, blanket, reflector, etc. are known, the radius of the pressure vessel can be determined. Knowing the pressure vessel radius, Eq. A-26 can be used to determine the maximum allowable working pressure.

Outline of Calculative Procedure. - The procedure used to determine the maximum allowable pressure is outlined below:

1. Obtain values of α, E, ν, k, and σ_a for vessel material at operating temperature. See Table A.2.2.
2. Obtain values of G_o and m from heat generation expression.
3. Choose a value for t_v and calculate mt_v.
4. Read value of $F(mt_v)$ off Fig. A.2.3.
5. Calculate G_v from Eq. A-39.
6. Calculate G_v/G_o and mt_s from Eq. A-40.
7. Calculate t_s.
8. Divide t_s into individual thicknesses as follows:
   a. Calculate $F(mt_{1s})$ from Eq. A-39, using $\sigma_{t,max} = 1.5 \sigma_a$ and $G_v = G_o$.
   b. Read mt_{1s} from Fig. A.2.3 and calculate t_{1s}.
   c. Enter mt_{1s} in Eq. A-40 and obtain $\frac{G_{2s}}{G_o}$.
   d. Calculate G_{2s} and enter in Eq. A-39 to determine t_{2s}.
   e. Proceed until t_s is divided. Reduce thickness of next to last shield, if shield is too thin.

9. Determine coolant passage thickness between thermal shields.

10. Obtain dimensions of core, blanket, reflector, thermal insulation, etc. from nuclear and thermal calculations, and calculate radius of vessel, R_v.

11. Calculate allowable pressure from Eq. A-26 for vessel thickness used in step 3.

Table A.2.2 lists the values for the material properties necessary for calculating the thermal stress.

Table A.2.2. Properties of SA-212-Gr. B Steel at 600°F

Property	Value	Reference
α, $\frac{\text{in.}}{\text{in. }^{\circ}\text{F}}$	8.34×10^{-6}*	143
E, psi	26.7×10^{6}	143
ν, dimensionless	0.296	143
σ_a, psi	17,400	140
k, $\frac{\text{Btu}}{\text{hr ft }^{\circ}\text{F}}$	25	144

* Mean value in going from 500°F to 700°F.

A P P E N D I X B

Xenon Control in Fluid Fuel Breeder Reactors

APPENDIX B

Xenon Control in Fluid Fuel Breeder Reactors[a]

1.0 Introduction

The importance of xenon control in a breeder reactor cannot be overemphasized. In a typical fluid-fuel reactor the poisoning effect of xenon amounts to about a 5% neutron loss per neutron absorbed in fuel if the xenon concentration is allowed to reach equilibrium. This loss is serious enough that it can seriously jeopardize the breeding performance of a reactor, and, conversely, any significant reduction in xenon concentration is reflected in greatly improved breeding gain. Improved breeding gain influences the economic potential of the system by allowing larger credits for material produced and thereby decreases the fuel cycle cost.

Fluid-fuel breeder reactors, such as the AHBR, MSBR, and the LBBR, lend themselves very conveniently to effective xenon control. For each of these, two methods of control are available - removing iodine before significant decay or removing xenon shortly after formation. A combination of these two methods might also be used. The choice of method depends largely upon the chemical and kinetic behavior of iodine and xenon in the system at the operating conditions. Direct removal of iodine has the additional advantage of reducing the biological hazard in event of an accident that releases the radioactive contents of the reactor.

The reduction of the poisoning effect depends directly upon the rate of removal of iodine and/or xenon. Considerably longer processing periods for xenon removal can be tolerated for a reasonably low xenon poison fraction if iodine removal is practiced (see Fig. B.1.1). The curve is drawn for processes that have 100% removal efficiency; for lower efficiencies the processing period would have to be shortened, i.e., the fuel and fertile streams would have to be processed more often.

---

[a] Based primarily on the work of Burch, Watson, and Weeren, Ref. 8.

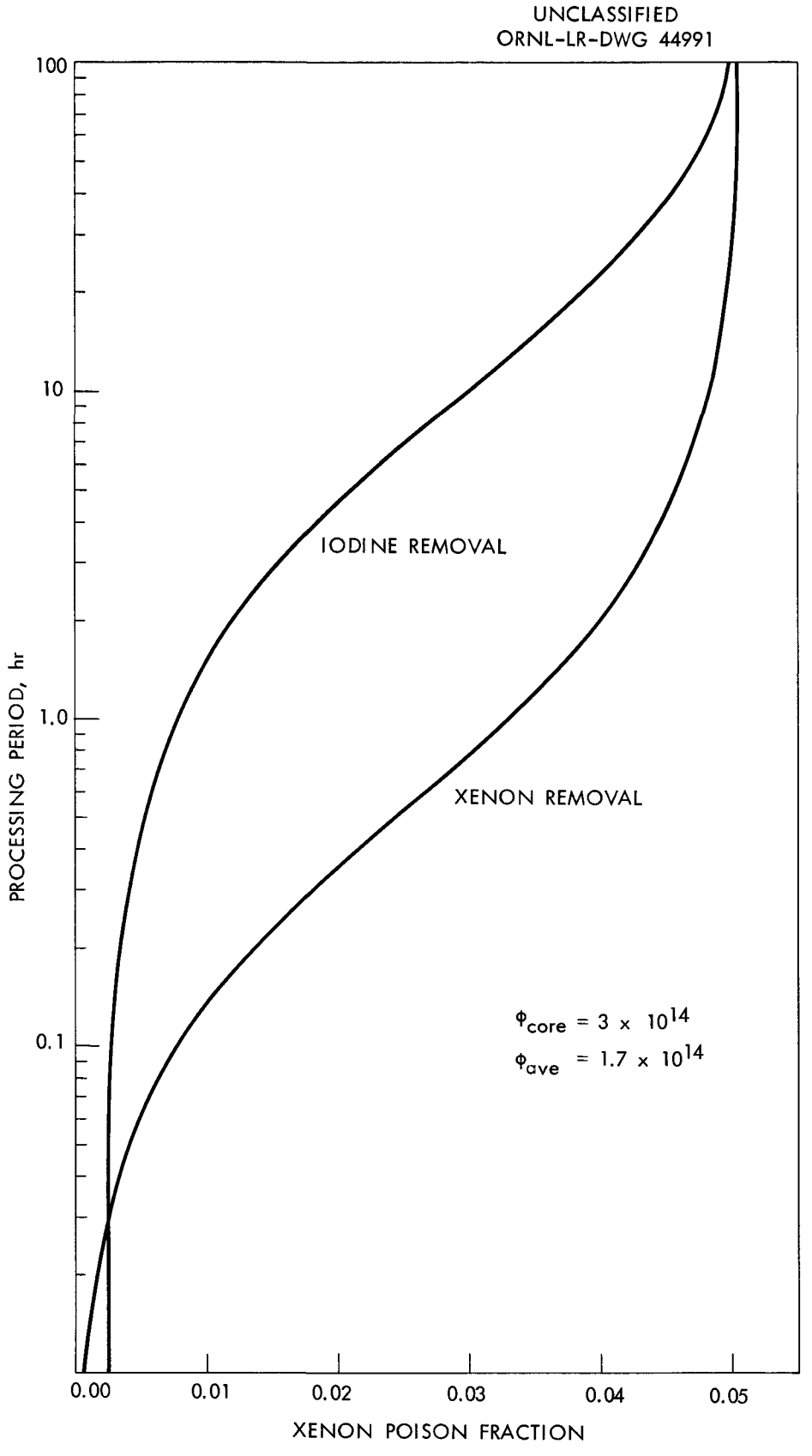

Fig. B.1 1 Processing period vs xenon-poison fraction.

Poison Fraction Calculation. - The poison fraction attributive to xenon is defined as the ratio of neutron absorptions by xenon to neutron absorptions in fuel under equilibrium conditions. Upon considering all of the ways by which xenon may be removed from the reactor, an expression for the poison fraction can be obtained which is

$$pf\ (Xe) = \frac{\eta\ Y_{Xe}^{t}}{\nu} \left[\frac{C_{Xe}^{a}}{\lambda_{Xe} + C_{Xe}^{a} + \frac{1}{T_{Xe}}} \right] , \qquad \text{(B-1)}$$

where

η = neutrons born per fuel absorption,
ν = neutrons born per fission,
Y_{Xe}^{t} = total Xe yield per fission (direct + indirect),
C_{Xe}^{a} = reaction rate coefficient (defined in Appendix H),
λ_{Xe} = decay rate of Xe,
T_{Xe} = average cycle time for Xe removal.

This is the equation that pertains when the only control over xenon poisoning is by xenon removal according to some process having a cycle time T_{Xe}.

When xenon poisoning is controlled by processing for iodine removal with no additional processing for xenon removal, the poison fraction is given by

$$pf\ (Xe) = \frac{\eta}{\nu} \left[\frac{C_{Xe}^{a}}{C_{Xe}^{a} + \lambda_{Xe}} \right] \left[Y_{Xe}^{d} + \frac{\lambda_{I}\ Y_{I}^{t}}{\lambda_{I} + \frac{1}{T_{1}}} \right] . \qquad \text{(B-2)}$$

Symbols not previously defined are

Y_{Xe}^{d} = direct fission yield of Xe per fission,
T_{1} = average cycle time for iodine removal,
Y_{I}^{t} = total iodine yield per fission (direct + indirect).

On the other hand, if both iodine and xenon removal methods are employed, the poison fraction expression becomes

$$pf\ (Xe) = \frac{\eta}{\nu} \left[\frac{C_{Xe}^{a}}{\lambda_{Xe} + C_{Xe}^{a} + \frac{1}{T_{Xe}}} \right] \left[Y_{Xe}^{d} + \frac{\lambda_{I}\ Y_{I}^{t}}{\lambda_{I} + \frac{1}{T_{1}}} \right] . \qquad \text{(B-3)}$$

It is not necessary to include a term in Eqs. B-2 and B-3 to account for neutron captures in iodine because the capture cross section is small. Inefficiencies in the removal processes are accounted for by decreasing the cycle times T_{Xe} and T_I. The curves of Fig. B.1.1 and plots of Eqs. B-1 and B-2.

Xenon and Iodine Diffusion into Graphite. - It should be pointed out that the above analysis does not account for poisoning from xenon which may become trapped in reactor structural material and be unavailable to removal techniques. For example, this might occur in the MSBR and LBBR by xenon (or iodine) diffusion into interstices of the graphite moderator. This phenomenon has been studied by Burch, Watson, and Weeren (8) in considerable detail.

In the MSBR and LBBR, fuel solution is in direct contact with graphite which, even though designated as "impervious", offers a large network of interconnected pores into which xenon and iodine might diffuse. Once inside the graphite the only mechanism of removal is burnout. The concentration inside the graphite is limited by the burnout rate and the diffusion rate. Burch and co-workers considered only diffusion through open pores and not diffusion through the lattice cell. There is evidence (41, 62) that xenon diffusion through the lattice cell is from six to eight orders of magnitude lower than diffusion through the pores.

Xenon poison fraction is plotted in Fig. B.1.2 as a function of the diffusion coefficient for certain assumed values of neutron flux for a MSBR and LBBR. The curves are taken from Burch's study which was made for the neutron flux levels noted on the graph. In this current breeder study, the neutron fluxes are approximately 8×10^{14} and 9×10^{14} respectively for the MSBR and LBBR. Xenon diffusion coefficients are probably of the order 10^{-4} - 10^{-6} for which xenon poisoning is about 1.2% for the MSBR and 2.5% for the LBBR if no xenon removal process is employed. A marked decrease in xenon poisoning is illustrated in Fig. B.1.3 which shows the effect of processing the gas phase to decrease the equilibrium concentration in the fuel.

A further calculation for the MSBR is reported in Sec. 3.0 of this appendix.

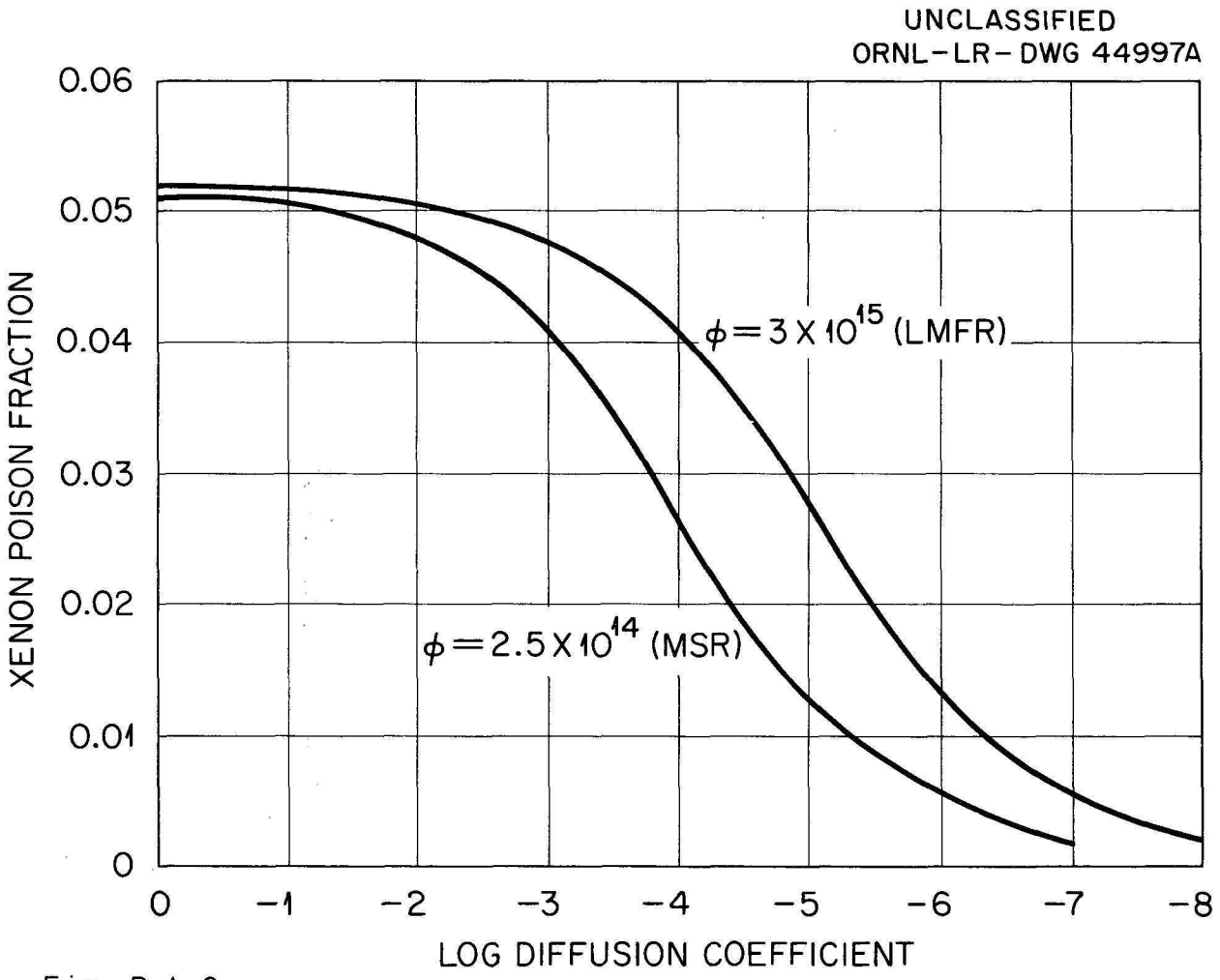

Fig. B.1.2.

Xenon Poison Fraction vs Diffusion Coefficient and Core Flux. Assumes Only Equilibration of Fission Gases in Expansion Tank. No Gas Phase Removal of Xenon From Expansion Tank.

The behavior of iodine with respect to its diffusion into graphite is not well known, and it is difficult to predict just how much xenon poisoning in the interstices of graphite might be due to iodine. However, it is believed that fission product iodides will be stable in MSBR and LBBR fuel solutions. Before the importance of iodine diffusion can be assessed, experimental data under in-pile conditions will probably be required.

2.0 Aqueous Homogeneous Breeder Reactor

The AHBR fuel solution is well suited for xenon control by either iodine removal or xenon stripping. Each of these methods has been studied (53, 54, 55, 56) in regard to the Homogeneous Reactor Experiments conducted at the Oak Ridge National Laboratory, and the iodine-removal method has been successfully applied to an operating reactor. Xenon poisoning in the pelletized ThO_2 blanket can be controlled only be removing the pellets from the reactor and dissolving. Xenon and iodine will be trapped inside and adsorbed on pellet surfaces, and no practical method of purging appears possible. Consequently, the equilibrium xenon poisoning in the fertile stream will be that associated with the frequency with which ThO_2 is removed for Thorex processing for recovery of bred material.

Iodine Removal. - Considerable development effort (58, 59) has been expended in the HRE program to study the behavior of iodine in aqueous systems, and iodine removal offers a promising means of controlling xenon poisoning. Iodine may be removed from the reactor fuel by low pressure processing of a continuous let-down stream or by concentration of iodine in a small volume of condensate at high pressure. For a large breeder reactor installation the latter method seems to be preferable, and in the study of Burch, et al, (8) it is suggested that a system as described below be used.

A by-pass stream of core solution is pumped continuously through the pressurizer; however, just prior to entering the pressurizer the solution is contacted in a jet eductor with a vapor stream consisting of a mixture of oxygen and D_2O vapor. Under these conditions the equilibrium distribution of iodine greatly favors the vapor phase. In the pressurizer the two phases separate, the liquid phase returning to the core and the vapor phase flowing to a partial condenser. A portion of the D_2O vapor is condensed, and the

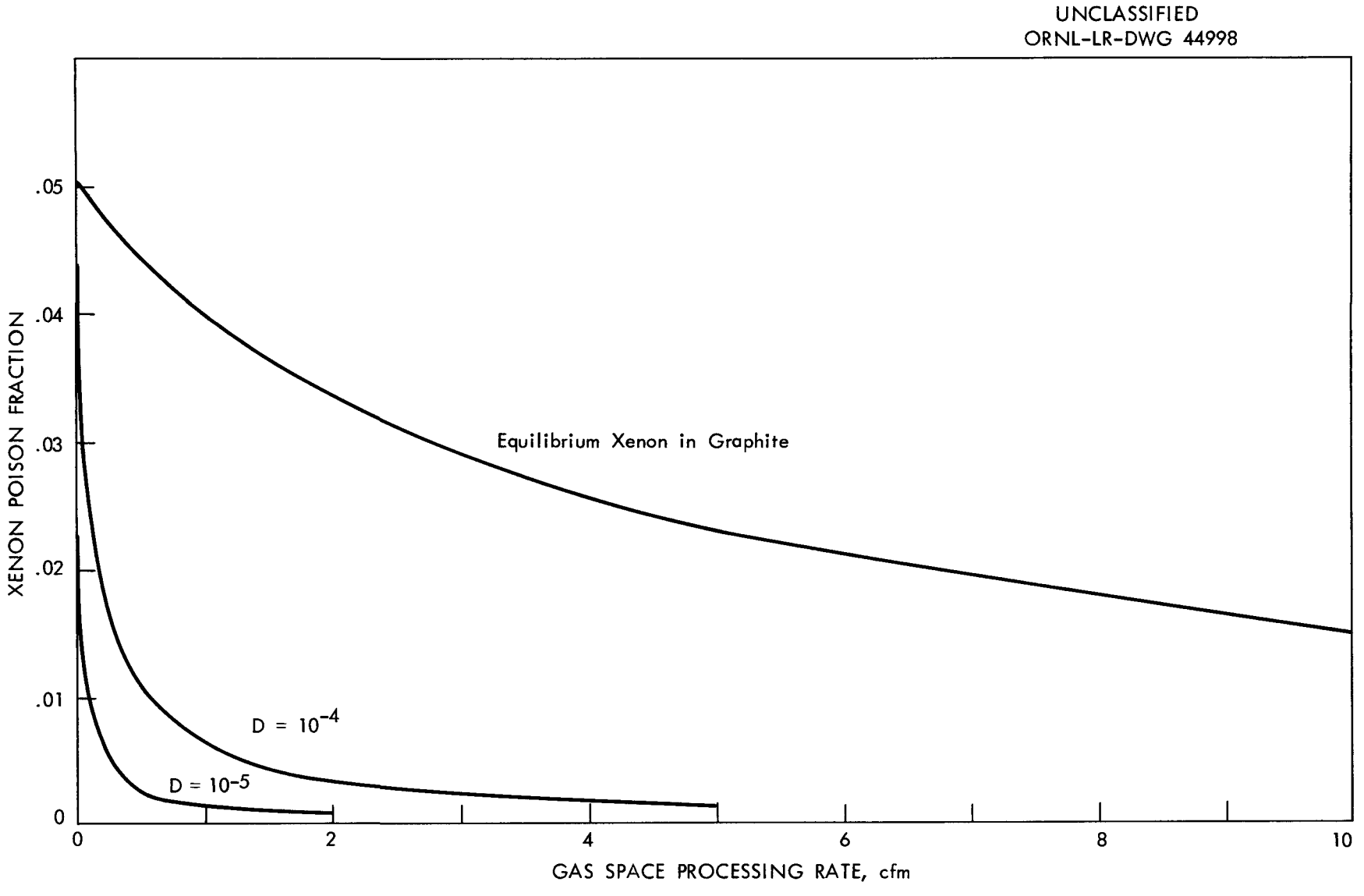

Fig. B.1.3. Xenon poisoning as a function of gas processing rate and diffusion coefficient in a molten salt reactor. Volume of gas space being processed = 35 ft^3.

remainder is recirculated to the eductor. Make-up vapor is supplied by boiling in the pressurizer; make-up oxygen is supplied from an external source.

Equilibrium conditions in the partial condenser are such that iodine greatly favors the liquid phase and is thereby withdrawn with the condensate. It might be noted that this process will not be effective for xenon removal because the vapor phase from the partial condenser is recirculated to contact more fuel solution. The rate at which iodine is removed from the system will increase with increased flow of recycle gas and amount of condensate withdrawn. The effectiveness of this type of purge is illustrated in Fig. B.2.1, and the resulting xenon poisoning to the system is shown in Fig. B.2.2. This latter figure has been drawn for certain assumed conditions of behavior of I-135 as noted by the parameters. The parametric study is presented because the behavior of iodine in an operating reactor is not completely understood. Measurements (63) in the HRE-2 have not been entirely successful in explaining the distribution of iodine throughout the system. One explanation of the discrepancy between measurements and calculations is that some of the iodine is adsorbed on the walls of pipes and other parts of the system.

The remainder of the processing system after the partial condenser is concerned with isolating the iodine to allow its decay. This is accomplished by allowing the condensate to flow through a pressure let-down valve into an evaporator. Steam strips iodine from solution and carries it to a trap containing silver-coated wire mesh. Iodine reacts chemically with the silver and is retained until it decays to xenon. Effluent xenon and steam pass from the trap through a condenser to reclaim the heavy water. Xenon passes to a charcoal adsorption bed for retention.

Xenon Stripping. - Direct stripping of xenon with radiolytic $D_2 + O_2$ appears to be an efficient but rather complex way of achieving low xenon poison fractions. Approximately 8 ft^3/min of radiolytic gas are produced in uniform distribution over the core for each megawatt of power providing an excellent mechanism for carrying fission gases. A portion or all of the radiolytic gas may be removed through a pressure-reducing system to purge xenon; the radiolytic gases are recombined and the resulting heavy water is recovered.

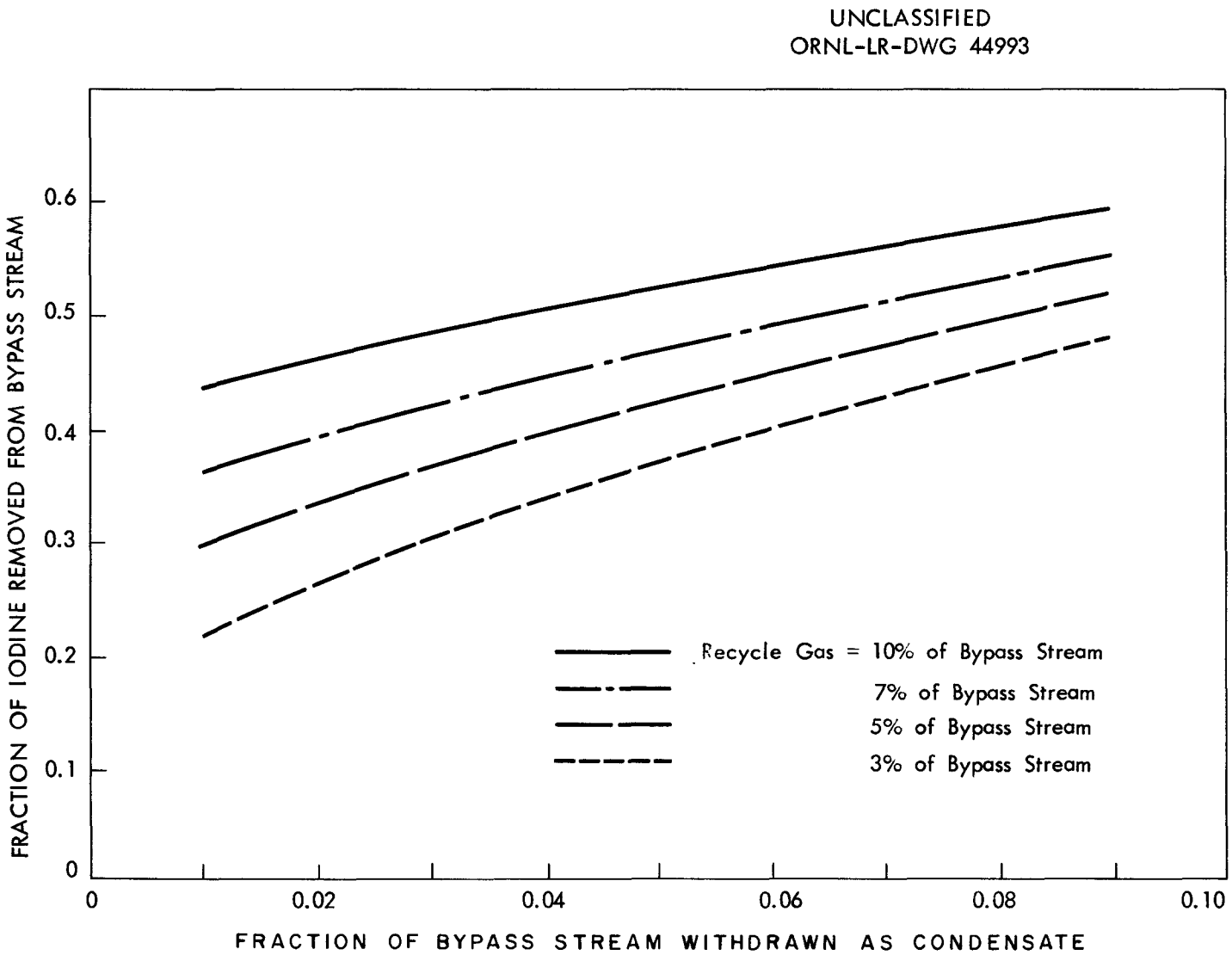

Fig. B.2.1. Iodine Removed from Bypass Stream at Various Flow Rates of Condensate and Recycle Gas.

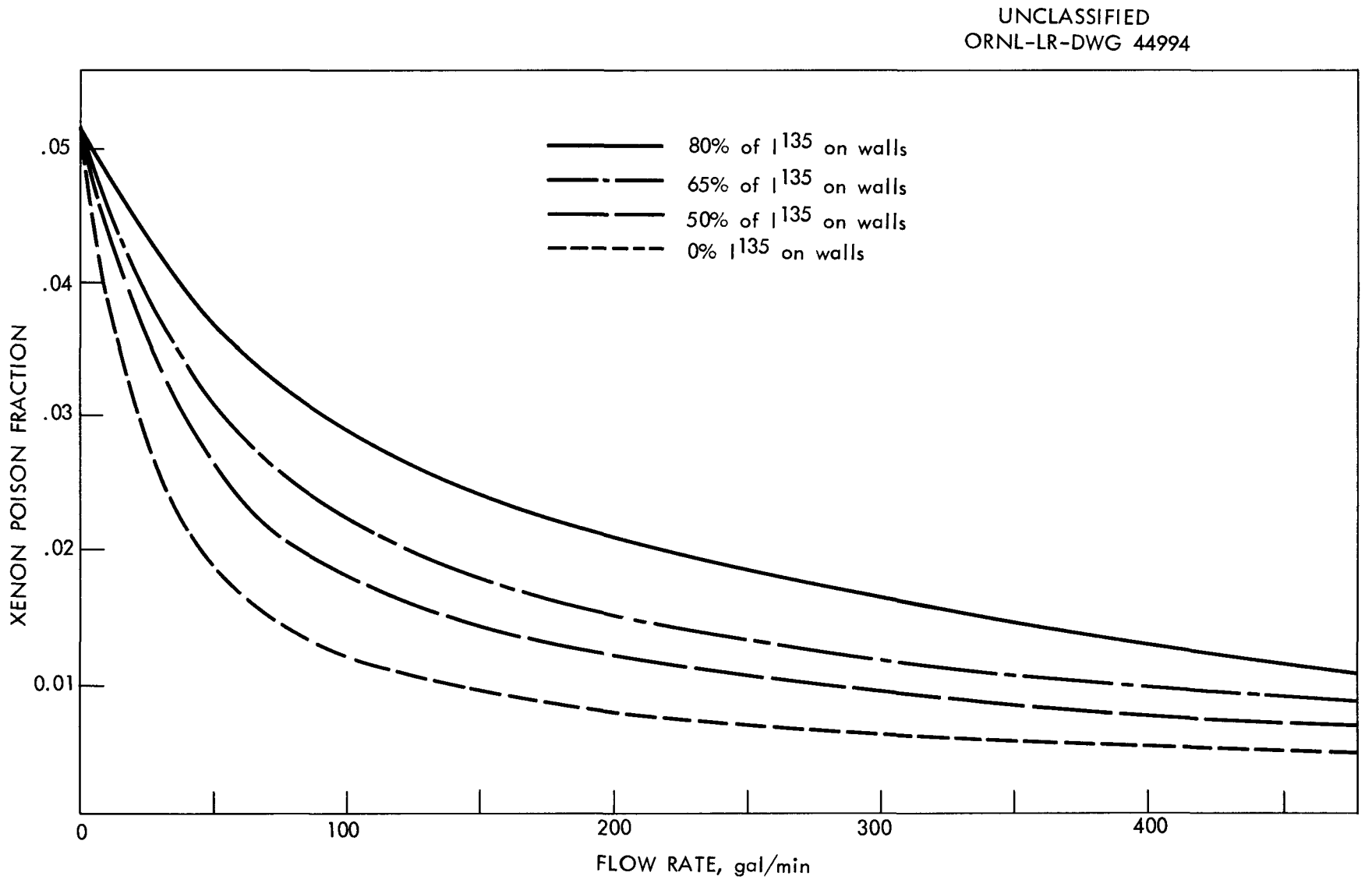

Fig. B.2.2. Xenon poisoning in a 500 Mw_t homogeneous reactor for various flows through pressurizer (40% removal of I^{135} in pressurizer assumed).

There are, however, potential disadvantages to the radiolytic gas-stripping process. First, this scheme requires handling relatively large volumes of an explosive gas mixture. Secondly, there are mechanical difficulties associated with a pressure-reduction system which has to operate over a range of as much as 2000 psi while passing a mixture of entrained liquid and gases. Also it might be that the charcoal beds would be required to handle large volumes of carrier gas which would probably be oxygen. On the favorable side, however, the gas-stripping process would permit reducing the amount of copper which is included in aqueous fuels to catalyze $D_2 + \frac{1}{2} O_2$ recombination, thereby resulting in neutron savings.

Calculated curves (8) showing the xenon poisoning of an aqueous system as a function of radiolytic gas processing are presented in Fig. B.2.3

3.0 Molten Salt Breeder Reactor

Iodine Removal. - Controlling xenon poisoning by iodine removal has not been seriously considered for the MSBR. It is expected that iodine will exist in molten salt solutions in the form of ionic iodides which should be soluble. No known method is available for removing these iodides. As mentioned above, xenon poisoning might be enlarged by the adsorption of iodides on graphite surfaces; however, not enough is known of this phenomenon to permit making a conclusive statement.

Gas-Sparging. - Two basic methods have been proposed for purging xenon with an inert gas, probably helium, from the MSBR -- sparging the fuel solution or sparging an inert gas chamber which provides large interfacial contact between gas and liquid phases. It appears that either method will be successful. Because of its extreme simplicity, continuous gas phase processing was adopted by Burch and co-workers (8) for calculations in regard to this study. Some of their pertinent results have been presented above in Fig. B.1.3.

The process consists of providing a sweep-gas passing through a surge chamber which provides the interfacial contact area. The equilibrium between xenon and molten salt is such that xenon greatly favors the gas phase. Smith and Ward (65) report the solubility of xenon in molten 63-37 mole % $LiF-BeF_2$ to be 0.25×10^{-8} moles/cm^3-atm at 1150°F. After leaving the surge chamber, xenon is adsorbed on charcoal and retained for decay.

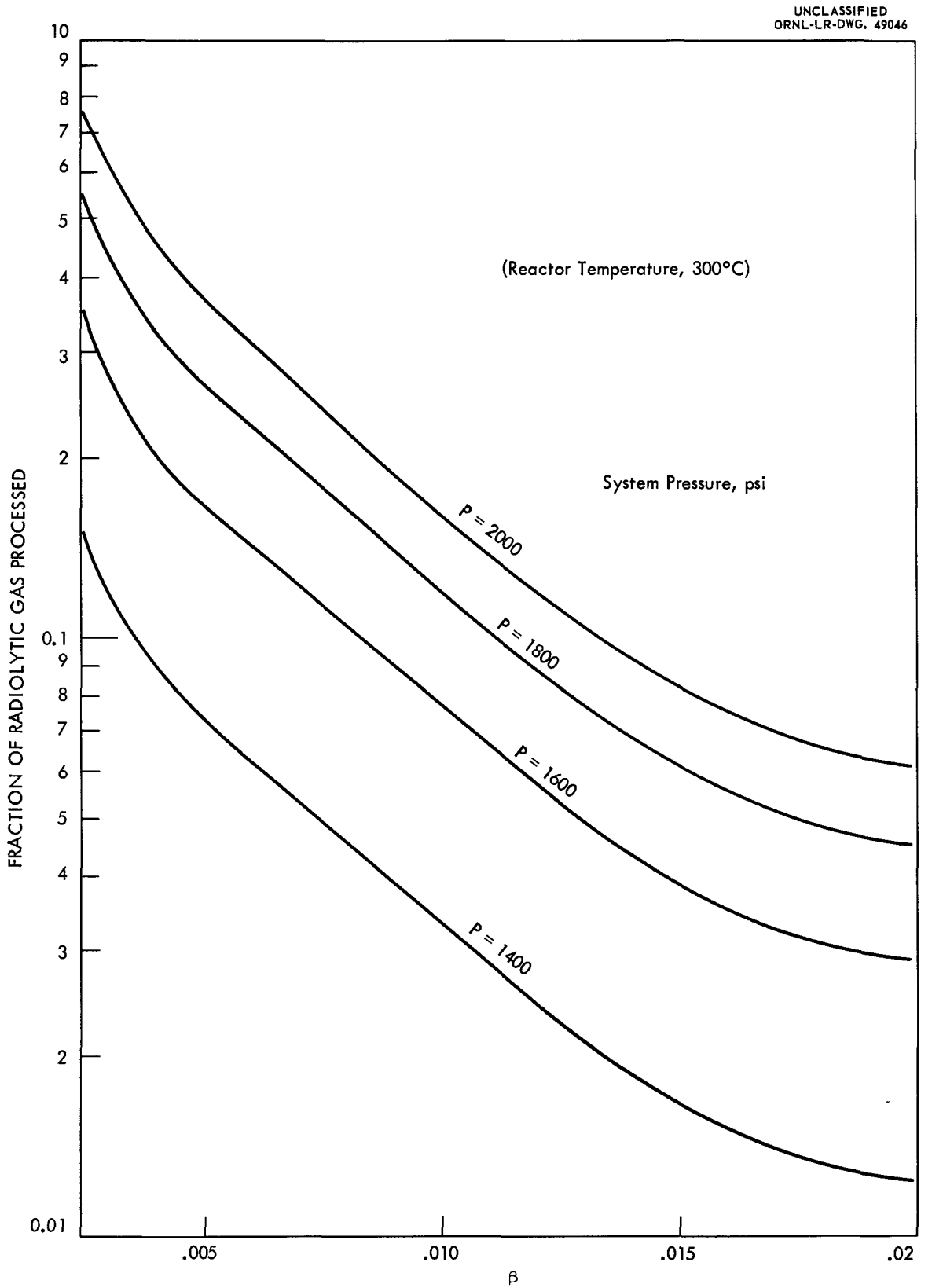

Fig. B.2.3. Fraction of the total production of radiolytic gas (D_2 + 1/2 O_2) which must be let down to maintain a desired xenon poison fraction (β).

The total number of Xe atoms in volume $A\Delta x$ at time $t + \Delta t$ is equal to the number present at time t plus the number of sources during time period Δt minus the number of losses during the same period of time. Under the assumption that no fissioning occurs in the graphite, the only source term for Xe will be the diffusion of Xe into the volume element. The losses consist of neutron absorptions in Xe, the radioactive decay of Xe and the Xe diffusion out of the volume element. These terms may be collected into the mathematical statement of Eq. B-4.

$$N(x,t + \Delta t)\, A\Delta x = N(x,t)\, A\Delta x + J_{in}\, A\Delta t - \overline{\sigma_a \phi} N(x,t)\, A\Delta x\, \Delta t$$

$$- \lambda N\,(x,t)\, A\Delta x\, \Delta t - J_{out}\, A\, \Delta t \qquad \text{(B-4)}$$

where:

$N(x,t)$ = the Xe concentration at position x at time t, atoms/cm^3,
A = the graphite area, cm^2,
Δx = the incremental graphite thickness, cm,
J_{in} = the Xe atoms diffusing into the incremental volume, atoms/cm^2-sec,
J_{out} = the Xe atoms diffusing out of the incremental volume, atoms/cm^2-sec,
$\sigma_a \phi$ = the energy integrated Xe reaction coefficient, sec^{-1},
λ = the Xe decay coefficient, sec^{-1}.

If we divide Eq. B.4 by $A\Delta x\Delta t$ and collect terms, we obtain Eq. B-5

$$\frac{N\,(x,t + \Delta t) - N\,(x,t)}{\Delta t} = - (\overline{\sigma_a \phi} + \lambda)\, N\,(x,t) + \frac{J_{in} - J_{out}}{\Delta x}\,. \qquad \text{(B-5)}$$

We will now assume Flick's-law diffusion, i.e.,

$$J = - D\, \frac{\partial N(x,t)}{\partial x}$$

where D is the Xe diffusion coefficient, cm^2/sec.

Xenon Removal by Sparging Side-Stream with Helium. - The core of the Molten Salt Breeder Reactor (MSBR), is constructed of 8-in.-square graphite rectangles. These rectangles are machined at the corners to form vertical passages of circular cross section. The fuel salt passes through the core in graphite tubes of bayonet construction which are inserted into the passages as shown in Fig. B.3.1. A small stream of blanket solution flows between the bayonet tube and the graphite moderator.

The blanket of the molten salt reactor is processed continuously by the fluoride volatility process. Because of this very rapid processing, very little fissioning occurs in the blanket stream, and the Xe concentration is extremely low. It is assumed that negligible amounts of xenon will diffuse from the fuel salt through the graphite bayonet tube and into the fertile stream. This assumption results in negligible error if diffusion coefficients are less than 10^{-4} cm^2/sec.

Because the ratio of tube wall thickness to tube diameter is small, the calculations may be performed in slab geometry. The calculational model is shown in Fig. B.3.2.

The problem has been broken into two parts. The first part is the solution for the slab of thickness "a", taking the origin at the center of the slab, and the second part is the solution for a semi-infinite slab taking the origin at the surface of the slab.

3.1 Derivation of the Xe Diffusion Equation

Since slab geometry is satisfactory for the solution of this problem, this derivation will be for slab geometry, as shown.

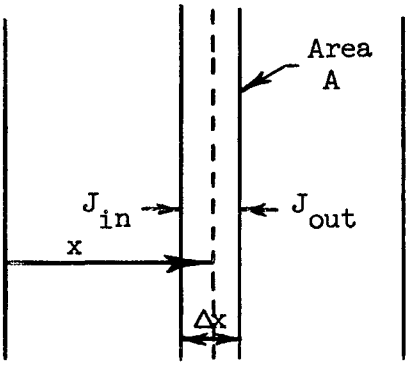

UNCLASSIFIED
ORNL-LR-DWG 56859

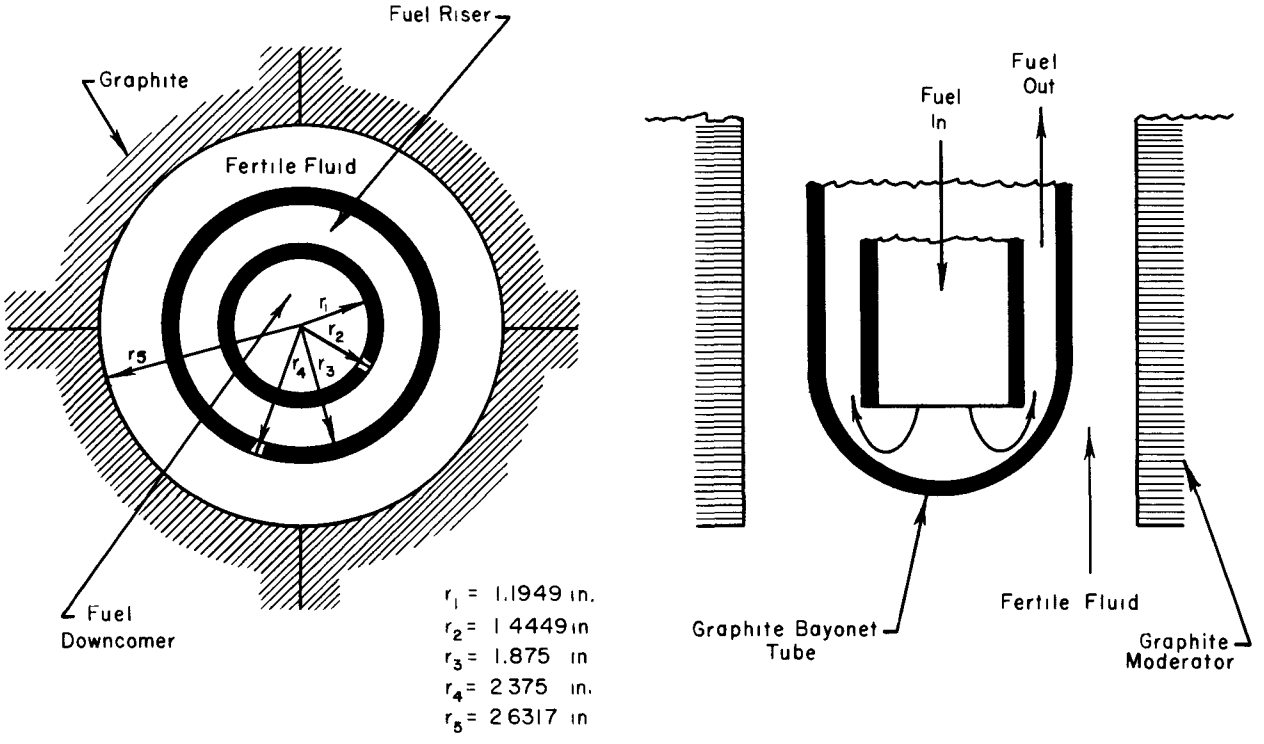

M S B R FUEL ELEMENT

Fig. B.3.1

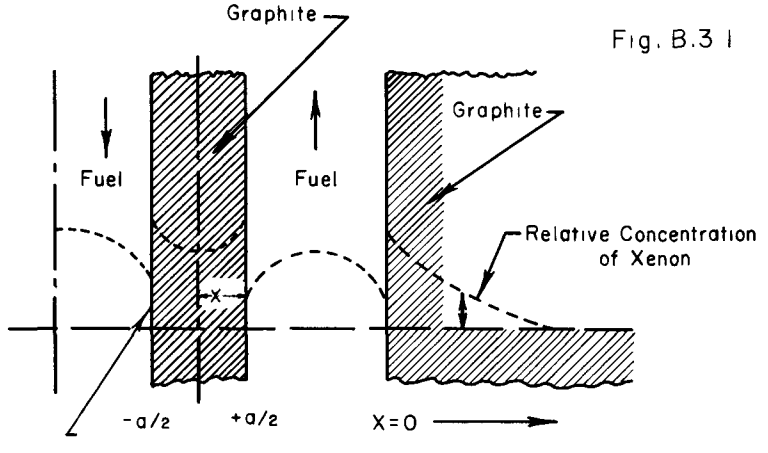

COMPUTATIONAL MODEL

Fig. B.3.2

Then $J_{in} = J(x,t) = - D\frac{\partial N(x,t)}{\partial x}$

and $J_{out} = J(x + \Delta x,t) = - \frac{D\partial N(x + \Delta x,t)}{\partial x}$

Equation B-5 may not be rewritten.

$$\frac{N(x,t + \Delta t) - N(x,t)}{\Delta t} = (\overline{\sigma_a \phi} + \lambda) N(x,t) + D \frac{\frac{\partial N(x + \Delta x,t)}{\partial x} - \frac{\partial N(x,t)}{\partial x}}{\Delta x} \quad \text{(B-6)}$$

We now take the limit as Δt and Δx approach 0 and obtain the time dependent diffusion equation

$$\frac{\partial N(x,t)}{\partial t} = + \frac{D\ \partial^2 N(x,t)}{\partial x^2} - (\overline{\sigma_a \phi} + \lambda) N(x,t) \quad \text{(B-7)}$$

Since the problem of interest is the steady state problem, Eq. B-7 is rewritten as Eq. B-8.

$$D \frac{d^2 N(x)}{dx^2} - (\overline{\sigma_a \phi} + \lambda) N(x) = 0 \quad \text{(B-8)}$$

3.2 Derivation of the Fuel Stream Equation

A schematic flow diagram for the Molten Salt Breeder Reactor is shown in Fig. B.3.4

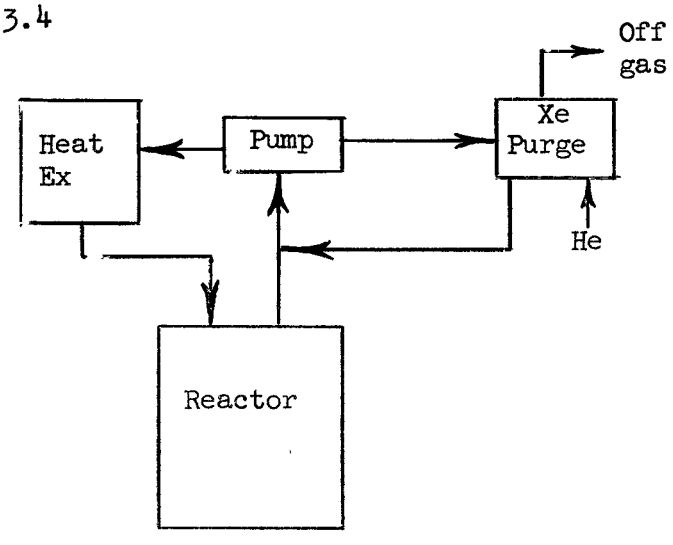

The rate of change of the Xe concentration in the fuel stream will be equal to the rate at which Xe is added to the fuel stream minus the rate of removal.

$$\frac{d\bar{N}}{dt} V = Y\sum_f \phi v - \overline{\sigma_a \phi}\, \bar{N} v - \frac{\bar{N} V}{T} - J_o A_T - \lambda \bar{N} v \qquad \text{(B-9)}$$

where

$Y\sum_f \phi v$ = the number of Xe atoms produced in the fuel stream per second,

$\overline{\sigma_a \phi}\, Nv$ = the number of neutron absorptions by Xe in the fuel stream per second,

$\frac{\bar{N} V}{T}$ = the number of Xe atoms removed per second from the fuel stream by purging,

$J_o A_T$ = the number of Xe atoms diffusing out of the fuel stream per second into the graphite,

$\lambda \bar{N} V$ = the number of Xe decays in the fuel stream per second.

This equation may be solved in the steady state for the average Xe concentration in the fuel stream.

$$\bar{N} = \frac{Y\sum_f \phi - J_o A_T/v}{\overline{\sigma_a \phi} + \frac{V}{Tv} + \lambda \frac{V}{v}} \qquad \text{(B-10)}$$

The diffusion current at the salt-graphite boundary may be obtained from Flick's law evaluated at x = 0, Eq. B-11.

$$J_o = D \left.\frac{\partial N(x)}{\partial x}\right|_{x = 0} \qquad \text{(B-11)}$$

Since the Xe concentration falls off very rapidly in the graphite, the concentration near the surface may be approximated even in the finite slab as $N(x) = No,g\ \epsilon^{-\beta x}$, and J_o may be approximated by Eq. B-12

$$J_o \tilde{=} D\beta No,g \qquad \text{(B-12)}$$

The factor C has been defined to be the ratio of the Xe concentration in the graphite at the graphite salt boundary to the average Xe concentration in the fuel salt, Eq. B-13.

$$C = \frac{No,g}{\overline{N}} \tag{B-13}$$

Equation B-10 can now be solved explicitly for the average concentration giving Eq. B-14.

$$N = \frac{Y\sum_f \phi}{\overline{\sigma_a \phi} + \lambda \frac{V}{v} + \frac{V}{vT} + CD\beta\, A_T/v} \tag{B-14}$$

3.3 Coupling Conditions at Graphite-salt Interface

In order to estimate the ratio of the Xe concentration in the graphite at the graphite-salt interface to the average concentration of Xe in the fuel stream, C, it is necessary to establish a mass transfer equation. By analogy with the Dittus-Boelter equation, Eq. B-15 is obtained.

$$\frac{\left| J_o \right| D_e}{(\overline{N} - No,s)\, D_{NS}} = 0.023 \left(\frac{\mu}{\rho D_{NS}} \right)^{0.4} \left(\frac{D_e G}{\mu} \right)^{0.8} \tag{B-15}$$

where

$\left| J_o \right|$ = the rate of diffusion of Xe into the graphite walls, atoms/cm^2-sec,

D_e = the equivalent diameter, cm. $D_e = 4A/Pw$ where A is the flow area and Pw is the wetted perimeter,

$\overline{N}$ = the mean concentration of Xe in the fuel stream, atoms/cm^3,

No,s = the concentration of Xe in the salt at the graphite-salt interface, atoms/cm^3,

D_{NS} = the diffusion coefficient of Xe in the salt, cm^2/sec,

μ = the viscosity of the salt, gm/cm-sec,

ρ = the density of the salt, gm/cm^3,

G = the mass flow rate of salt per unit of flow area, gm/sec-cm^2.

As observed above, the Xe concentration falls off very rapidly in the wall, and J_o may be approximated by $D\beta No,g$.

The value of No,g is related to No,s by Henry's law, Eq. B-15

$$No,s = 1.807 \times 10^{15} P(N) \qquad (B-16)$$

where P(N) is the partial pressure of Xe in atmospheres. The value of 1.8×10^{15} for the constant was calculated from a value of 3×10^{-9} moles/cc atm at 1200°F, cited by Watson and Evans (3).

The general gas law, Eq. B-17, holds for Xe in the graphite.

$$F_g P(N) = No,g R(\Theta) \qquad (B-17)$$

where

F_g = the volume fraction of voids in the graphite,
R = the universal gas constant, 136.2×10^{-24} atom/°K-atoms/cm^3,
N = the graphite temperature, °K.

Substitution of P(N) in Eq. B-17 into Eq. B-16 and transposing terms gives Eq. B-18

$$No,g = \frac{No,s\ F_g}{1.807 \times 10^{15}\ R\Theta} \qquad (B-18)$$

For the reactor operating at 1180°F, and with a graphite void fraction of 0.10, Eq. B-18 becomes:

$$No,g = 440\ No,s \quad . \qquad (B-19)$$

We now substitute No,g/440 for No,s in Eq. B-15 and obtain Eq. B-20.

$$\frac{D\beta\ No,g\ De}{(\overline{N} - \frac{No,g}{440})\ D_{NS}} = 0.023 \left(\frac{\mu}{\rho D_{NS}} \right)^{0.4} \left(\frac{DeG}{\mu} \right)^{0.8} \qquad (B-20)$$

Table B-1 gives a list of the parameters required for the solution of Eq. B-20.

Table B-1

$D = 10^{-5} - 10^{-7}$ cm^2/sec	$\mu = 0.0783$ gm/sec-cm
$\beta = 18.3 - 183$ cm^{-1}	$\rho = 1.91$ gm/cm^3
De = 6.08 cm	G = 1400 gm/sec-cm^2 (Ref. 147)
$D_{NS} = 3 \times 10^{-5}$ cm^2/sec	

Substitution of the parameters in Table B-1 into Eq. B-21, and manipulation yields the following equation for C as a function of $D\beta$.

$$C = \frac{No,g}{\bar{N}} = \frac{2.19 \times 10^{-2}}{4.93 \times 10^{-5} + D\beta} \qquad \text{(B-21)}$$

For diffusion coefficients of 10^{-5} and 10^{-7}, C has values of 94.2 and 324, respectively. These values of C were used in plotting the curves on Fig. B.3.3.

3.4 Solution of Diffusion Equation

As has been shown, the steady state equation for diffusion of Xe into graphite may be written:

$$D \frac{d^2 N(x)}{dx^2} - (\overline{\sigma_a \phi} + \lambda) N(x) = 0 \qquad \text{(B-8)}$$

For the finite slab shown in Fig. B.3.2, with the boundary condition that the Xe concentration No,g in the graphite at the surface is the same at $\pm$ a/2, the solution of Eq. B-8 is:

$$N(x) = \frac{No,g \cosh \beta x}{\cosh \beta a/2} \qquad \text{(B-22)}$$

where

$$\beta = \left[\frac{\overline{\sigma_a \phi} + \lambda}{D} \right]^{1/2}$$

The solution to Eq. B-8 for the semi-infinite slab shown in Fig. B.3.2 is

$$N(x) = No,g \quad \epsilon^{-\beta x} \tag{B-23}$$

The total neutron absorptions by Xe circulating in the fuel stream are given by Eq. B-24.

$$A_f = \overline{\sigma_a \phi}\, \overline{N}\, v \tag{B-24}$$

where

v = the volume of fuel in the reactor core, cm^3,

$\overline{N}$ = the mean concentration of Xe in the fuel stream, $\frac{atoms}{cm^3}$.

The neutron absorptions by Xe which has diffused into the graphite are given by Eq. B-25

$$A_g = \frac{\overline{\sigma_a \phi}\, C\, \overline{N}}{\beta} \left[2A_1 \tanh \beta\, a/2 + A_2 \right] . \tag{B-25}$$

where

C = the ratio of the Xe concentration in the graphite at fuel-graphite boundary to the average Xe concentration in the fuel stream,

A_1 = the mean area of the graphite in the inner graphite tube, $cm^2 = \frac{\pi}{2} (R_1 + R_2) L$, where L is the length of the tubes,

A_2 = the inside area of the graphite in the outer graphite tube, cm^2.

The ratio of Eq. B-25 to Eq. B-26 is:

$$\frac{A_g}{A_f} = \frac{C}{v\beta} \left[2A_1 \tanh \beta a/2 + A_2 \right] . \tag{B-26}$$

The Xe concentration in the fuel stream is given by Eq. B-14.

$$\bar{N} = \frac{Y\sum_f \phi}{\overline{\sigma_a\phi} + \lambda + \frac{V}{vT} + CD\beta A_T/v}$$

where

Y = the yield of Xe, atoms/fission,
$\sum_f\phi$ = the number of fissions per sec per cm^3 of fuel stream,
A_T = the surface area of the graphite, cm^2,
V = the circulating fuel stream volume in the primary system, cm^3,
T = the Xe removal cycle time, sec.

The total neutron losses to Xe, neutrons absorbed in Xe per neutron absorbed in fuel, is given by Eq. B-27.

$$A = \left(1 + \frac{A_g}{A_f}\right) f_{1,1}\, C_a\, \bar{N}\, \eta \qquad \text{(B-27)}$$

where

$f_{1,1}$ = the fuel stream volume fraction in the core,
C_a = the reaction rate coefficient, neutrons absorbed in Xe per Xe atoms per cm^3 per neutron born in the reactor,
η = the number of neutrons produced per neutron absorbed in fuel.

The parameter C_a is obtained from a multigroup diffusion equation calculation of the MSBR. This number is computed from Eq. B-28:

$$C_a = \int_{u=o}^{\infty} \int_{\substack{\text{reactor}\\ \text{volume}}} \sigma_a(u)\, \psi\,(\vec{r},u)\, d^3r\, du \qquad \text{(B-28)}$$

where

$\sigma_a(u)$ = the neutron absorption cross section of Xe at lethargy u, barns,
$\psi(\vec{r},u)$ = the neutron flux at position $\vec{r}$ per unit lethargy per neutron born per second in the reactor, $\frac{\text{neutron-cm}}{cm^3\text{-sec-neutron born/sec}}$.

Table B-2 is a list of the calculational data for solving Eq. B-27. This equation has been solved for a graphite having 10% accessible voids and a reactor power of 1180 Mw for diffusion coefficients of 10^{-5} and 10^{-7} cm^2/sec, and is plotted in Fig. B.3.3 as a function of Xe removal cycle time.

Table B-2

$Y = 0.06$ Xe atoms/fission	$v_2 = 1.6 \times 10^6$ cm^3
$\sum_f \phi = 0.2175 \times 10^{14}$ fissions/cm^3 sec	$A_1 = 0.584 \times 10^6$ cm^2
$\overline{\sigma_a \phi} = 3.32 \times 10^{-3}$ sec^{-1}	$A_2 = 0.828 \times 10^6$ cm^2
$\lambda = 0.209 \times 10^{-4}$ sec^{-1}	$A_T = 2.00 \times 10^6$ cm
$V = 7.51 \times 10^6$ cm^3	$a = 0.317$ cm

$$C_a = 0.312 \times 10^{-15} \frac{\text{absorptions per Xe atom/cm}^3}{\text{neutron born}}$$

3.5 Results and Conclusions

From Fig. B.3.3 it will be observed that neutron losses to Xe can be kept to less than 0.005 neutrons lost to Xe per neutron absorbed in fuel with a processing time of 55 seconds. This cycle time will require a processing rate of about 110 ft^3/sec, which does not seem unreasonable.

If the diffusion coefficient is as large as 10^{-5} cm^2/sec, the cycle time is no shorter than 23 sec, corresponding to a processing rate of about 20 ft^3/sec.

UNCLASSIFIED
ORNL-LR-DWG 56887

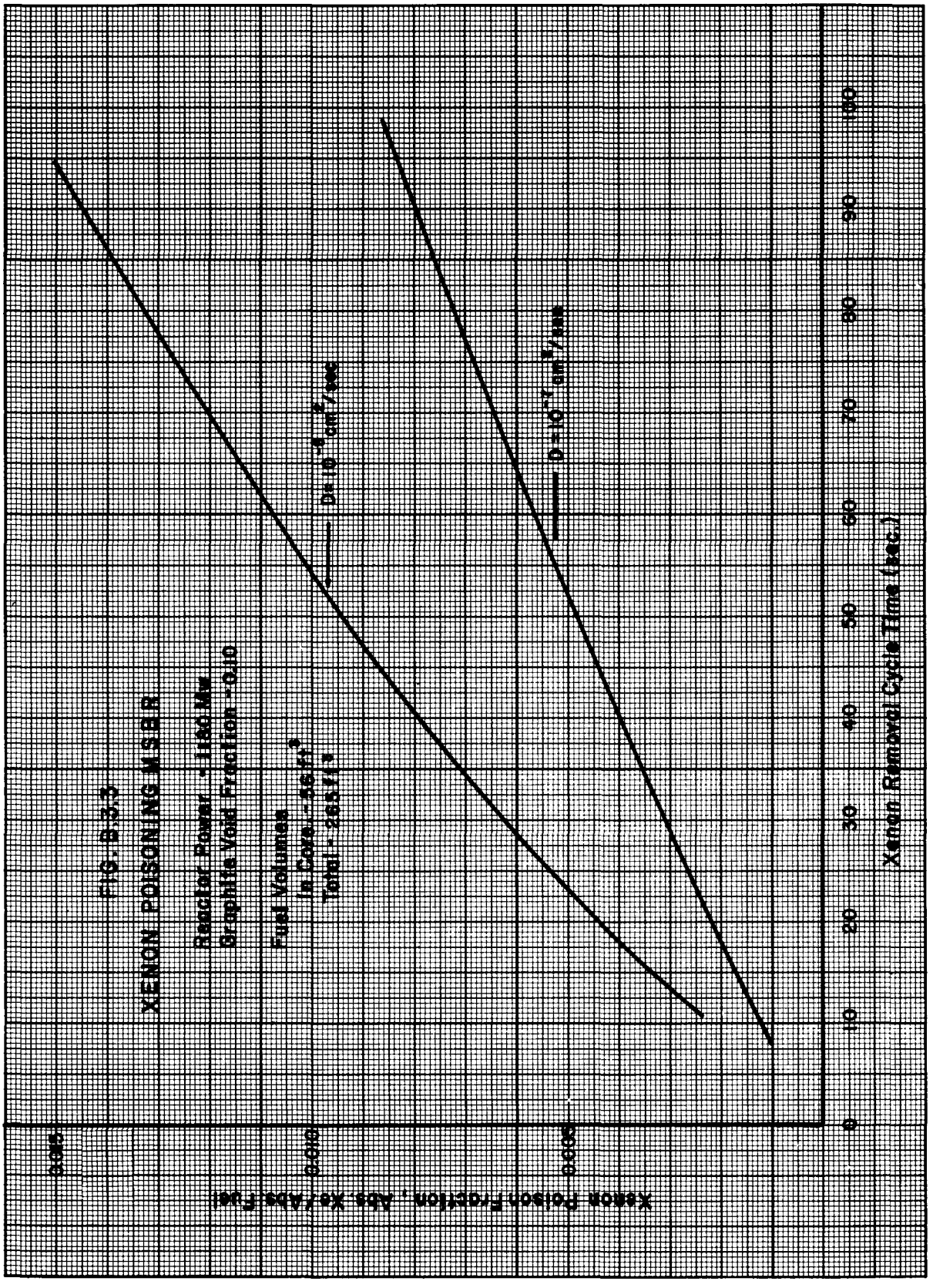

Nomenclature

A_1 = The mean area of graphite in the inner graphite tube, cm^2

A_2 = The inside area of the graphite in the outer graphite tube, cm^2

A_f = The neutron absorptions to Xe in the fuel stream

A_g = The neutron absorptions to Xe in the graphite

A_T = The wetted graphite surface area, cm^2

a = The thickness of the inner graphite fuel tube, cm

C = The ratio of Xe concentration in the graphite at the surface of the graphite-salt interface to the average concentration of Xe in the fuel stream

D = The diffusion coefficient of Xe in the graphite, cm^2/sec

D_e = The equivalent fuel tube diameter, cm
$D_e = 4A/Pw$ where A is the flow area, Pw is the wetted perimeter

D_{NS} = The diffusion coefficient of Xe in the fuel salt, cm^2/sec

F_g = The void volume fraction in the graphite

$f_{l,l}$ = The fuel streams volume fraction in the reactor core

G = The fuel mass flow rate per unit of flow area, $gm/cm^2/sec$

J = The net diffusion current of Xe, $atoms/cm^2\text{-}sec$

J_o = The diffusion of Xe into the graphite at the graphite-salt interface, $atoms/cm^2\text{-}sec$

J_{in} = The diffusion current of Xe into volume element $A\Delta x$, $atoms/cm^2\text{-}sec$

J_{out} = The diffusion current of Xe and of volume element $A\Delta x$, $atoms/cm^2\text{-}sec$

N(x) = The Xe concentration in the graphite at position x, $atoms/cm^3$

$\overline{N}$ = The average concentration of Xe in the fuel stream, $atoms/cm^3$

No,g = The concentration of Xe in the graphite at the graphite-salt interface, $atoms/cm^3$

Nomenclature (Continued)

$N_{o,s}$ = The concentration of Xe in the salt at the graphite-salt interface atoms/cm^3

$P(N)$ = The partial pressure of Xe in the graphite, atmospheres

R = The universal gas constant, atmosphere/^oK - $\frac{atom}{cm^3}$

T = The Xe removal cycle time, seconds

t = Time, sec

V = The fuel stream circulating volume, cm^3

v = The fuel stream volume in the reactor core, cm^3

Y = The number of Xe atoms produced per fission, atoms/fission

$\beta = \left[\frac{\overline{\sigma_a \phi} + \lambda}{D}\right]^{1/2}$, cm^{-1}

η = The number of neutrons produced per neutron absorbed in fuel

λ = The Xe decay coefficient, sec^{-1}

μ = The coefficient of viscosity for fused salt, gm/sec-cm

ρ = The density of molten salt, gm/cm^3

$\sigma_a(u)$ = The neutron absorption cross section for Xe at lethargy u, barns

$\overline{\sigma_a \phi}$ = The energy integrated Xe reaction coefficient, sec^{-1}

$\sum_f \phi$ = The number of fissions per cm^3 of fuel in the reactor core, fissions/cm^3

C_a = The reaction rate coefficient, neutrons absorbed in Xe per Xe atom per cm^3 per neutron born in the reactor

$\psi(\vec{r},u)$ = The neutron flux at position r per unit lethargy per neutron born per second in the reactor, $\frac{\text{neutron-cm}}{cm^3\text{-sec}\ \frac{\text{neutron born}}{^oK\ \text{sec}}}$

Θ = The reactor operating temperature, ^oK

4.0 Liquid Bismuth Breeder Reactor

The problems of maintaining low xenon poisoning in the LBBR are similar to those of the MSBR. Iodine is expected to exist in the form of iodides associated with other fission products or in an ionized state in which removal is probably quite difficult. Consequently it appears that gas removal is the most feasible method of purging xenon. The techniques should be almost exactly the same as those used in the MSBR. The solubility of xenon in liquid bismuth is of the same order of magnitude as its solubility in molten fluoride salts (66). There is insufficient data available to permit calculating xenon poisoning in the LBBR that would be different from that obtained for the MSBR. It appears reasonable to assume that xenon poisoning can be maintained at a tolerable level by adequate gas sparging.

Dwyer and Eshaya (66) report a few measurements on the behavior of iodine and xenon in irradiated fuel in contact with graphite capsules. Their results indicated that diffusion rates of xenon into graphite were somewhat higher than those of iodine, and that there was a tendency to collect at fuel-graphite and fuel-metal interfaces. In the LBBR, segregation at graphite-fuel interfaces could be very serious. However, segregation at metal-fuel interfaces would not be a problem since these surfaces are out of the fission zone. Xenon formed by decay on metal surfaces could quickly be removed by gas sparging; xenon formed on graphite surfaces might diffuse into the graphite and constitute considerable poison.

5.0 Heat Removal from Fission Gases

The heat removal from the beta decay of fission gases is a problem common to all reactors. Burch, et al (8) made calculations on the heat generation by fission gases for a 500 Mwt reactor, and their results are plotted as heat generation rate versus decay period in Fig. B.5.1

Since the beta decay heat-release rate decreases rapidly, it appears that the most practical processing method is to hold the fission gases about two days in a decay tank before passing them through the charcoal beds. The decay tank could be a water-cooled vessel having heat transfer properties superior to charcoal. Since charcoal is not a good heat conductor, it is

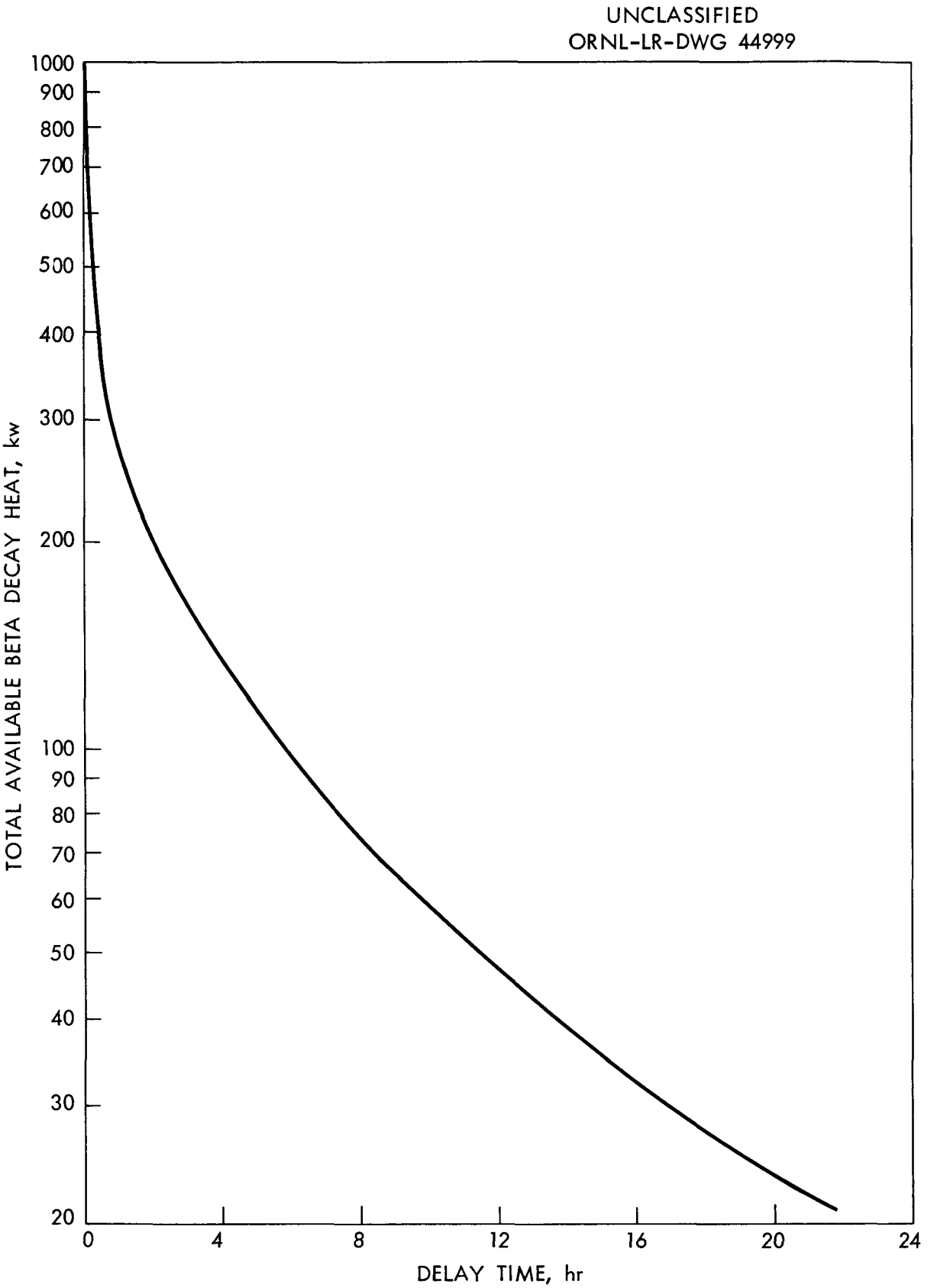

Fig. B.5.1. Fission gas beta decay heat vs delay time for 500 mw reactor.

desirable to maintain a low heat release rate at that point so the charcoal cross section to gas flow can be large. Even under favorable heat release conditions, charcoal has to be packed in relatively small diameter tubes. For example, for this 500 Mwt system, Burch calculates a bed consisting of approximately 4000 ft of 1/2-in. tubing, 9200 ft of 1-in. tubing, 5200 ft of 1-1/2-in. tubing, and 6800 ft of 2-in. tubing. The several sections would be tandem in the enumerated order.

APPENDIX C

Chemical Reprocessing Methods and Cost Bases

3.0 (Continued)

APPENDIX C

Chemical Reprocessing Methods and Cost Bases

The five breeder reactors investigated in this study require three basically different chemical processes in their fuel and fertile stream processing operations, viz., fluoride volatility plus aqueous fluoride dissolution, solvent extraction from aqueous nitrate solution, and fused salt extraction plus zinc slagging. The type of process that is used is peculiar to the chemical and physical nature of the individual fuel or fertile stream, and in some cases two different processes might have to be used for the same reactor. Furthermore, the physical nature of the fuel or fertile material requires in some cases that special and often complex head-end treatments be applied to prepare irradiated material for the principal recovery operations. These head-end treatments are necessary to convert material to the required chemical state and can contribute appreciably to the processing cost. The several processes are in various states of development from that of a demonstrated operation on a pilot plant scale (e.g., solvent extraction by the Thorex process) to a laboratory operation as is the case for fused salt extraction.

Processing operations for each of the breeder reactors in this study is described below; a summary of the operations is given in Table C.1.1. Cost data for the several processes have been obtained from the most recent studies and operational experience. In instances where no cost figures were available, estimates were made.

1.0 Aqueous Homogeneous Breeder Reactor

Fuel Stream Processing. - Three distinct operations are required in processing the fuel stream of the AHBR in order to keep neutron poisons at a tolerable level: solid-liquid separation in a hydroclone, peroxide precipitation, and fission gas sparging. Each of these operations is designed to remove a specific poison or group of poisons (see Fig. 5.1.2).

Table C.1.1. Chemical Processing Methods for Five Thorium Breeder Reactors

Reactor	Fuel Stream		Fertile Stream	
	Process	State of Development	Process	State of Development
AHBR	FP + corrosion product solids removal by hydroclone; Ni removal by D_2O_2 precipitation; residual U from above steps processed with fertile stream	Demonstrated in HRE-2; Bench scale	Thorex	Pilot plant
MSBR	Fluoride volatility for U recovery; HF dissolution for rare earth removal plus salt discard to remove soluble FP's	Pilot plant Laboratory	Fluoride volatility for U recovery; Salt discard for FP removal	Pilot plant
LBBR	Salt extraction plus zinc slagging	Laboratory	Special head-end to separate ThO_2 from Bi plus modified Thorex	Head-end in laboratory state; Thorex demonstrated in pilot plant
GGBR and DGBR	Special head-end to leach U from graphite plus Thorex	Head-end in laboratory state; Thorex in pilot plant	Thorex	Pilot plant

Hydroclone Operation. - Under AHBR operating conditions (~ 280°C) certain of the fission products, notably the rare earths, plus Fe and Cr corrosion products form insoluble oxides which can be removed by centrifugal force in a hydroclone. A small stream of fuel solution is removed continusouly from the circulating fuel stream, passes through the hydroclone, and returned to the primary fuel loop. The circulating rate is such that the entire fuel volume is processed several times each hour. The main circulating pump supplies the pressure drop required by the hydroclone. Solids separated by the hydroclone are collected over a specified operation period, which might vary from one to three days, after which time the hydroclone system is isolated from the reactor and the contents drained to the next processing step.

The solids are dissolved in 10.8 m H_2SO_4, stored for 90 days to allow fission products to decay, and processed in the Thorex plant for uranium recovery. This stream might be processed separately or concurrently with the fertile stream depending on the type of product that is desired for sales. It is estimated that the solids will be about 10 wt % uranium. The storage period is necessary to decrease the amount of activity in the Thorex plant where solvent degradation from radiation damage can result in large uranium and solvent losses.

Peroxide Precipitation. - Soluble fission products as well as nickel and manganese from stainless steel corrosion are removed from the fuel stream by precipitating uranium as UO_4. A small side-stream of fuel solution is continuously withdrawn, held for seven days for fission product decay, and treated with D_2O_2 which precipitates UO_4. The process rate is governed by the allowable nickel concentration in the fuel stream, nickel being the principal neutron poison removed by this process. A permissible nickel poison level as great as 0.0014 neutrons absorbed per fuel absorption was established as a compromise between increased inventory and processing charges on the one hand and neutron savings on the other. In this system the corrosion rate of type 347 stainless steel is 0.0003 in. per year at a specific area of 42.6 ft^2/Mwt core power; this leads to a processing rate of about 2400 liters/day per station and an equilibrium nickel concentration in the fuel of 0.00167 m. The corrosponding manganese concentration is 0.00025 m. At this concentration Mn contributed about 0.0004 to the poison fraction.

The fission and corrosion products in solution are allowed to cool for 90 days and then mixed with the fertile stream-feed to the Thorex plant for recovery of unprecipitated uranium. Fission and corrosion products are segregated in the main waste stream from the Thorex plant. The precipitate of UO_4, 3.6 kg U-233/day when the fuel concentration is 1.5 g U-233/liter, is dissolved in D_2SO_4 and returned directly to the core.

Xenon Control. - The largest single poison in the reactor is Xe-135, and its control is important enough that processes have been devised for its removal. Appendix B has been devoted to a discussion of these processes.

Higher breeding performance can be obtained in the AHBR if xenon control is accomplished by radiolytic gas-stripping rather than by the iodine removal process. It is not necessary to let down all of the radiolytic gas to reduce xenon poisoning to a tolerable level (see Fig. B.2.3); however, in this study it was assumed that all radiolytic gas would be let down making it unnecessary to add any copper catalyst to the fuel solution. Omitting the copper allowed an additional savings in neutrons because copper is an appreciable poison. Further benefit is obtained by utilizing the heat of $D_2 + \frac{1}{2} O_2$ recombination in a flame recombiner to superheat steam.

The 2000 psi curve of Fig. B.2.3 indicates that complete gas let-down should reduce xenon poisoning to about 0.0025 neutrons absorbed per absorption in fuel. In the AHBR however, a more conservative value of 0.005 was assumed to be the equilibrium xenon poisoning because it was felt that enough uncertainty in the behavior of xenon and iodine existed that perhaps the theoretical figure would be low. For example, the accumulation of iodine precursor on metal surfaces might be more serious than anticipated. Nevertheless, it was believed that in any case stripping would be effective enough to attain the 0.005 value in the fuel stream.

Approximately 8 ft^3/min at standard conditions of radiolytic gas are produced per thermal megawatt. This gas plus the fission gases and iodine are routed through a flame recombiner and then to a condenser. Condensed heavy water is pumped back into the reactor while the fission gases are vented to a charcoal adsorber for retention. Some of the iodine accompanying the stripping gas will almost certainly accompany the condensate back to the reactor, providing an additional reason for using a conservative figure for the equilibrium poisoning.

Fertile Stream Processing

The fertile stream of the AHBR consists of pellets of ThO_2 approximately 1/8 in. x 1/8 in. right cylinders. After a specified irradiation period, which was varied in this study, the pellets are discharged to the fertile stream processing plant for separation by solvent extraction of thorium and bred uranium from fission products and subsequent partition of thorium and uranium. The Thorex process, which has been demonstrated at ORNL, is used to process the fertile stream; feed rates are variable in the range 220-1060 kg Th/day, corresponding to fertile stream loadings of about 13-4 g (Pa + U-233)/kg Th.

As mentioned above, waste streams from the hydroclone and peroxide precipitation are also processed in the Thorex plant for residual uranium recovery.

ThO_2 Pellet Dissolution. - Pellets of ThO_2 are dissolved in HNO_3, and the resulting aqueous solution is stored for 10 days to permit fission products to decay. At this point the waste streams from fuel reprocessing may be added. The specification of 10-days cooling is an extrapolation of current Thorex technology which is based upon processing material that has been cooled 30 days or longer. The short-cooled material may be expected to create heat removal and solvent degradation problems in later process steps.

Dissolution produces large volumes of nitrogen oxides which contain radioactive fission gases such as I_2, Xe, and Kr. It will be necessary to pass the stream over $AgNO_3$ for I_2 removal and then through charcoal beds to capture Xe and Kr. Nitrogen oxides are absorbed in water generating nitric acid which is recycled to the dissolution steps.

Solvent Extraction. - The aqueous solution of Th, U, Pa, fission product, and corrosion product nitrates is contacted in a solvent extraction column with tributyl phosphate which extracts thorium and uranium leaving all other components in the aqeuous phase. Thorium and uranium are partitioned in additional solvent extraction-stripping operations as diagrammed in Fig. C.1.1. The product of the extraction is aqueous solutions of $UO_2(NO_3)_2$ and $Th(NO_3)_4$. Meanwhile the aqueous waste stream of fission and corrosion products plus Pa-233 is held for 200 days to permit Pa to decay.

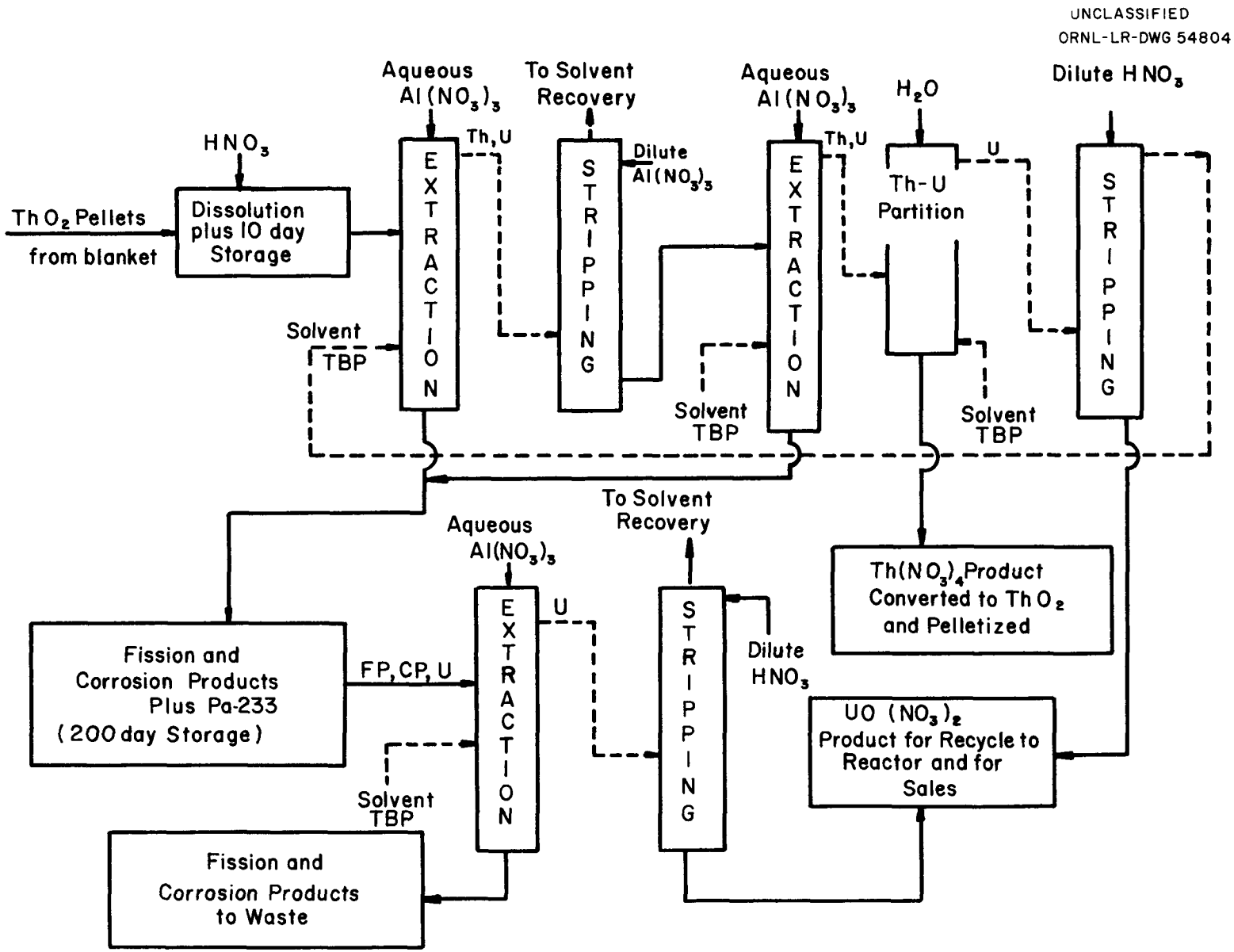

FIG. C.1.1 SCHEMATIC FLOW SHEET OF THOREX PROCESS

Initially about 7-20% of the fertile material production is present as Pa in this stream; at the end of the storage period all but 0.64% of this Pa has decayed. It is not economical to hold the waste for longer periods to allow more decay since the cost of additional tanks is more than the value of the additional uranium. The waste solution is recycled through a solvent extraction step to recover uranium.

ThO_2 and UO_2SO_4 Preparation. - The products of the Thorex plant are aqueous nitrate solutions of thorium and uranium. Thorium is converted to the oxide by oxalate precipitation plus firing, and the ThO_2 is then pelletized. Uranium is converted to the oxide and dissolved in heavy sulfuric acid. Thorium oxide is recycled to the blanket for additional irradiation; uranyl sulfate is recycled to the reactor core while the excess production is sold.

Although the processing steps shown in Fig. C.1.1 produce thorium and uranium products that are sufficiently decontaminated from fission products that activity from this source is not a problem in direct handling, activity from heavy isotopes, particularly U-232 and Th-228, will make it necessary to handle the products remotely. These nuclides accumulate and give off appreciable activity in thorium that has undergone long irradiation. The fuel reconstitution step is not made very difficult by a remote handling restriction since the operations are relatively simple; however, the pelletizing operation is rather severely hampered by this requirement because of the mechanical nature of the process.

Process Losses. - Based on pilot plant experience, it was assumed that uranium losses in chemical processing would be no greater than 0.03% of throughput. Thorium losses in such short-cooled processing have been taken at 2.5% (49) of the throughput. Protactinium losses depend upon the length of time that the Pa-233 is held for decay. A study (81) was conducted to optimize fissionable inventory in the processing system with regard to the number of Pa-233 decay and reprocessing cycles indicating that on this basis alone four or five cycles would be desirable. However the capital investment associated with larger extraction equipment and additional tankage could not be justified in terms of the savings on inventory. Nevertheless it was

necessary to retain Pa-233 for about eight half lives (200 days) to preclude excessive damage to the breeding gain. After this time 0.64% of the Pa-233 initially present is lost.

Thorex Plant Cost

Capital investment cost of the Thorex plant was based upon the work of Ferguson (7) which was later extended by Guthrie (49) to cover processing conditions encountered in this study. The basic study by Ferguson should be reasonably accurate since it was based upon advanced Thorex technology and considerable experience with the Thorex pilot plant at the Oak Ridge National Laboratory. For this current study, however, it was desirable to assume more stringent processing conditions than those employed in current Thorex processing cycles in order to take advantage of technological advances that might occur before breeder reactors are built. For example, it has been assumed that irradiated ThO_2 can be processed after 10 days cooling; whereas 30-day cooled material is the most radioactive that has been processed by current methods. No extrapolation was made in fuel stream processing, and the current practice of cooling irradiated fuel for 90 days was adopted. Furthermore, it was assumed that the small fuel streams, hydroclone underflow plus the waste stream from peroxide precipitation, could be blended with the fertile stream and processed without any additional investment in the Thorex plant over that required for the fertile stream alone.

The 10-day cooling period assigned to the irradiated fertile material enhances fuel yields and lowers inventory charges. However, as explained above, a large fraction (78%) of Pa-233 accompanying the fertile stream remains undecayed and is not recovered in the initial extraction. The fuel yield of the reactor would be seriously impaired if this Pa-233 were not recovered. This protactinium accompanies the fission product waste, and an additional 200-day storage is necessary to allow decay to uranium, which is recovered in a recycle step. The plant investment for this type of operation increases over that of a long-cooled, single-decay operation for several reasons, viz., increased off-gas disposal, increased analytical problems, increased solvent damage and cleanup, increased tankage for Pa-233 decay, and lower plant capacity due to the recycle operation. Guthrie (49) estimated that an increase of 20% in the investment over that of a plant for long-cooled, single-decay operation would suffice.

Further uncertainty in the chemical processing plant investment occurs in the charges made for the untested operations of converting the product of the Thorex plant into ThO_2 pellets. Because of the rapid turnover of the Thorex and refabrication cycles, the recovered thorium and uranium will be too radioactive from Th-228 and U-232 daughters respectively for direct handling; therefore remote refabrication techniques must be assumed for both fuel and fertile streams. Remote refabrication of the fluid fuel offers no problem; however, the pelletizing operation is more diffccult. If it were desired to have direct handling of thorium, it would be necessary to hold thorium for several years, perhaps four to ten years, to allow 1.9-year Th-228 to decay. This of course would create an intolerable thorium inventory and make it advisable to consider discarding thorium. The large inventory and storage problems prompted the choice of remote thorium refabrication for this study.

The cost figures upon which the investment in the Thorex plant is based were presented* in Table 4.A and Fig. 4.2.1 of Sec. 4.2.6. The accompanying discussion compares the values adopted for use in this study with those previously reported (145, 146). The upper curve of Fig. 4.2.1 was used for these cost estimates because it reflects the investment for operation with 10-day initial ThO_2 cooling and with recycle of extraction column raffinate after 200-day storage for Pa-233 decay. This curve includes the capital cost of dissolution equipment for ThO_2, Thorex solvent extraction equipment for thorium and uranium decontamination, solvent recovery equipment, conversion equipment for preparing ThO_2 from $Th(NO_3)_4$, and equipment for remotely fabricating ThO_2 pellets.

---

* This portion of this report is issued under separate cover but is identified by same ORNL memorandum number as this appendix.

2.0 Molten Salt Breeder Reactor

A flow diagram of the chemical reprocessing system for the MSBR is shown in Fig. C.2.1. The processing operation consists of three parts: fuel salt purification, uranium recovery from the fertile stream, and helium sparging to remove fission gases from the fuel salt.

Fuel Salt Purification

Fluoride Volatility. - A small, side-stream of fuel salt is removed from the main fuel-salt circulating loop and contacted with fluorine gas. Uranium hexafluoride is volatilized according to the reaction

$$UF_4 + F_2 \rightarrow UF_6 ,$$

which goes to completion leaving negligible uranium in the molten salt. The UF_6, which in addition to U-233 contains all of the higher isotopes of uranium, is burned in hydrogen, reducing the hexafluoride to the tetrafluoride. A portion of the UF_4 is routed to sales, the remainder is recycled to the reactor.

HF Dissolution. - Uranium-free salt flows from the fluorinator into a dissolver to which is added a 90% HF-10% H_2O solution. The salt and a number of the fission products are soluble in the acid; however, a number of the most serious neutron poisons, including principally the rare earths, are insoluble. These are removed by filtration.

The solution of salt and acid is evaporated for HF recovery, the salt being recrystallized. The soluble fission products, including mainly the alkali metals and alkaline earths such as Sr, Ba, Te, Se, Nb, Cd, Ag, Tc, etc., are removed by discarding a portion of the fuel salt on a prescribed cycle. The recovered salt plus make-up LiF-BeF_2 is fortified with UF_4 from spent-fuel cycle and the fertile-stream cycle and returned to the reactor.

Cycle Times. - Two cycle times are associated with the fuel cycle - that determined by the number of days it takes to process the total fuel stream volume and that determined by the number of days required to discard the fuel salt inventory. The first of these determines the poisoning due to the rare earths, and the second determines the poisoning due to the alkali metals and alkaline earths. Also it is apparent that a given poisoning can

UNCLASSIFIED
ORNL - LR - DWG 54768

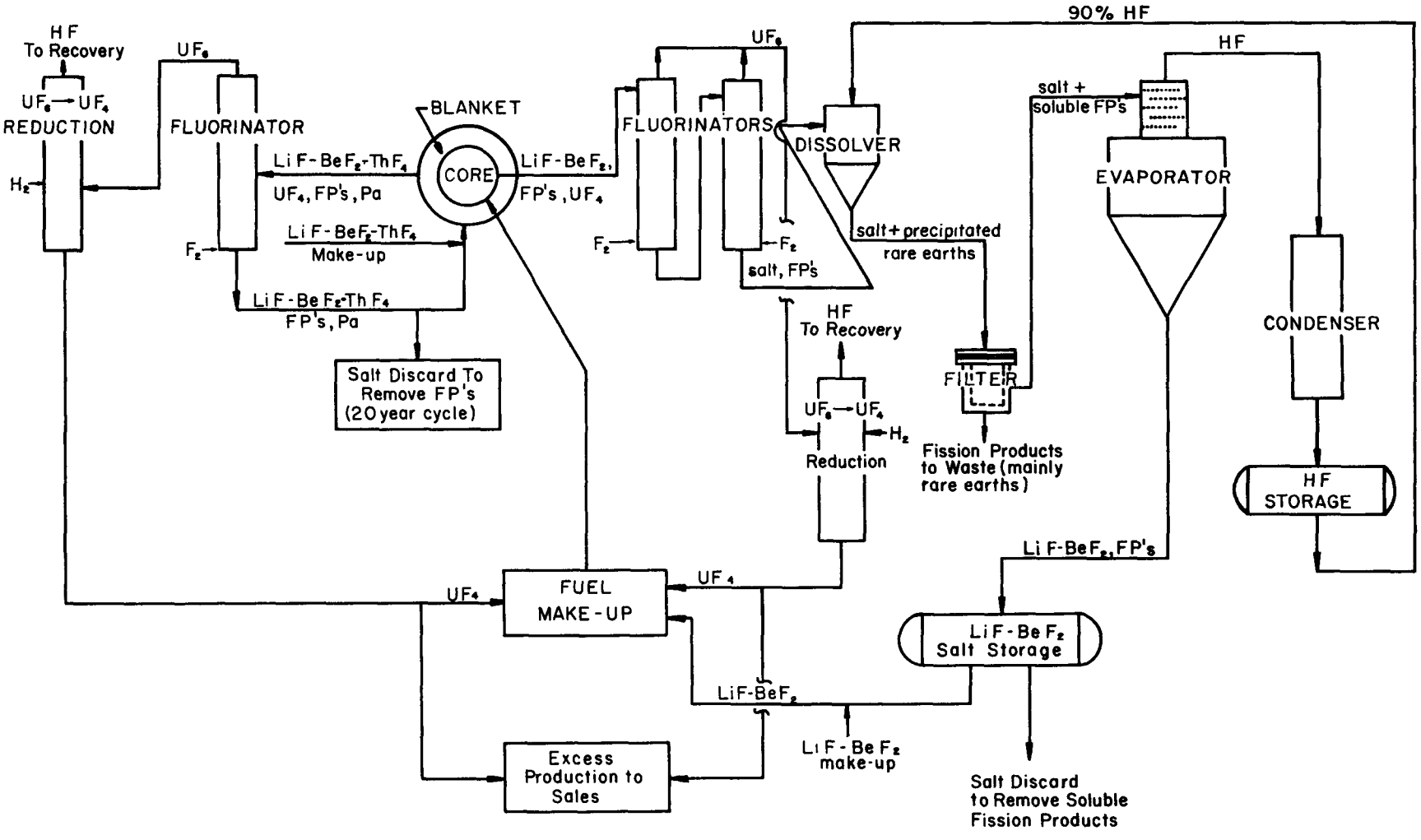

FIG. C.2.1 SCHEMATIC FLOW DIAGRAM OF MOLTEN SALT BREEDER REACTOR FUEL & FERTILE STREAM PROCESSING

occur for a number of combinations of these two cycle times. The fuel stream cycle time determines the size and hence the capital investment in the processing plant; the fuel-salt discard cycle determines the charge of replacement of the fuel-salt inventory. For a given, total fission product poison level, there is a combination of the two cycle times which gives the minimum cost. This optimization was made in this study so that all results are reported for optimum conditions.

Product Composition. - Four alternate methods are available for selecting the product that is diverted to sales: (1) spent fuel, (2) pure bred material, (3) feed mixture formed by mixing all recovered spent fuel and bred material, and (4) selected withdrawal of spent fuel and bred material to make the product isotopic composition the same as the overall system composition. The last alternate was chosen for these calculations because less ambiguity would exist in calculating the doubling time.

Fertile Stream Processing

Fluoride Volatility. - The fertile stream is processed in the fluoride volatility step only. Molten salt from the blanket circulating system is withdrawn at a specified rate and contacted with elemental fluorine. As in the fuel-stream cycle, UF_6 is volatilized and reduced to UF_4 with H_2. A portion of the UF_4 is diverted to sales, and the remainder is recycled to the reactor core with the recovered spent fuel.

In the MSBR at fertile-stream cycle times less than 100 days, fewer than 3.5% of the total fissions occurs in the fertile stream. Consequently, it is unnecessary to purify this stream in an HF dissolution step as was done for the fuel salt. The fission product concentration can be maintained at a sufficiently low level by periodically discarding a small portion of the salt and replacing with fresh make-up. In this study a 20-year replacement cycle was used.

It is observed that protactinium is not removed from the fertile salt in this process. Protactinium builds up in the blanket system until its decay rate is just equal to the rate at which U-233 is being removed. The effect of Pa-233 on the neutron economy is controlled by adjusting the volume of the fertile stream, larger volumes giving fewer neutrons losses to protactinium.

Process Losses. - The reaction of UF_4 and F_2 in the fluoride volatility steps is rapid and goes to completion so that there is no measurable loss of uranium. The only operation in which losses might occur is the reduction of UF_6 to UF_4 by hydrogen gas. If there is incomplete reaction at this point, uranium loss in the exhaust HF stream will occur. Uranium losses in the processing cycle were taken as equivalent to 0.0022 neutrons per neutron absorbed in fuel regardless of the processing rate, and the losses were assumed to occur entirely in the $UF_6 \rightarrow UF_4$ reduction step. Plant experience (61) in the reduction step has shown that this unit process can be carried out with almost arbitrarily small process loss. In fact losses are customarily smaller than random errors in sampling and analysis. Uranium losses no greater than 0.01% of throughput are considered attainable with a reasonable amount of operation care.

No allowance has been made for protactinium losses in processing. Protactinium could be lost if it were volatilized in the fluoride volatility step and suffered incomplete reduction in the subsequent operation. Laboratory and pilot plant data do not show any volatilization of protactinium.

Fission Gas Removal

Xenon-135 is such a serious neutron poison that in a breeder reactor special methods of control are necessary. In this system the fuel salt, perhaps the fertile salt also, is sparged with a stream of helium to purge fission gases. After removal the fission gases are adsorbed on charcoal and retained for decay. In summary these are the processing steps for controlling fission gas concentration; the subject has been treated in considerable detail in Appendix B.

Processing Plant Cost

Fuel Stream Processing. - The capital cost of the fuel stream processing plant was based upon a cost study by Weinrich (31), who estimated the capital charges for a plant to process continuously about 20 ft^3/day of fuel salt. A plant of this capacity is within the region of interest of this study. Weinrich's data were reviewed by Chemical Technology Division personnel* for

---

*W. G. Stockdale, D. O. Campbell, and W. L. Carter.

comparison with more recent cost data and cost estimating practices at Oak Ridge National Laboratory, and, as a result his data were adjusted upward. These data and the ORNL revised figures are presented in Table C.2.1. The ORNL estimate is approximately twice that of Weinrich. These estimates were made from functional flowsheets representing the best available design information on the fluoride volatility and HF dissolution processes.

In optimizing MSBR systems to obtain the most economic combination of fuel processing plant cost and fuel salt replacement cost, it was necessary to extrapolate the ORNL cost estimate in Table C.2.1 to both smaller and larger plants. The extrapolation was made by assuming that the capital cost is proportional to the 0.6 power of the processing rate. This method of extrapolating cost data has been found reasonably accurate when applied to the chemical industry as a whole and to plants which process nuclear reactor materials.

There is a limit, however, to the extrapolation in the region of low processing rates because at some low rate, which may not be well defined, it is economic to change from continuous to batch processing methods. In this study it was assumed that the lower limit of continuous processing would occur around 7 ft^3/day, which corresponds to a fuel cycle time of 75 days. (The fuel stream volume was constant at 530 ft^3.) When the fuel cycle time is 75 days, the extrapolated cost curve (Fig. C.2.2) indicates that the capital investment is about $5 million. Furthermore, it was felt that the investment in a batch plant would not be sensitive to further increases in the cycle time; consequently, the $5 million value was assumed to apply to all plants having cycle times greater than 75 days. A batch processing plant was estimated by Weinrich to cost $3.4 million; the above figure allows a premium of $1.5 million over Weinrich's estimate.

Fertile Stream Processing. - The fertile stream is processed only in a fluoride volatility step and therefore requires much less equipment than the accompanying fuel stream processing plant. Weinrich (31) included the fertile stream plant as an integral part of his fuel stream plant design and did not make a complete separate breakdown of the two costs. However it was possible to prepare a cost estimate for the fertile stream plant by

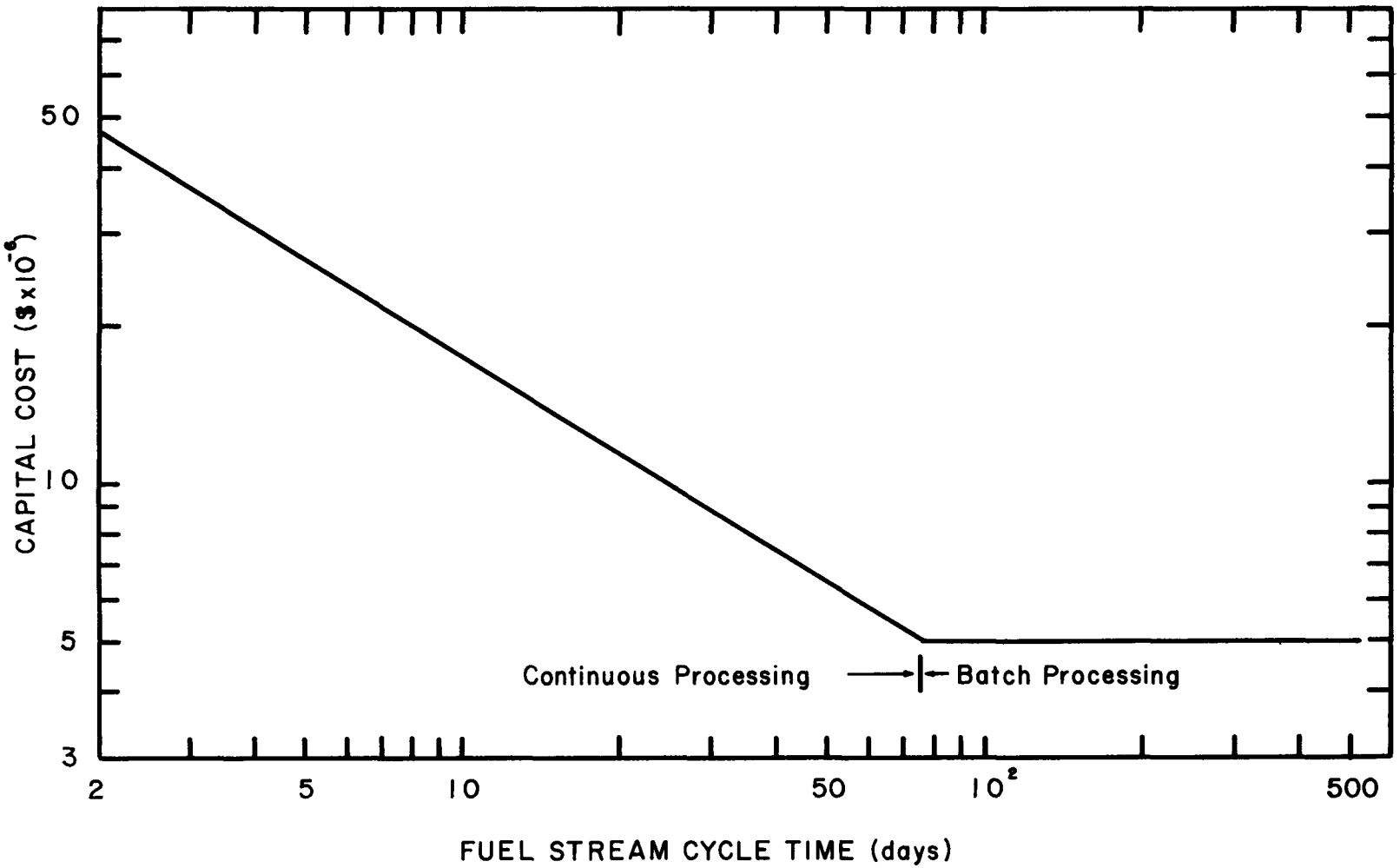

FIG. C.2.2 CAPITAL COST OF FUEL STREAM PROCESSING PLANT FOR A MOLTEN SALT BREEDER REACTOR

Table C.2.1. Cost Estimate of Facilities for Continuous Processing of Molten Salt Breeder Reactor Fuel Stream. Weinrich's Cost Estimate Compared with Revision made by ORNL

	Weinrich's Estimate ($)	ORNL Estimate ($)
Tanks and Vessels (Core Salt Section)		
Core salt hold tanks	19,500	39,000
Core salt fluorinators	16,500	33,000
UF_6 chemical traps	31,900	63,800
UF_4-UF_6 reduction tower	8,600	17,200
Vibrators, filters, burners, etc.	5,000	10,000
HF dissolving tank	24,000	48,000
HF evaporators	101,000	180,500
HF condensing tower	23,100	46,200
HF storage tank	41,300	82,600
KOH scrub tower	3,500	7,000
Miscellaneous storage and utility tanks	20,000	20,000
Sub-Total	294,400	547,300
Installed cost (=1.35 x cost)	397,440	738,800
Coolers (Core Salt Section)		
UF_6 gas coolers	3,600	3,600
Reduction tower vent cooler	3,000	3,000
HF vapor desuperheater	9,600	9,600
HF condensing tower vent cooler	6,000	6,000
Circulating HF cooler	48,000	48,000
Circulating H_2O chiller	2,400	2,400
Sub-Total	72,600	72,600
Installed cost (=1.10 x cost)	79,860	79,860
Vessels and Tanks (Blanket Salt Section)		
Blanket salt hold tanks	9,800	
Blanket salt fluorinator	5,500	Fertile stream
UF_6 chemical trap	3,600	processing esti-
Sub-Total	18,900	mated separately
Installed cost (=1.35 x cost)	25,500	

Table C.2.1. (Continued)

	Weinrich's Estimate ($)	ORNL Estimate ($)
Coolers (Blanket Salt Section)		
UF_6 cooler	2,400	
Installed cost (= 1.10 x cost)	2,640	
Miscellaneous Equipment		
Pumps	40,000	65,700
Agitators	6,000	6,000
Filters	20,000	30,000
Freon refrigeration system	160,000	160,000
Fuel reconstitution system	60,000	80,000
Electric heating furnaces	148,000	148,000
Pipe heating equipment	60,000	60,000
F_2 + H_2 gas supply systems	20,000	20,000
F_2 compressors	20,000	20,000
Sub-Total	534,000	589,700
Installed cost (= 1.35 x cost)	720,900	796,140
Sub-Total of installed cost of major equipment	1,226,300	1,614,800
Attendant Facilities		
Special instrumentation	76,000	76,000
General instrumentation	60,000	60,000
Panelboards and alarms	24,000	24,000
Sub-Total	160,000	160,000
Installed cost (= 1.40 x cost)	224,000	224,000
Piping, Painting, Scaffolds, etc., Installed Cost		
Special piping	4,500	4,500
General piping[a]	231,000	1,210,100
Equipment footings and foundations[b]	138,000	181,500
Pipe insulation	8,000	8,000

Table C.2.1 (Continued)

	Weinrich's Estimate ($)	ORNL Estimate ($)
Equipment insulation	20,000	20,000
Electrical distribution, lighting, etc.	144,000	144,000
Painting[c]	28,000	36,300
Remote operating equipment	75,000	75,000
Field testing and inspection	25,000	25,000
Operating and safety supplies	15,000	15,000
Freight[d]	37,000	48,400
Sub-Total	725,500	1,767,800
TOTAL INSTALLED COST	2,175,840	3,606,600
Contingency[e]	217,580	901,650
TOTAL DIRECT MATERIALS AND LABOR	2,393,400	4,508,300
Fees and Expenses		
Contractor's field expense[f,g]	119,670	2,254,150
Contractor's overhead fee[h,g]	359,010	
Engineering and design[i]	478,700	901,660
Purchasing and shop inspection[j]	119,700	225,400
Estimated Cost of Additional Facilities		
Sampling facilities		70,000
Ventilation		10,000
Waste removal		50,000
cells and buildings	1,500,000[k]	1,700,000
Laboratory		50,000
Mock-up cell		20,000
Crane		60,000
TOTAL ESTIMATED PLANT COST	4,970,500	9,849,500

Footnotes for Table C.2.1.

(a) Estimated by Weinrich as 25% of major equipment purchase price.
Estimated by ORNL as 100% of major equipment purchase price.

(b) Estimated as 15% of major equipment purchase price.

(c) Estimated as 3% of major equipment purchase price.

(d) Estimated as 4% of major equipment purchase price.

(e) Estimated by Weinrich as 10% of total installed cost.
Estimated by ORNL as 25% of total installed cost.

(f) Estimated by Weinrich as 5% of total direct materials and labor cost.

(g) Sum of contractor's field expense and overhead fee taken by ORNL as 50% of total direct materials and labor cost.

(h) Estimated by Weinrich as 15% of total direct materials and labor cost.

(i) Estimated as 20% of total direct materials and labor cost.

(j) Estimated as 5% of total direct materials and labor cost.

(k) Weinrich allowed $1,500,000 for additional facilities that might be shared with reactor operation.

extracting specific items from Weinrich's estimate and including allocations for instruments, buildings, etc. ORNL pricing procedures were applied to prepare the estimate given in Table C.2.2.

This tabulation presents values that are applicable to a plant processing fertile stream at a rate of 20 ft^3/day, the same basis upon which the fuel stream processing plant was designed. For this rate it was estimated that the capital investment would be about $1.8 million dollars. These values were plotted in Fig. C.2.3; the remainder of the graph was obtained by assuming the cost was proportional to the 0.6 power of the processing rate.

Table C.2.2.

Cost Estimate of Facilities for Continuous Processing
of Molten Salt Breeder Reactor Fertile Stream

	Estimated Cost ($)
Tanks and Vessels	
Salt hold tank	20,000
Fluorinator	20,000
UF_6 chemical traps	43,000
UF_6-UF_4 reduction towers	12,000
Vibrators	10,000
UF_6 gas coolers	3,600
Reduction tower vent cooler	3,000
Pumps	8,000
Filters	2,900
Agitators	6,000
Freon refrigeration	23,500
Bred material reconstitution	8,800
Electric heating furnaces	50,000
Pipe heaters	8,800
F_2 supply	2,900
F_2 compressor	2,900
Sub-total	225,400
Installed cost (= 1.35 x cost)	304,290
Attendent Facilities	
Special instruments	40,000
General instruments	30,000
Panelboards and alarms	15,000
Sub-total	85,000
Installed Cost (= 1.40 x cost)	119,000

Table C.2.2. (Continued)

Installed Cost of Piping, Insulation, Painting, etc.	Estimated Cost ($)
Special piping	3,000
General piping (= 100% of major equipment cost)	225,400
Equipment footings and foundations (= 15% of major equipment cost)	33,800
Pipe insulation	1,200
Equipment insulation	3,000
Electrical distribution	21,000
Painting (= 3% of major equipment cost)	6,800
Remote operating equipment	11,000
Field testing and inspection	3,700
Operating and safety supplies	2,200
Freight (= 4% of major equipment cost)	9,000
Sub-total	320,100
Total installed cost	743,400
Contingency (= 25% of total installed cost)	185,800
TOTAL DIRECT MATERIALS AND LABOR	929,200
Contractor's field expense and overhead (= 50% of total direct materials and labor)	464,600
Engineering and Design (= 20% of total direct materials and labor)	185,800
Purchasing and shop inspection (= 5% of total direct materials and labor)	46,500
Additional Facilities Shared with Fuel Salt Processing Facilities	
Sampling	10,300
Ventilation	1,500
Cells and buildings	100,000
Laboratory	7,400
Mock-up cell	2,900
TOTAL ESTIMATED PLANT COST	1,748,200

UNCLASSIFIED
ORNL-LR-DWG 54793

FIG. C.2.3 CAPITAL COST OF MSBR FERTILE STREAM PROCESSING PLANT

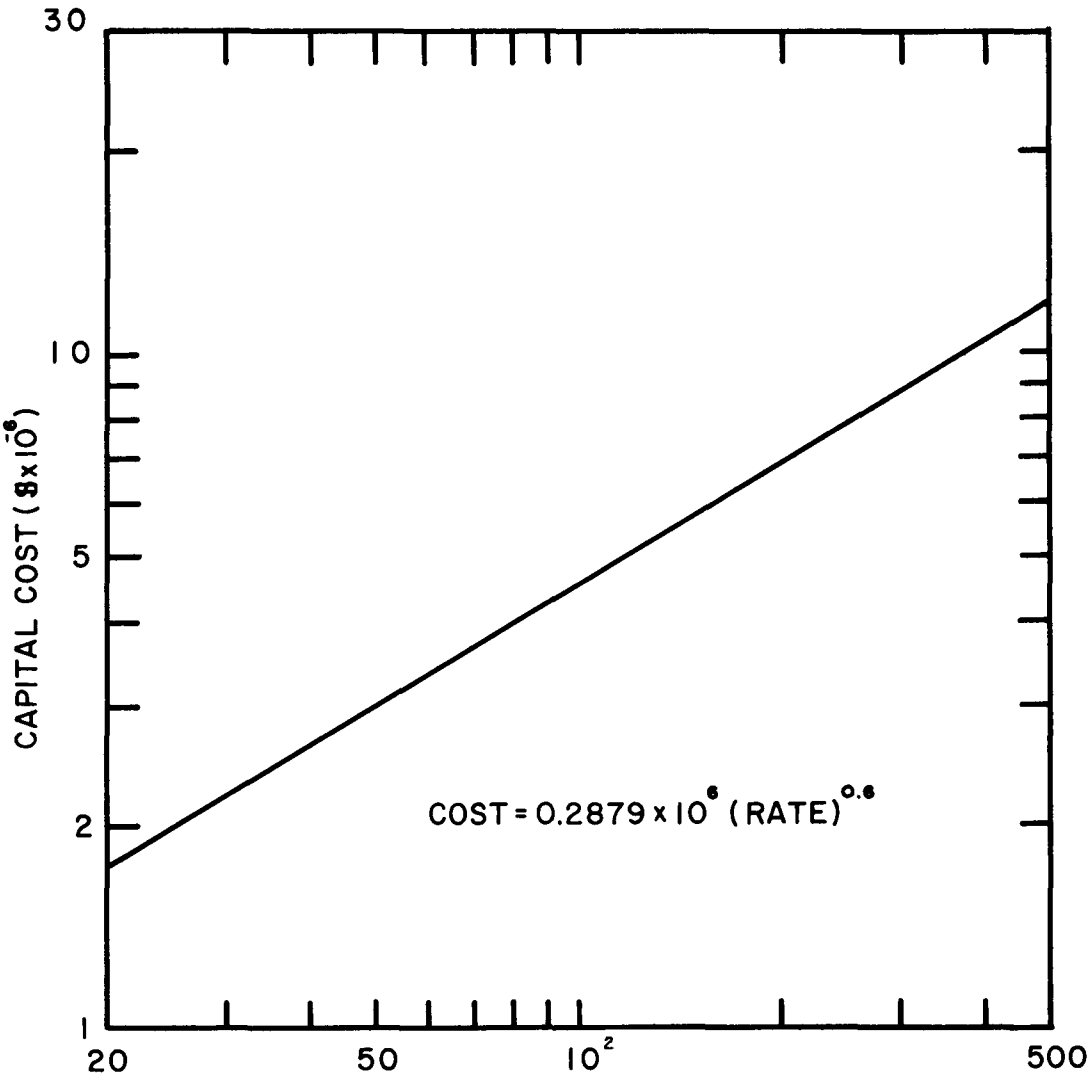

3.0 Liquid Bismuth Breeder Reactor

Four primary operations are associated with processing fuel and fertile streams of the LBBR. The fuel stream processing consists of fused salt extraction and zinc slagging processes for removal of FPS* and FPN** groups of fission products respectively. Fertile stream processing consists of an argon flotation process to separate ThO_2 from Bi-ThO_2 slurry and a modified Thorex process to recover bred uranium and thorium. The accompanying description of these processes and flow diagrams are abstracted from Babcock and Wilcox Company report BAW-1171, The Liquid Metal Thorium Breeder Reactor, by Thomas, et al (22).

Fuel Stream Processing

Fused Salt Extraction. - The FPS group of fission products is selectively removed from the spent fuel by being oxidized to chlorides with a fused salt mixture which is the ternary eutectic NaCl-KCl-$MgCl_2$ (m.p. = 396°C) containing $BiCl_3$. A side-stream of spent fuel flows through two extraction columns in series (see Fig. C.3.1) in which it is contacted with the fused salt. The salt flows concurrently with the fuel and enters the second column first. Temperatures in the extraction are maintained at 930°F, a value slightly above the solubility limit of uranium in bismuth. In column 2 zirconium and FPS are extracted along with some of the uranium. The uranium is recovered in the first column by operating it at reducing conditions. The proper oxidation-reduction conditions are maintained in two columns by controlling the $BiCl_3$ concentration in the salt fed to the second column.

Processed fuel leaves the second column and returns to the reactor. However, considerable magnesium, a fuel additive for inhibiting corrosion and increasing fuel stability, is extracted in the two columns; make-up magnesium is necessarily added to the recovered fuel.

---

* FPS = fission products which form compounds more stable than the corresponding uranium compounds.

** FPN = fission products which form compounds less stable than the corresponding uranium compounds. This group is subdivided into FNP-I characterized by being more stable than the corresponding Bi compound and FPN-II characterized by being less stable than the corresponding Bi compound.

Fig. C.3.1 Typical Fused Salt Process Flow Sheet for LBBR Fuel Stream Processing

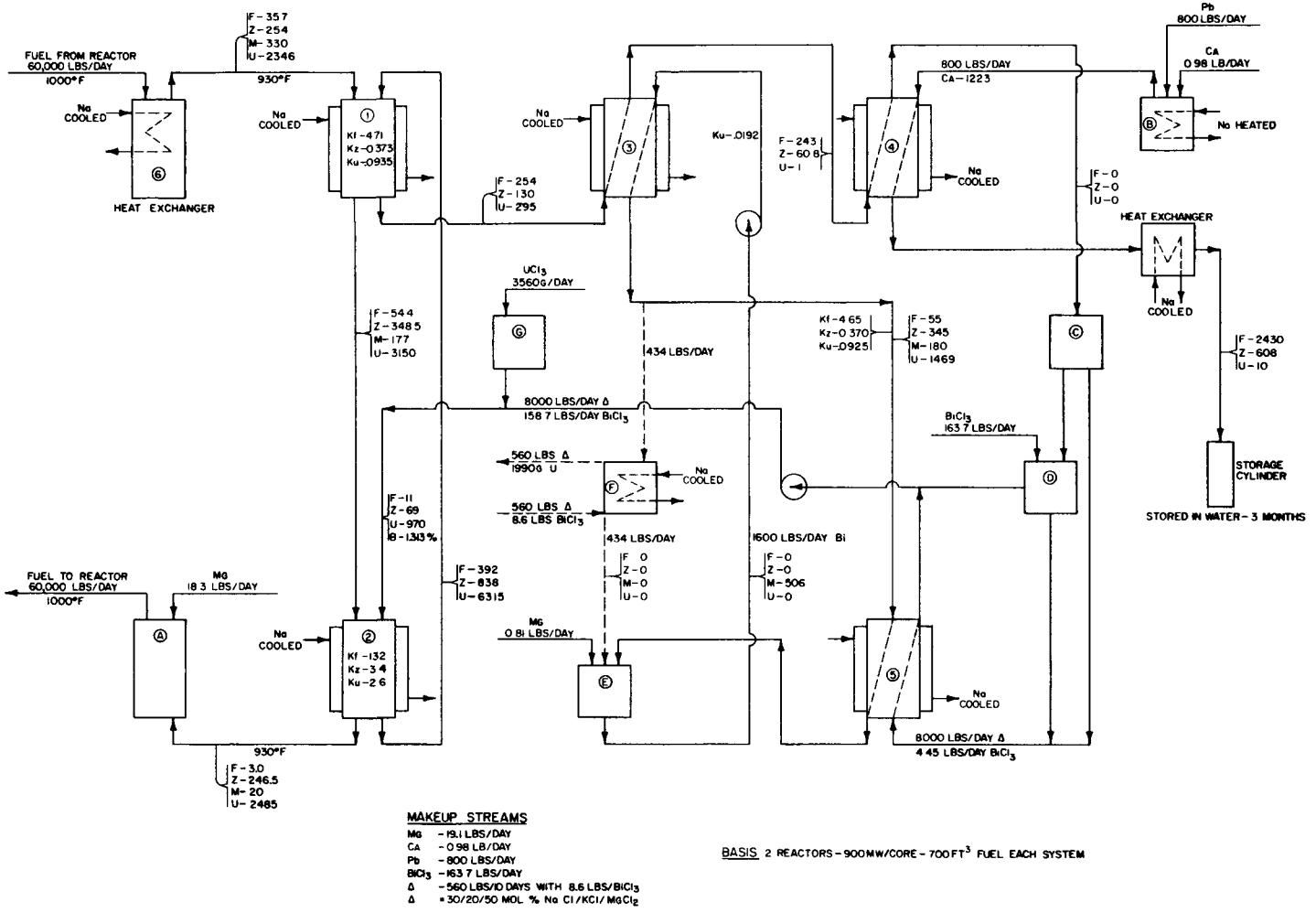

MAKEUP STREAMS

Mg	- 19.1 LBS/DAY
Ca	- 0 98 LB/DAY
Pb	- 800 LBS/DAY
$BiCl_3$	- 163 7 LBS/DAY
Δ	- 560 LBS/10 DAYS WITH 8.6 LBS/$BiCl_3$
Δ	= 30/20/50 MOL % Na Cl/KCl/$MgCl_2$

BASIS 2 REACTORS - 900 MW/CORE - 700 FT^3 FUEL EACH SYSTEM

Salt Recovery. - The remainder of the operations shown in Fig. C.3.1 are designed to recover the fused salt and its small uranium content while isolating the FPS fission products. Uranium is recovered in column 3 by scrubbing the salt with a Bi-Mg stream; at the same time most of the zirconium and a small amount of FPS are extracted. The Bi-Mg stream flows to column 5 in which a countercurrent fused NaCl-KCl-$MgCl_2$ stream extract almost completely the uranium, zirconium, and the few fission products. The fused salt then returns to column 2 to begin the sequence of operations again. The Bi-Mg stream cycles indefinitely between columns 3 and 5, picking up solutes from the outgoing salt in column 3 and delivering them to the incoming salt in column 5. Column 3 operates under reducing conditions, Mg being the reductant; column 5 operates under oxidizing conditions, $BiCl_3$ being the oxidant.

The fused salt leaving column 3 carries the bulk of the FPS, some zirconium, and the non-recoverable uranium. The salt flows to column 4 in which a stream of molten Pb-Ca extracts the FPS, zirconium, and uranium. The salt is thus pruified and returns to the process to begin the cycle again via columns 5 and 2. The FPS and zirconium are concentrated in the Pb-Ca mixture to about 10 times their concentration in the salt and stored for decay.

Mo, Ru, Rh, and Te Removal. - These four fission products are members of the FPN group, and their solubilities in bismuth are so low (estimated at 1-5 ppm at 400°C) that they can be precipitated on a cold surface. It is proposed to circulate continuously a sidestream of fuel solution over a "cold finger" so constructed that it can conveniently be removed. The four fission products deposit on the cold surface. The surface temperature must be kept below the lowest system temperature which is 1000°F but not so low that uranium will precipitate. The flow rate provides a complete turnover of the fuel volume every 24 hours.

Zn Slagging. - The remainder of the FPN group is removed in a batch-operated zinc slagging operation. Approximately 220 gal/week of fuel solution is withdrawn (see Fig. C.3.2) and treated with a ternary eutectic of NaCl-KCl-$MgCl_2$ to which has been added just enough Bi as $BiCl_3$ to oxidize uranium. The salt extracts the uranium, zirconium, and the FPS. The fuel

Fig. C.3.2 Zinc Slagging Process Flow Sheet for FPN Removal from LBBR Fuel Stream

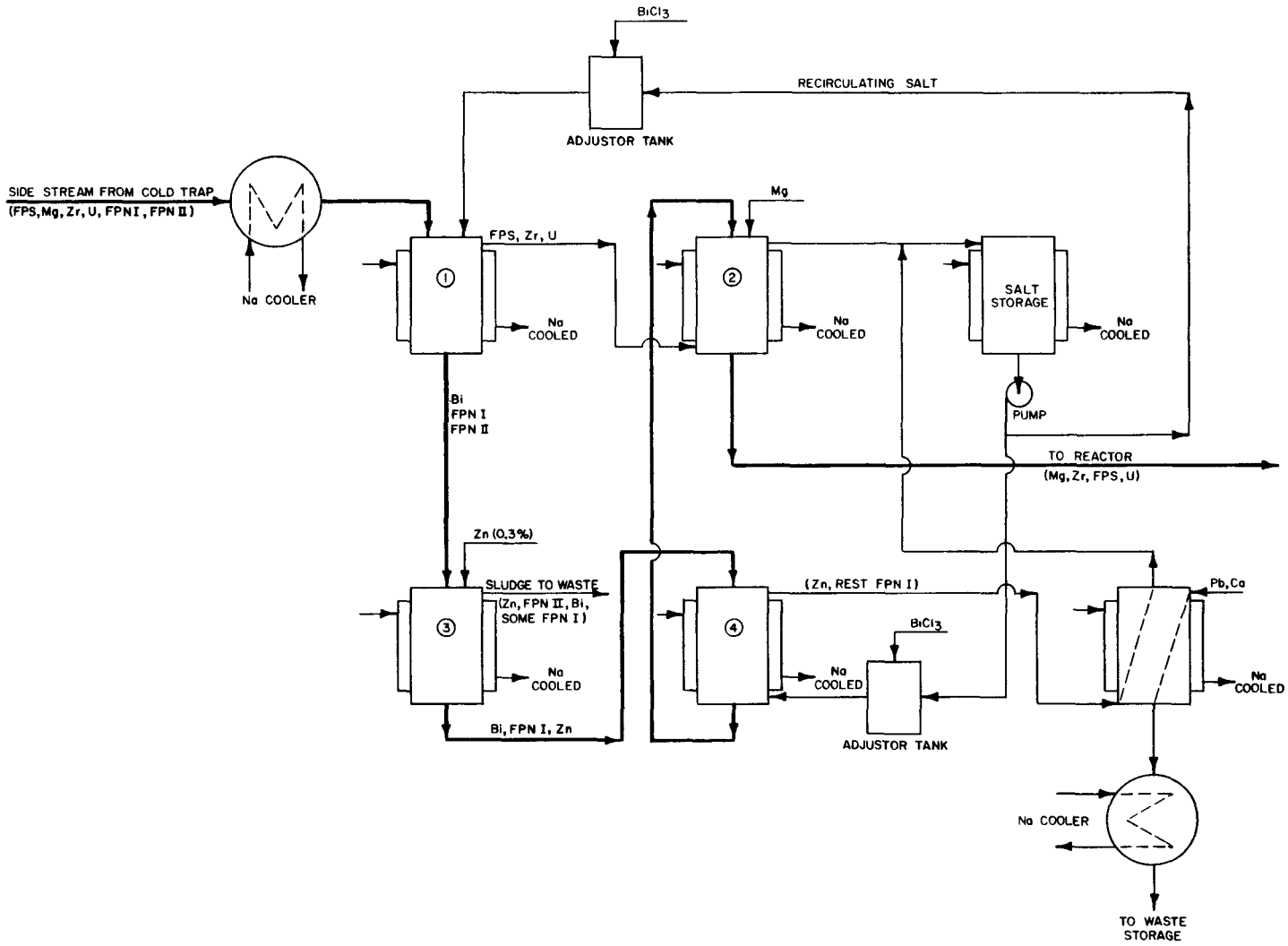

stream flows to the slagging vessel where it is mixed with molten Zn. Upon cooling to around 570°F, the FPN elements (especially the FPN-II) form intermetallic compounds with Zn and float as a slag on top of the bismuth. The slag is discarded to waste.

Bismuth, zinc, and most of the FPN-I elements flow to an oxidizing vessel where contact with $BiCl_3$ in the ternary molten salt ozidizes FPN-I and Zn and removes them from bismuth. The stripped bismuth then flows to vessel 2 where it is contacted with salt from vessel 1. Enough magnesium is added to transfer all of the uranium and most of the zirconium to the bismuth. Before the bismuth is returned to the reactor, its magnesium, chromium, and iron content may be brought up to reactor levels.

The molten salt which has been used to isolate the FPN-I group is cleaned by contact with a Pb-Ca mixture as described above. Lead, containing the fission products, is stored for decay. The recovered salt cycles through the process again.

Process Losses. - No large-scale operating data on the fuel stream process from which process losses can be computed are available. However, based on laboratory and bench-scale results as reported in BAW-1171 (22), it has been assumed that uranium and protactinium losses in both fuel and fertile stream processing would correspond to a neutron loss of 0.0032 neutrons per neutron absorbed in fuel.

Fertile Stream Processing

The fertile stream in the LBBR consists of a 12 wt % ThO_2 slurry in bismuth. The stream is irradiated in the blanket until the desired loading, i.e., Pa-233 + U-233 content, has been reached and is then processed for U, Pa, and Th recovery and their separation from fission products. The recovery is accomplished by a modified Thorex process after a special head-end treatment.

Head-End Treatment. - The head-end treatment consists of separating the ThO_2-Bi slurry as depicted by the flow sheet of Fig. C.3.3. The process stream is contacted with argon in a phase separator at 1000°F to float ThO_2 particles which are skimmed off in a manner similar to slagging operations in the metallurgical industry. Thorium oxide particles are assumed to carry approximately their

Fig. C.3.3 Head-End Process Flow Sheet for LBBR Fertile Stream Processing

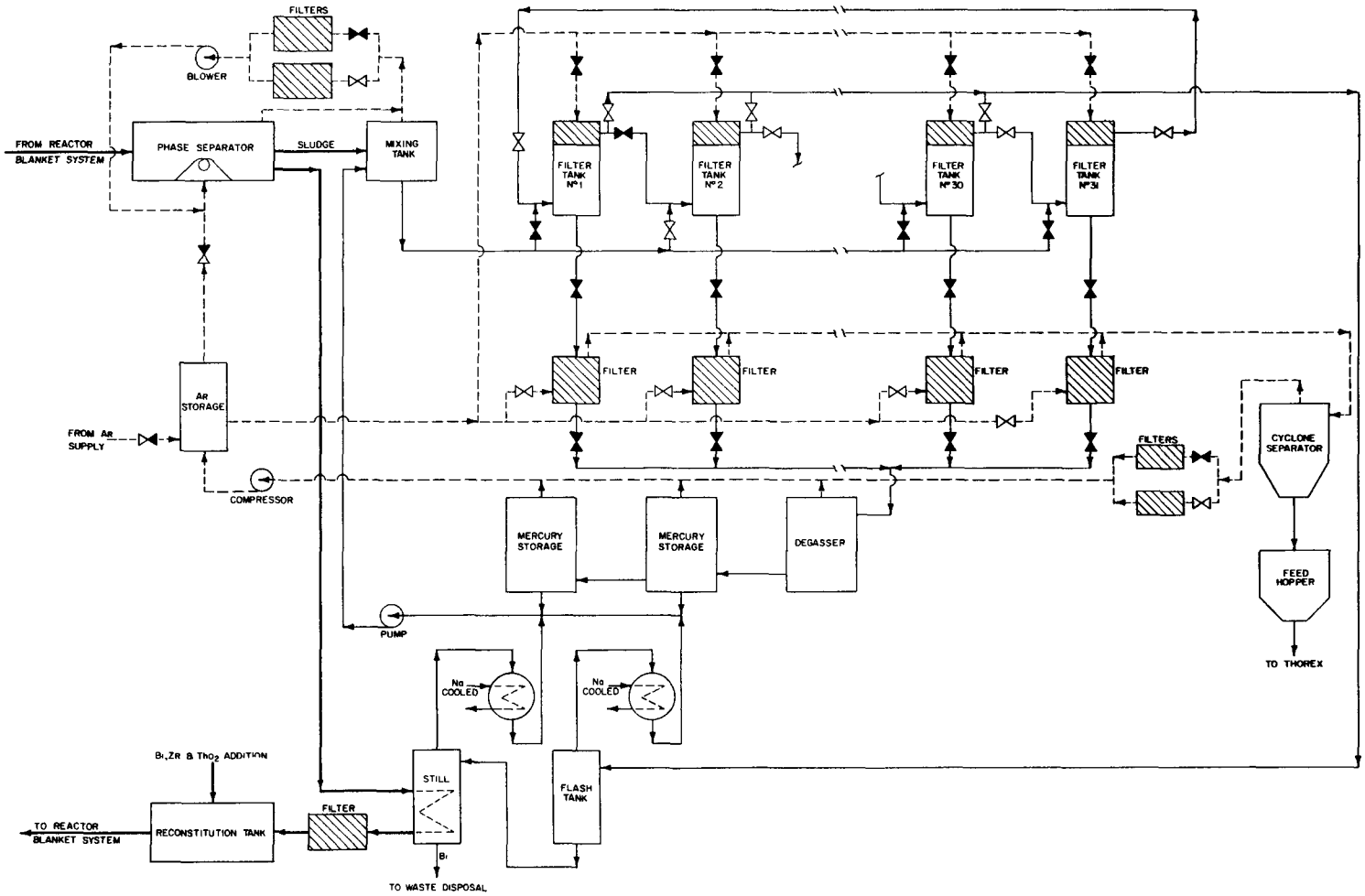

weight of bismuth. Argon is continuously recycled through filters for removing entrained particles.

The ThO_2-Bi sludge and "clean" bismuth stream leave the phase separator via different routes. Bismuth gives up some of its heat to operate the mercury still before being reconstituted with ThO_2 and make-up Bi preceding its recycle to the blanket system. Zirconium is also added at this point to enhance corrosion resistance.

The sludge is washed with mercury to dissolve bismuth and filtered. Each filter is designed to hold one day's accumulation of ThO_2, and while the cake is on the filter, mercury is circulated through it to remove fission product and Pa-233 decay heat. The filter vessel acts as the decay storage vessel and, since a 10-day storage is specified before Thorex, 11 filters are required. At the end of the storage period, the cake is blown off the filter with argon onto another filter which removes the last traces of mercury. Argon transport is again used to carry the ThO_2 powder to the feed system for the Thorex plant, the argon-ThO_2 separation being made in a cyclone separator.

The remaining operation in the head-end treatment is to recover bismuth from the circulating mercury stream. The mercury system operates at almost the saturation temperature of mercury at a pressure of 180 psia, the heat being supplied by the decay energy of fission products and Pa-233 in the filter cakes. The high-pressure, Hg-Bi solution is flashed in an evaporator to accomplish the primary separation. Most of the mercury is vaporized and returned to the system after condensation. Liquid bismuth containing the rest of the mercury is distilled; the still bottoms contain less than 1 ppm mercury. Recovered bismuth returns to the fertile stream circulating system.

The principal points of uncertainty in the process are: (1) the ability of liquid metal filters to stand up in the high temperature mercury service, (2) the economics of separating bismuth and mercury to the point where there is no danger of poisoning the reactor with mercury, and (3) the ability of ThO_2 particles to retain their integrity without sintering or fusing during the storage period.

Thorex Process. - The Thorex process used to decontaminate and recover uranium and thorium is almost identical to that described above for the AHBR, and the description will not be repeated here. Briefly, the process is as follows: Thorium dioxide powder from the head-end treatment is dissolved in concentrated nitric acid and contacted with tributyl phosphate (TBP) in a solvent extraction operation. In this way thorium and uranium are separated from fission products and protactinium. In subsequent solvent extraction steps, thorium and uranium are further decontaminated and partitioned from each other. The waste stream containing Pa-233 is held 200 days to allow Pa decay and recycled to solvent extraction to recover the uranium.

Thorium, which leaves the solvent extraction plant as $Th(NO_3)_4$, is converted to the oxide by oxalate precipitation and firing. After grinding to 10μ-size particles, ThO_2 is slurried in bismuth and recycled to the reactor blanket.

Uranium Reconstitution. - The uranium product of the Thorex plant is $UO_2(NO_3)_2$ in aqueous solution which must be converted to UCl_3 so it can be put into bismuth solution. The solution is denitrated in a continuously-operated, fluidized-bed denitrator of ever-safe geometry. The product is UO_3. The tri-oxide is dissolved in HCl and fed to an electrolytic cell. The electrolysis, carried out under a CO_2 atmosphere, reduces uranium to the trivalent state. The cell product is UCl_3 which is dried and returned to the fuel feed stream via the fused salt extraction system as shown in Fig. C.3.1.

Excess uranium production would probably be withdrawn as $UO_2(NO_3)_2$ at the end of the solvent extraction step or as UO_3 after the denitration step.

Process Losses. - As stated above it was assumed that uranium and protactinium losses from both fuel and fertile stream processing would correspond to no more than 0.0032 neutrons per neutron absorbed in fuel. Thorium losses from the Thorex system were assumed to be 2.5% of the throughput. This seemingly high loss was chosen because of the uncertainty of operating Thorex with such short-cooled material.

Fission Gas Removal

It is proposed to remove fission gases from the core and blanket systems by sparging with helium. The principal fission gas requiring removal is Xe-135 which, if allowed to accumulate, can destroy the breeding potential of the LBBR. Krypton is, of course, removed at the same time. The poisoning attributive to xenon as a function of sparging rate has been discussed in Appendix B. Fission gases are too radioactive for release to the atmosphere and must be retained on charcoal for decay.

Processing Plant Cost

Fuel Stream Processing Plant. - The capital charges of the fuel stream processing system have been estimated by Thomas, et al (22), and their value was used throughout this study. The fuel stream processing rate was not varied from the rate used by Thomas so that these charges remained constant. A value of $2.5x10^6 was assigned to the fuel processing cycle; this value corresponded to a 12-day cycle time.

A consideration of the details of the plant shows that the components are small in size and leads to the conclusion that the capital cost will be insensitive to changes in capacity. If this is true, there is little to be gained by increasing the processing cycle time because the unit cost, mills/kwhr, will remain the same while the neutron losses to fission products will increase, thus decreasing the breeding credit and the fuel yield. It was concluded that Thomas, et al, have rather well optimized the fuel stream processing rate, and therefore the rate and capital costs were not varied in this study.

Fertile Stream Processing Plant. - The estimate of Guthrie (49) was used to fix the cost of the Thorex plant. The basis of this estimate has been discussed above in the section dealing with the AHBR; capital cost versus capacity curves are given in Fig. 4.2.1. Guthrie's estimate did not include any charges for the special head-end treatment required by the LBBR. This portion of the plant was estimated from Thomas's data to cost $1.7x10^6, a figure that was applicable to the conditions of this study since processing rates were in the range estimated by Thomas. For the portions of the study in which the rates differed from those of the Babcock and Wilcox study, the

head-end process was still assumed to cost $1.7x10^6$. This assumption is partially justified by the fact that the head-end process cost is only about 10% the total fertile stream processing plant cost. It was further felt that the accuracy with which the initial estimate was made did not justify relatively minor refinements.

4.0 Graphite-Moderated, Gas-Cooled Breeder Reactor and Deuterium-Moderated, Gas-Cooled Breeder Reactor

The GGBR and DGBR have similar fuel and fertile streams, and similar processing methods may be used on the two streams. The basic process for both streams is the Thorex process. However irradiated fuel must be subjected to a head-end treatment to separate the graphite carrier and fuel portion of the fuel elements. Each of these reactors operates with solid fuel elements composed of UO_2 dispersed in a graphite matrix; irradiated GGBR elements are approximately 2 wt % uranium, and the DGBR elements are approximately 24 wt % uranium. In each case about two-thirds of the uranium is fissionable atoms.

The fertile stream for each reactor is ThO_2 pellets, 1/8 in. x 1/8 in. cylinders as described above for the AHBR.

Fuel Stream Processing

Three head-end processes have been investigated for the preparation of suitable Thorex feed solution from irradiated uranium-graphite fuels. These are (1) a burning process to destroy the graphite followed by HNO_3 dissolution of the residue, (2) grinding the fuel element to a fine mesh followed by a concentrated HNO_3 leach to dissolve uranium, and (3) direct disintegration of the solid fuel element by fuming HNO_3. All of these processes have been investigated on a laboratory scale by Bradley and Ferris (82, 83). The latter process appears to offer engineering advantages over the other two and for this reason is considered for processing the fuel elements of the GGBR and DGBR. Before processing, the fuel elements are held for 90 days to allow fission products to decay.

Head-End Treatment. - The head-end treatment consists of using 90% nitric acid as an intercalating agent to disintegrate the uranium-graphite fuel matrix and dissolve the uranium. When placed in boiling acid, the elements swell and crumble to a porous powder yielding their uranium content

to the acid. The slurry is then filtered and the residual graphite is washed with water to remove absorbed uranium-bearing solution (see flowsheet Fig. C.4.1). Over 90% of the uranium present is recovered in the first leaching; a second boiling nitric acid leach on the graphite residue recovers practically all of the remaining uranium. Since the fission products are soluble in nitric acid, they will accompany the filtrate and uranium in the wash solutions.

The leach solutions are about 21 m in HNO_3 (83); whereas, if large volumes of wash water are used, the wash solutions may be rather weakly acidic. Neither solution is exactly suitable for direct feed to the Thorex plant. Each solution is evaporated; the raffinates are then mixed and adjusted to Thorex feed composition which is 0.2-0.4 m acid deficient. Nitric acid is recovered in the evaporation and reused in subsequent leaches.

The efficiency of uranium recovery from the graphite depends upon the concentration of uranium in the graphite; this is shown in Fig. C.4.2 (83). Uranium recovery decreases with decreasing uranium concentration in the fuel. At concentrations greater than about 1.5 wt % U, recoveries of 99% or better are obtainable. However at uranium concentrations less than about 1.5 wt % U, the recovery decreases rapidly. Bradley and Ferris (83) suggest that in this range the fuel element be ignited to destroy the graphite followed by dissolution of the residue in nitric acid if extremely high uranium recovery is required. DGBR fuel elements, which contain about 24 wt % U at discharge, are well within the region of very efficient uranium recovery; on the other hand GGBR elements, containing only about 2 wt % U, are approaching the concentration range where the fuming nitric acid leaching process may not give the desired recovery.

Thorex Process. - The Thorex process employed for the GGBR and DGBR fuels is the same as described above for the AHBR. Briefly the following procedure would be followed: uranyl nitrate solution plus fission products from the head-end treatment is contacted with tributyl phosphate in a sequence of extraction and stripping operations to isolate uranium and fission products in separate streams. The same equipment used for processing the fertile stream can be used. Waste solutions of fission products are sent to permanent storage; some $UO_2(NO_3)_2$ is diverted to sales and the remainder is recycled to the core.

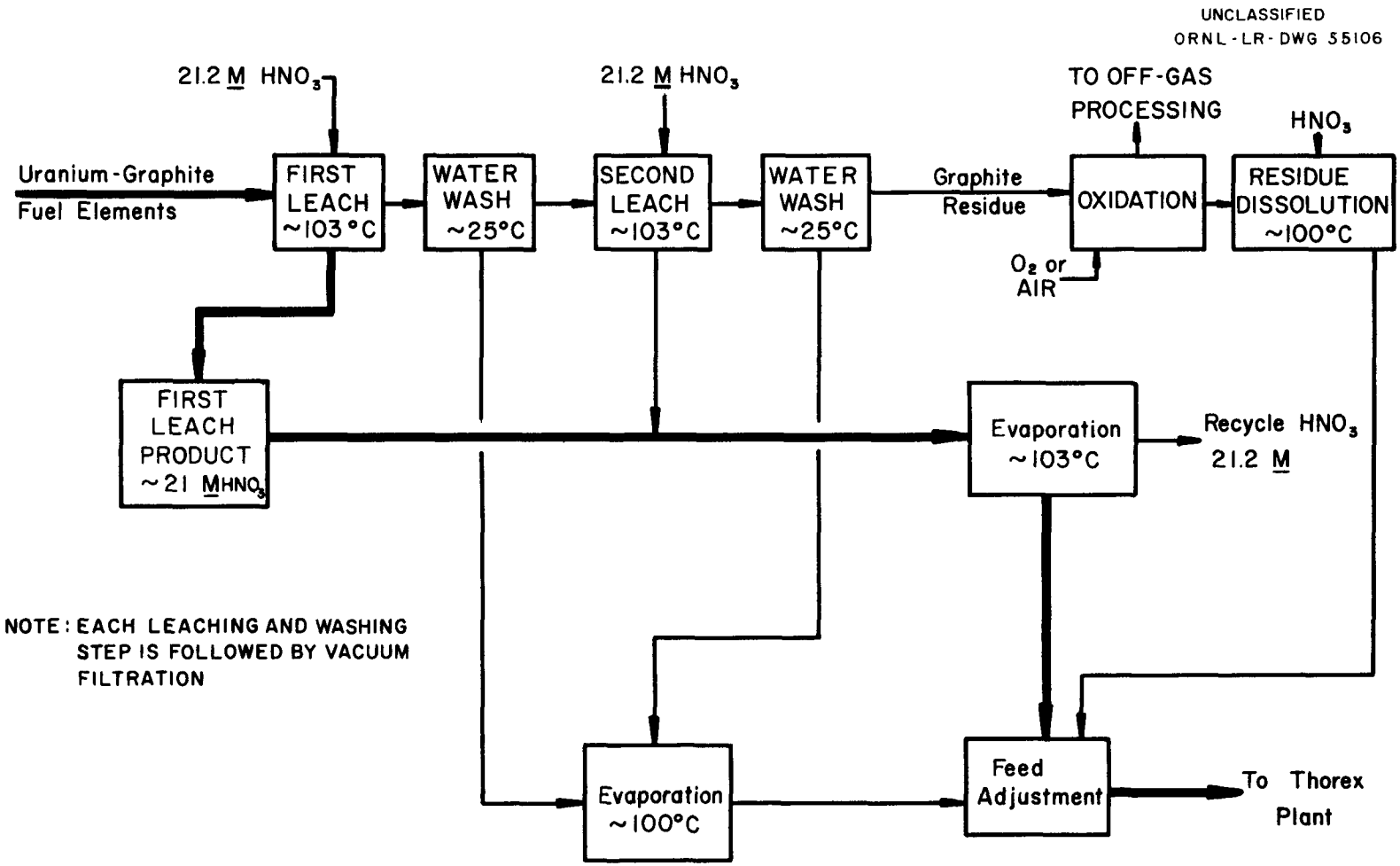

FIG. C.4.1 SCHEMATIC FLOW DIAGRAM FOR RECOVERING URANIUM FROM IRRADIATED URANIUM-GRAPHITE FUELS BY TREATMENT WITH FUMING NITRIC ACID.

(After Bradley and Ferris ORNL CF 60-3-65)

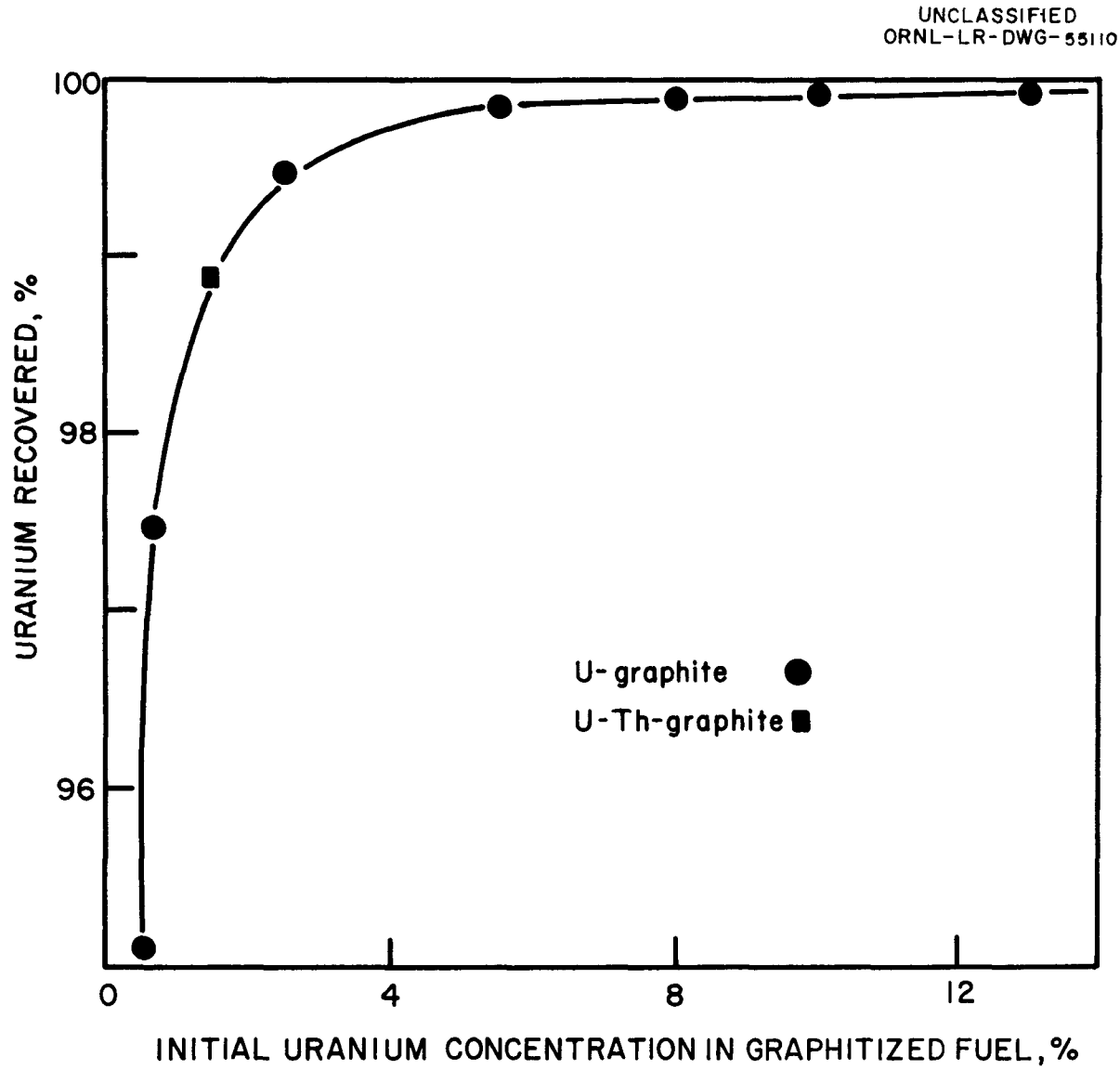

FIG: C.4.2 Efficiency of Uranium Recovery from Uranium-Graphite Fuels as a Function of Uranium Concentration. Leach Solution: 90% HNO_3

(After Bradley and Ferris ORNL CF 60-3-65)

Fuel Reconstitution. - New fuel elements are fabricated by soaking preformed graphite fuel plates, inserted in reusable graphite casings, in $UO_2(NO_3)_2$ solution made up of recovered spent fuel plus recovered bred material. After the desired uranium content is attained, the elements are fired at about 800°C to convert the nitrate to the oxide and then charged to the reactor. The reusable graphite casings are protected from the $UO_2(NO_3)_2$ solution during the soaking step by a coating of wax or other volatile compound that is vaporized during the firing step.

All operations in fuel refabrication must be performed remotely because of the activity from U-232 and its daughters.

Process Losses. - Loss of fissionable or potentially fissionable material occurs at three points in the processing cycle: (1) in the graphite residue or the residue after burning in the head-end treatment, (2) in the waste streams from the solvent extraction plant, and (3) as undecayed Pa-233 after the 200-day storage period. Based on laboratory data for mechanism 1 and on pilot plant experience for mechanism 2, it was assumed that no more than 0.1% of the product would be lost per pass of fuel through the processing plant for each of these mechanisms. Loss due to undecayed Pa-233 is 0.64% of the Pa-233 throughput.

Thorium losses in fertile stream processing for such short-cooled material have been taken as 2.5% of the throughput.

Fertile Stream Processing

The fertile streams of both the GGBR and the DGBR are ThO_2 pellets. In each case these pellets are dissolved in HNO_3, stored 10 days for cooling, and processed in a Thorex plant for recovery of uranium and thorium. The operations for these two reactors are identical to those discussed above for processing ThO_2 from the AHBR.

Fission Gas Treatment

There is no reliable method for predicting the amount of fission gas that will escape from a uranium-graphite fuel element under irradiation nor is there a method for processing these gases out of a fuel element while still in the reactor core. For these reasons it has been assumed in the nuclear calculations that all gases are retained within the fuel element and

build up to an equilibrium value. From the standpoint of neutron economy this is important only in the case of Xe-135. It is infeasible to chemically process fuel elements on a cycle short enough to reduce xenon below its burn-out concentration. In fact in order for xenon diffusion from the element into the circulating helium coolant to be an important factor in poison control, the mean diffusion time must be of the order of a few minutes. Experimental data will be necessary before the importance of diffusion can be evaluated. The circulating coolant gas can be processed for fission gas removal by withdrawing a side stream and passing it through charcoal beds. Xenon and krypton are adsorbed, and the helium is reclaimed. If iodine is present, contacting the gas stream with silver nitrate at an elevated temperature ($\sim 175^{o}C$) will effectively remove the iodine.

Off-Gas Treatment

Off-gases from the dissolution reactions in the head-end treatment and from fertile material dissolution contain oxides of nitrogen as well as fission gases and some iodine. Oxides of nitrogen can be recovered by absorption in water and the resulting acid reused. Iodine can be reacted with silver nitrate and held for decay. Xenon and krypton can be absorbed on charcoal and retained for decay. If the graphite residue of the head-end treatment has to be burned to recover uranium undissolved in the fuming HNO_3 dissolution, there will be large quantities of carbon dioxide to be processed. However at this point fission gas as well as iodine concentration should be quite small having been removed in the dissolution step. If this is the case, processing the CO_2 stream may not be a formidable problem. It might be sufficient to pass the CO_2 through an iodine trap and exhaust the remainder to the atmosphere through a tall stack. If it is necessary to retain the CO_2, absorption in hydrated lime may be used.

Processing Plant Cost

The bases upon which the cost of the Thorex plant were based have been presented above in the discussion of AHBR fertile stream processing in Sec. 4.2 of the body of this report and in Sec. 1.0 of this appendix. The same capital costs were used for the Thorex plant for the GGBR and the DGBR; these values as a function of processing rate have been presented in Fig. 4.2.1 and 4.2.2.

The investment in head-end treatment equipment, required for the GGBR and DGBR but not for the AHBR, is included in the upper curve of Fig. 4.2.1. Since there was considerable uncertainty in estimating the cost of head-end equipment, this equipment was assumed to cost the same as that for heavy water recovery in AHBR processing.

Fertile stream processing costs for the GGBR and DGBR are identical to that of the AHBR.

Capital investment in equipment for remote fabrication of uranium-graphite fuel elements is rather difficult to predict because of untested operations. The operations must be done remotely because of the activity associated with the presence of U-232 in the recycle stream. A "guesstimate" of the cost was prepared by Guthrie (49) based on a fabrication cost of $1.5 per gram of fissionable isotope in a plant having a capacity of 5 kg/day. This charge is about the same as current (1960) cost for fabricating MTR and APPR fuel elements. Guthrie states that "beryllia or prefabricated graphite shapes would be extra. To achieve these costs great technical advances would have to be made in fuel element design and fabrication technology. Based on current technology, the investment might be of the order of ten times that shown in" Fig. 4.2.3.

The costs given in Fig. 4.2.3 were used in this study for processing the fuel in the GGBR and DGBR. An additional allowance at the rate of $2 per pound for replacement of the graphite fuel plates was made.

A P P E N D I X D

Neutron Losses to Pa-233 in Batchwise Operated Blankets

A P P E N D I X D

Neutron Losses to Pa-233 in Batchwise Operated Blankets

1.0 Analysis of Batch-Operated Blanket

The equilibrium reactor program ERC-5 (86) computes the neutron losses to Pa-233 with the assumption that the blanket is continuously mixed so that the Pa-233 is uniformly distributed throughout the blanket system. The blanket of the AHBR is separated into three concentric rings, and each ring is divided into 20 sectors containing ThO_2 pellets. The pellets in each sector are shifted daily from one blanket ring to the next. This "batchwise" shifting results in neutron losses to Pa-233 which are greater than those predicted by ERC-5. This Appendix describes the analysis which was used to estimate the neutron losses to Pa-233 in the AHBR.

Time Dependent Differential Equation. - The time dependent differential equation for the concentration of Pa at radius r and time t is given by Eq. D-1.

$$\frac{dN_{13}(r,t)}{dt} = \int_u \sigma_{o2}(u)\ \phi(r,u)\ N_{o2}\ du - \int_u [\lambda + \sigma_{13}(u)\ \phi(r,u)]\ N_{13}(r,t)du \quad \text{(D-1)}$$

where:

$N_{13}(r,t)$ = the atomic concentration of Pa-233 at radius r and time t, atoms/cm^3,

$\sigma_{o2}(u)$ = the microscopic capture cross-section of thorium at lethargy u, cm^2,

$\phi(r,u)$ = the neutron flux at radius r per unit lethargy u, neutron-cm/cm^3-sec-unit lethargy,

N_{o2} = the concentration of thorium in the blanket, atoms/cm^3,

λ = the decay constant for Pa-233, sec^{-1},

$\sigma_{13}(u)$ = the microscopic absorption cross-section of Pa-233 at lethargy u, cm^2.

The relative neutron flux (n-cm/cm^3-neutron born) as a function of position and lethargy may be obtained by solving the group diffusion equations, and the absolute flux is readily obtained when the power is specified. The integration of the product of cross-section and flux over lethargy may then be immediately performed. This integration will hence forth be denoted as

$$\overline{\sigma\phi(r)} = \int_{u=o}^{\infty} \sigma(u)\ \phi\ (r,u)\ du\ .$$

Losses for Batchwise Mixing. - The initial condition for the blanket is that at the beginning of a cycle. The concentration of Pa-233 in a given ring is uniform and equal to the mean concentration of the same batch in the preceding ring at the end of the previous cycle, see Table D.1.1.

Table D.1.1. Initial Concentration

i	1	2	3
$N_{13}^{i}\ (t=0)$	$L \int_{r_3}^{r_3+\Delta r_3} \frac{N_{13}(r,t_R)\ 2\pi r dr}{V_3}$	$L \int_{r_1}^{r_1+\Delta r_1} \frac{N_{13}(r,t_R)\ 2\pi r dr}{V_1}$	$L \int_{r_2}^{r_2+\Delta r_2} \frac{N_{13}(r,t_R)\ 2\pi r dr}{V_2}$

where: t_R is the residence time in each ring, V is the volume of a ring, Δr is thickness of a given ring, and L is the length of the reactor.

Using these initial conditions, Eq. D-1 may now be integrated.

$$N_{13}(r,t) = \frac{\overline{\sigma_{o2}\phi(r)}N_{o2}}{\lambda+\overline{\sigma_{13}\phi\ (r)}} \left[1 - e^{-[\lambda+\overline{\sigma_{13}}\phi(r)]t}\right] + N_{13}^{i}\ (t=0)\ e^{-[\lambda+\overline{\sigma_{13}}\phi(r)]\ t} \qquad \text{(D-2)}$$

During the residence time, t_R, the losses to Pa-233 will be

$$C = L \int_{t=0}^{t=t_R} \int_{r_1}^{r_3+\Delta r_3} N_{13}(r,t)\ \overline{\sigma_{13}\ \phi}(r)\ 2\pi r dr\ dt\ . \qquad \text{(D-3)}$$

Losses for Continuous Mixing. - For continuous mixing, in the limit (i.e., infinite rate of mixing), $N_{13}(r,t)$ becomes independent of r. The equation of continuity then becomes

$$\frac{dN_{13}^*}{dt}(V_1+V_2+V_3) = \int \overline{\sigma_{o2}\phi(r)}\, N_{o2}\, 2\pi rLdr - \int (\lambda+\overline{\sigma_{13}\phi(r)})\, N_{13}^*\, 2\pi rLdr. \quad \text{(D-4)}$$

Where the star refers to the fact that N_{13} is uniform throughout the blanket. Since N_{13}^* is constant at equilibrium, $dN_{13}^*/dt=0$, and equation D-4 can be solved for N_{13}^*.

$$N_{13}^* = \frac{\int N_{o2}\, \overline{\sigma_{o2}\phi(r)}\, 2\pi rLdr}{\int (\lambda+\overline{\sigma_{13}\phi(r)})\, 2\pi rLdr} \quad \text{(D-5)}$$

During a time, t_R, the losses to Pa-233 for the case of continuous mixing become:

$$C^* = N_{13}^* \int_{t=0}^{t_R} \int_{r_1}^{r_3+\Delta r_3} \overline{\sigma_{13}\phi(r)}\, 2\pi Lrdr\, dt. \quad \text{(D-6)}$$

The quantity $\frac{C-C^*}{C^*}$ is the fractional increase of neutron losses to Pa-233 at finite residence times relative to the loss incurred with rapid continuous mixing. This fractional increase in neutron losses has been computed numerically using the IBM-704 program PLSB-1. The results are plotted in Fig. D.1.1 as a function of residence time in the blanket for the reactor described in Sec. 5.1, operating at a power level of 910 Mwt.

From Fig. D.1.1 it can be seen that the neutron losses to Pa-233 can be held to about 1% of the losses calculated by ERC-5 by shifting the thorium in the blanket from one ring to the next every third day.

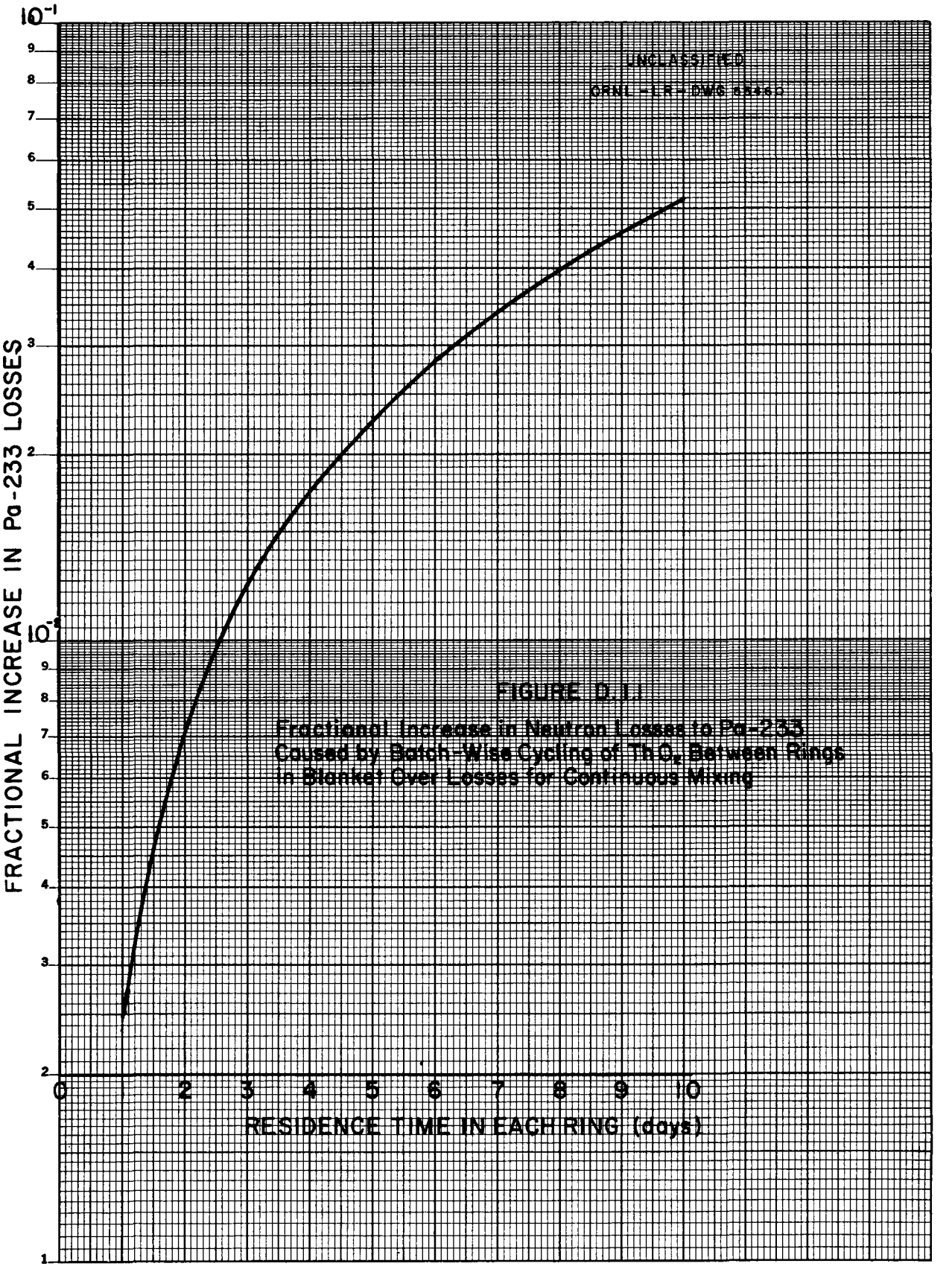

FIGURE D.I.1

Fractional Increase in Neutron Losses to Pa-233 Caused by Batch-Wise Cycling of ThO_2 Between Rings in Blanket Over Losses for Continuous Mixing

APPENDIX E

Poison Fraction Calculations

APPENDIX E

Poison Fraction Calculations

1.0 Molten Salt Breeder Reactor

The total poison fraction generated by fission products in a reactor includes the contribution to neutron losses from fuel stream plus fertile stream fission products in both core and blanket regions. Since in the MSBR the number of fertile stream fissions is a small portion of the total fissions and to simplify the calculations, the total poison fraction was assigned to the fuel stream.

By definition,

$$\text{Poison fraction} = \sum_i \frac{\text{neutrons absorbed by i-th fission product}}{\text{neutrons absorbed in U-233 + U-235}}$$

$$= \sum_i \frac{N_{i,1}(f_{1,1}\phi_1\sigma_i^a + f_{1,2}\phi_2\sigma_i^a)V}{F_t\,\nu/\eta} \qquad \text{(E-1)}$$

where,

$N_{i,1}$ = atomic concentration of i-th fission product, atoms/cm^3,
$f_{1,1}$ = volume fraction of fuel stream in core,
$f_{1,2}$ = volume fraction of fuel stream in end blanket,
ϕ_1 = average neutron flux in circulating fuel, neutrons/cm^2-sec,
ϕ_2 = average neutron flux in end blanket, neutrons/cm^2-sec,
σ_i^a = absorption cross section for i-th atom, cm^2,
f_n = fraction fissions in fuel stream, assumed to be 1.0,
F_t = total fission rate in reactor, fission/sec,
ν = neutrons born per fission,
η = neutrons born per neutron absorbed in fuel,
V = total fuel stream volume, cm^3.

The atomic concentration, $N_{i,1}$, can be expressed in terms of known quantities by considering the steady state production and loss of the i-th atom. Equating the production rate to the sum of all removal rates, there obtains

$$\frac{F_t Y_i}{V} = N_{i,1}\lambda_i + N_{i,1}(f_{1,1}\phi_1\sigma_i^a + f_{1,2}\phi_2\sigma_i^a) + \frac{N_{i,1}E_i}{T_i} \qquad \text{(E-2)}$$

The value of $N_{i,1}$ from Eq. E-2 can be substituted into Eq. E-1 to obtain

$$pf = \sum_i \frac{\eta Y_i}{\nu} \left[\frac{f_{1,1}\phi_1\sigma_i^a + f_{1,2}\phi_2\sigma_i^a}{\lambda_i + f_{1,1}\phi_1\sigma_i^a + f_{1,2}\phi_2\sigma_i^a + \frac{E_i}{T_i}} \right] \qquad \text{(E-3)}$$

Symbols not previously defined are

Y_i = yield of i-th atom (for some nuclides this number had to be adjusted to account for the behavior of a precursor atom in the chemical processing schemes),
λ_i = decay constant of i-th atom, sec^{-1},
E_i = efficiency of removal of i-th atom in chemical processing,
T_i = cycle time for i-th atom in chemical processing, sec.

The quantity E_i/T_i in Eq. E-3 expresses the removal rate of the i-th atom in chemical processing. In MSBR processing T_i assumes two values, identified as T_1 and T_{1d}, the values being characteristic of the chemical behavior of an atom in processing. T_1 refers to those fission products whose removal is accomplished in the HF dissolution step; therefore, T_1 is the actual fuel stream cycle time through the chemical processing plant. T_{1d} is associated with those fission products whose removal is accomplished by discarding a portion of the uranium-free fuel salt each time the fuel stream is processed. The time T_{1d} is independent of the time T_1; there is, however, the restriction that T_{1d} must be greater than T_1. In the economic cases, T_{1d} will be several times larger than T_1.

The total poison fraction attributive to the fuel stream is the solution to Eq. E-3. Through this equation the total poison fraction is related to the cycle times T_1 and T_{1d} and thereby to the capital investment in the processing plant and the replacement cost of the fuel salt. Furthermore, it is possible to optimize these costs for a given poison fraction by the appropriate choices of T_1 and T_{1d}. This optimization was made in this study.

Solution of Poison Fraction Equations. - The total fission product poison fraction was conveniently calculated using the PF-9 code for the Oracle which solved Eq. E-3. Detailed knowledge of cross sections as a function of energy for the individual fission products is not available; however, reasonably reliable resonance integrals are known. It was necessary therefore to relate fission product absorptions to absorptions in another element for which more extensive cross section data are available. The element carbon was chosen.

In Eq. E-3 all of the terms are known except the terms $\phi\sigma$. From previous GNU or Cornpone calculations a reaction rate coefficient, C_c, for carbon can be computed as the quotient of total carbon absorptions at all energies in a region and the homogenized concentration of carbon atoms (see Appendix H). Using this quantity an effective thermal flux can be computed as

$$\phi_{th}^{eff} = \frac{F_t \nu C_c}{\sigma_c^{th} V/D_c} , \qquad (E-4)$$

in which σ_c^{th} is the thermal microscopic absorption cross section for carbon and D_c is its thermal disadvantage factor. The other quantities were defined above in Eq. E-1.

If it is desired to treat fission products as 1/v absorbers, it is only necessary to multiply both sides of Eq. E-4 by the thermal absorption cross section, σ_i^{th}, to obtain the absorption rate. The $\phi_{th}^{eff}\ \sigma_i^{th}$ so obtained may be used in Eq. E-3 in computing the poison fraction. On the other hand, a more pessimistic - but more realistic - computation is to include the resonance absorptions and in some manner adjust the thermal energy cross sections to reflect these resonances. An effective cross section was calculated for each fission product by including the resonance absorptions in the following manner:

The number of neutrons absorbed by a given (i-th) isotope can be expressed as a sum of thermal neutron absorptions plus an integration over the epithermal range.

$$A_i/V = N_i \, \phi^{th} \, \sigma_i^{th} + N_i \int_{E(th)}^{\infty} \phi(E) \, \sigma_i^a \, (E) \, dE$$

where V is the volume of the core. Assume now the slowing down density q is nearly uniform in energy.

$$q = \xi \Sigma_t^e \, E \, \phi(E) \cong \phi^{th} \Sigma_f^{th} \quad \nu/f$$

where f is the fraction of neutrons absorbed in the thermal group. Solving for $\phi(E)$, one has

$$\phi(E) \cong \phi^{th} \Sigma_f^{th} \, \nu/f \, \xi \Sigma_t^e \, E$$

which, put into the equation above for A_i, gives

$$\frac{A_i}{V} = N_i \, \phi^{th} \left[\sigma_i^{th} + \frac{\nu \Sigma_f^{th}}{f} \int_{E(th)}^{\infty} \frac{\sigma_i(E) \, dE}{\xi \Sigma_t^e \, E} \right]$$

But $\xi \Sigma_t$ is nearly a constant in energy (above thermal), and

$$\int_{E(th)}^{\infty} \frac{\sigma_i(E) \, dE}{E} \cong \text{Resonance Integral}$$

so that, approximately

$$\frac{A_i}{V} \cong N_i \, \phi^{th} \left[\sigma_i^{th} + \frac{\nu \Sigma_f^{th}}{f \xi \Sigma_t^e} \, x \, (RI)_i \right]$$

It therefore becomes convenient to define an "effective" thermal cross section, viz.:

$$\sigma_i^{eff} = \sigma_i^{th} + \frac{\nu \Sigma_f^{th}}{f \, \xi \Sigma_t^e} \, x \, (RI)_i \qquad \text{(E-5)}$$

where,

RI = resonance integral for i-th nuclide, cm^2,
$\sum_f^{th}$ = macroscopic fission cross section in reactor, cm^{-1}, at thermal,
$\xi \sum_t^e$ = slowing down power in reactor, cm^{-1}, epithermal range,
f = fraction of total fissions occuring at thermal energy,
ν = number neutrons born per fission.

The terms $\nu \sum_f^{th}$, $\xi \sum_t^e$, and f are computed by the GNU code for the IBM-704.

Both sides of Eq. E-4 can be multiplied by σ_i^{eff} from Eq. E-5 to obtain

$$\phi_{th}^{eff} \sigma_i^{eff} = \frac{F_t \nu C_c}{\sigma_c^{th} V/D_c} \left[\sigma_i^{th} + \frac{\nu \sum_f^{th}}{f \xi \sum_t^e} (RI)_i \right] . \qquad (E\text{-}6)$$

When the subscripts 1 and 2 are inserted to denote core region and end blanket region respectively, two expressions are obtained for insertion as the $\phi\sigma$ terms of Eq. E-3. These are

$$\phi_{th,1}^{eff} \sigma_i^{eff} = \frac{F_t \nu C_{c,1}}{\sigma_c^{th} V/D_c} \left[\sigma_i^{th} + \frac{\nu \sum_f^{th}}{f \xi \sum_t} (RI)_i \right] \qquad (E\text{-}7)$$

$$\phi_{th,2}^{eff} \sigma_i^{eff} = \frac{F_t \nu C_{c,2}}{\sigma_c^{th} V/D_c} \left[\sigma_i^{th} + \frac{\nu \sum_f^{th}}{f \xi \sum_t^e} (RI)_i \right] . \qquad (E\text{-}8)$$

The solution of Eq. E-3 revised by Eqs. E-7 and E-8 is the desired poison fraction.

Resonance Integrals. - Values of resonance integrals have not been reported for all 44 nuclides of Table E.1.1.

The ones reported by Nephew (38) were used, and, for the unavailable values, assumed or calculated values were used. When a calculation was made,

the method for infinite dilution described by Dresner (92) was used. In cases where there were insufficient physical data to allow the calculation, an assumed value was necessary.

Fission Products Included in Poison Fraction Calculation. - The fission products used in the poison fraction calculations were those recommended by Burch, Campbell, and Weeren (17). Forty-four nuclides that would make an appreciable contribution to the poisoning were chosen; these are listed in Table E.1.1. The isotopes of xenon are not included in this tabulation because the poisoning from xenon (primarily Xe-135) is large enough that it is treated separately, and a special processing method, gas sparging, must be employed to bring this value within tolerable limits. Hence the poison fraction calculated by Eq. E-3 for the fission products in Table E.1.1 excludes any xenon contribution.

The 44 fission products are divided into three groups which classify the elements more or less according to their chemical behavior in the system. The first group contains the metals that are noble relative to nickel and might be expected to be reduced and plate out on the walls of the system. Also included in this group are the iodines and bromine that are probably sensitive to removal by gas sparging and hence may behave like xenon. The noble metals and the halogens are treated as if they are removed from the fuel solution on a very fast cycle and thus contribute little to the poison fraction.

The second group contains the rare earths that are removed by precipitation in the HF-dissolution process and are thereby controlled by the fuel stream cycle time.

The third group contains the alkali and alkaline earth metals that are soluble in the HF-dissolution process and are removed by discarding the fuel salt on a specified cycle.

Gas Sparging and Effective Yield. - Fission product nuclides which are daughters of gaseous precursors will have "effective" yields that are smaller than their actual fission yield because the gas sparging operation removes a portion of the parent atoms before decay. The fraction of gaseous nuclides of a particular species which undergo decay before being sparged is

Table E.1.1. Fission Product Nuclides Included in Poison Fraction Calculations

Nuclide	Thermal Cross Section (barns)	Decay Constant (sec^{-1})	Yield	Resonance Integral[d] (barns)
Atoms removed by plating on walls or by gas sparging				
Rh-103	150	stable	0.029	1000
Mo-95	13.4	"	0.064	101
Ru-101	2.46	"	0.05	131
Mo-97	2	"	0.062	12.2
Ru-102	1.2	"	0.042	26.7
Ru-104	0.7	"	0.018	15.8
Mo-100	0.2	"	0.065	6.3
I-131	600	0.995×10^{-7}	0.029	25
I-129	11	stable	0.01	25
I-127	6.1	"	0.0025	167
Br-81	2.6	"	0.0013	83.2
Zr-93	4	"	0.065	43.9
Zr-91	1.5	0.666×10^{-9}	0.059	9.7
Atoms removed by precipitation in HF-dissolution				
Gd-157	0.16×10^{6}	stable	0.0001	462
Gd-Eu-155[a]	0.7×10^{5}	0.1281×10^{-7}	0.0003	1512
Sm-149	0.5×10^{5}	stable	0.007	0.219×10^{6}
Sm-Eu-151	7000	0.301×10^{-9}	0.0033	3315
Eu-153	400	stable	0.0013	1512
Nd-143	290	"	0.052	37.4
Sm-152	150	"	0.0021	2850
Pm-147	60	0.845×10^{-8}	0.015	2050
Nd-145	52	stable	0.029	310
Pr-141	11	"	0.056	16
Nd-146	9.8	"	0.022	10[c]
La-139	8.8	"	0.06	24.7
Nd-144	4.8	"	0.038	10[c]
Nd-148; La-140[a]	3	"	0.08	16.1
Ce-142	1.8	0.24×10^{-7}	0.059	10[c]
Y-89	1.4	0.106×10^{-7}	0.0271[b]	0.184
Ce-140	0.6	0.67×10^{-8}	0.063	10[c]
Nd-150	2.9	0.1824×10^{-9}	0.005	10[c]

Table E.1.1. (Continued)

	Atoms removed by fuel salt discard			
Cd-113	0.25×10^{5}	stable	0.0001	41.9
Sr-89	130	0.149×10^{-6}	0.0271(b)	193
Ag-109	84	stable	0.0003	1396
Ag-107	30	stable	0.002	198
Cs-135	15	"	0.00046(b)	375
Se-82	2	"	0.0025	0.347
Cs-137	2	0.732×10^{-9}	0.0308(b)	375
Sr-90	1	stable	0.059	10(c)
Ba-138	0.7	"	0.0144(b)	0.0021
Te-130	0.3	"	0.02	8.6

(a) Considered together because cross sections and/or yields are about the same.

(b) Yields are adjusted to reflect gas sparging of gaseous precursors on a 6-minute cycle.

(c) Assumed value of resonance integral since no data for calculating available.

(d) Except as indicated by footnote (c), values are from Nephew (reference 38) or calculated by method of Dresner (reference 92).

$$\frac{\lambda_{decay}}{\lambda_{decay} + \lambda_{sparge}} ,$$

where the terms designate the decay rate and the sparge rate. The effective yield then becomes

$$\text{Effective yield} = (\text{actual yield}) \frac{\lambda_{decay}}{\lambda_{decay} + \lambda_{sparge}} . \qquad \text{(E-9)}$$

For example consider Sr-89, a daughter of Kr-89, under conditions for which the average sparging time of the fuel stream is six minutes.

$$\text{Kr-89} \xrightarrow[3.2 \text{ min}]{} \text{Rb-89} \xrightarrow[15 \text{ min}]{} \text{Sr-89} \xrightarrow[50.4 \text{ d}]{} \text{Y-89}$$

$$\text{Effective yield of Sr-89} = (0.048) \left[\frac{\frac{0.693}{3.2}}{\frac{0.693}{3.2} + \frac{1}{6}} \right] = 0.0271$$

In this example the effective yield of Y-89 would be the same.

Where applicable, effective yields based on a six-minute sparge cycle were used in poison fraction calculations in this study.

Graphical Representation. - The solutions of Eq. E-3 for a large number of values of T_1 and T_{1d} are plotted in Fig. E.1.1.* The time T_1 is the cycle time for removal of fission products in the HF dissolution step. These are chiefly the rare earths and are those nuclides listed in the second group of Table E.1.1. T_{1d} is the cycle time for those atoms controlled by discard of the fuel salt. These are the alkali and alkaline earth metals and are listed in the third group of Table E.1.1. As mentioned above these times are independent of each other; however, the restriction that T_{1d} can be no smaller than T_1 applies. The nature of the processing scheme makes it impossible to discard salt faster than it is processed. The dashed curve of Fig. E.1.1 show the limiting condition of $T_1 = T_{1d}$.

It is observed that a given poison fraction may be obtained for a large number of combinations of T_1 and T_{1d}. In this study of the MSBR, optimum economic conditions were calculated using the poison fraction as

* In this figure, values of the abscissae have been divided by eta so that the poison fraction is expressed as neutrons absorbed in fission products per neutron born.

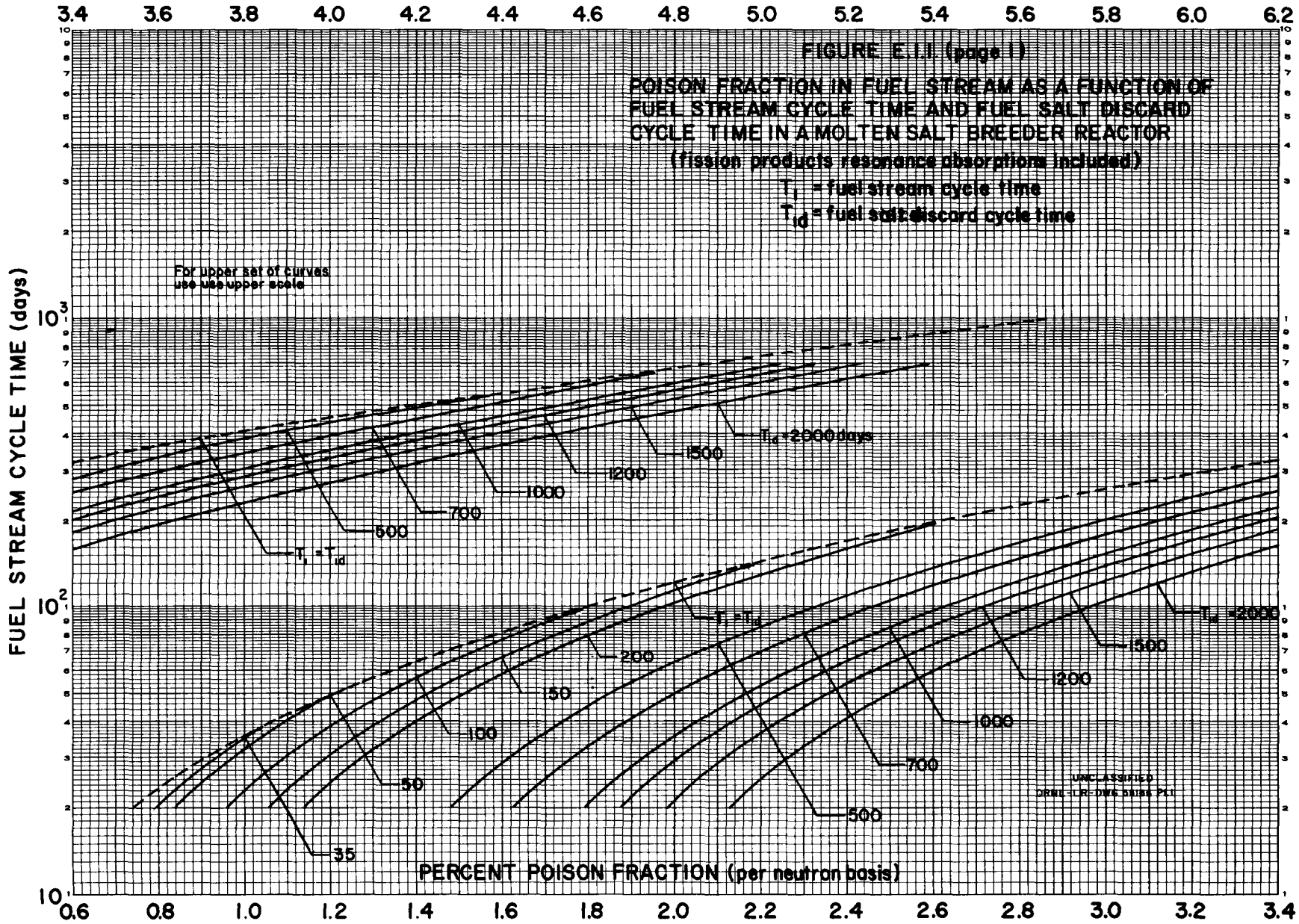
FIGURE E.1.1 (page 1)
POISON FRACTION IN FUEL STREAM AS A FUNCTION OF FUEL STREAM CYCLE TIME AND FUEL SALT DISCARD CYCLE TIME IN A MOLTEN SALT BREEDER REACTOR
(fission products resonance absorptions included)
T_1 = fuel stream cycle time
T_{id} = fuel salt discard cycle time
For upper set of curves use the upper scale
FUEL STREAM CYCLE TIME (days)
PERCENT POISON FRACTION (per neutron basis)
$T_1 = T_{id}$
T_{id} = 2000 days
1500
1200
1000
700
500
200
150
100
50
35
UNCLASSIFIED
ORNL-LR-DWG 51184 R1

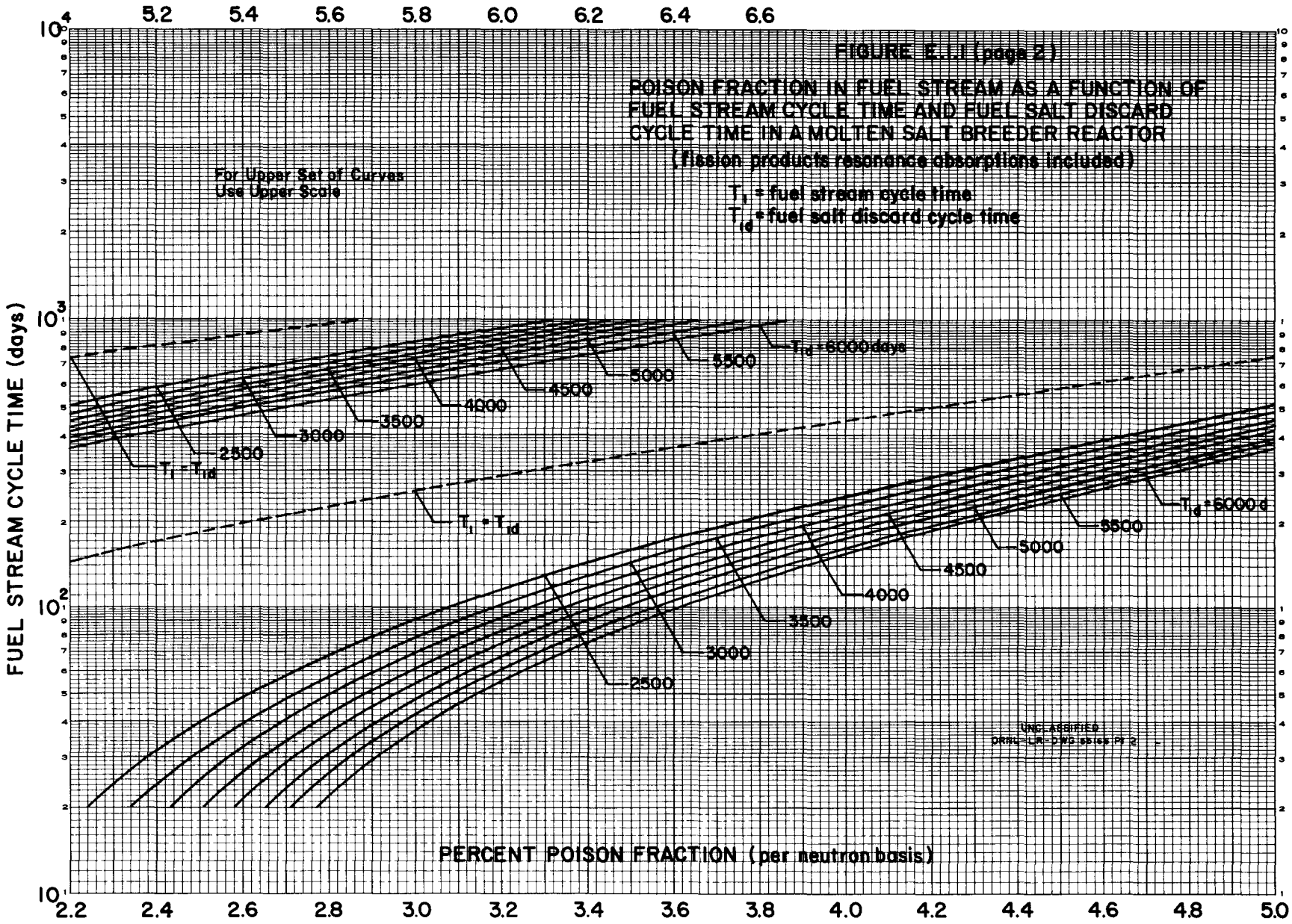
FIGURE E.LI (page 2)
POISON FRACTION IN FUEL STREAM AS A FUNCTION OF FUEL STREAM CYCLE TIME AND FUEL SALT DISCARD CYCLE TIME IN A MOLTEN SALT BREEDER REACTOR
(Fission products resonance absorptions included)
T_l = fuel stream cycle time
T_{id} = fuel salt discard cycle time
For Upper Set of Curves Use Upper Scale
FUEL STREAM CYCLE TIME (days)
PERCENT POISON FRACTION (per neutron basis)
$T_l = T_{id}$
$T_l = T_{id}$
T_{id} = 6000 days
T_{id} = 6000 d
5500
5000
4500
4000
3500
3000
2500
UNCLASSIFIED
ORNL-LR-DWG 65168 R1

a parameter. Fuel cycle costs were calculated at several combinations of T_1 and T_{1d} which gave the same poison fraction, and a graphical solution was used to determine the minimum fuel cycle cost and the corresponding fuel cycle time and fuel salt discard time.

Xenon Poison Fraction. - Xenon is controlled in both fuel and fertile streams of the MSBR by gas sparging (see Appendix B). It has been assumed that Xe-135 poison fraction can be maintained at 0.005 neutrons absorbed per neutron absorbed in fuel.

2.0 Liquid Bismuth Breeder Reactor

Poison fractions in the LBBR were not calculated in the manner as described above for the MSBR. Instead, the results computed by Thomas, et al (22), were used in this study because processing rates and conditions were made identical to those recommended by Thomas. The following discussion is a summary of the discussion in the reference report on computational methods, sources of data, and assumptions.

Poison Fraction Calculations. - The equilibrium concentration of any member of a fission product chain

$$A_0 \longrightarrow A_1 \longrightarrow \cdots \longrightarrow A_n$$

can be described by the equation

production = decay + burned + processed.

The number of atoms of the first member is then

$$N_0 = \frac{Y f}{\lambda_o + \beta + \sigma_o g_o \overline{\Phi}_2 + I_o \overline{\Phi}_1^1} \qquad \text{(E-10)}$$

The second member of the chain, N_1, is formed by decay of the first member, N_0. So

$$\frac{\lambda_o Y f}{\lambda_o + \beta + \sigma_o g_o \overline{\Phi}_2 + I_o \overline{\Phi}_1^1} = N_i \left(\lambda_1 + \beta + \sigma_1 g_1 \overline{\Phi}_2 + I_1 \overline{\Phi}_1^1\right) \qquad \text{(E-11)}$$

Identifying $C_o = \dfrac{\lambda_o}{\lambda_o + \beta + \sigma_o g_o \bar{\Phi}_2 + I_o \bar{\Phi}_1^1}$, (E-12)

there obtains

$$N_1 = C_o \frac{Y f}{\lambda_1 + \beta + \sigma_1 g_1 \bar{\Phi}_2 + I_1 \bar{\Phi}_1^1}$$

$$= C_o C_1 \frac{Y f}{\lambda_1} \quad \text{(E-13)}$$

Similarily,

$$N_n = C_o \cdot \cdot \cdot \cdot C_{n-1} \left(\frac{Y f}{\lambda_n + \beta + \sigma_n g_n \bar{\Phi}_2 + I_n \bar{\Phi}_1^1} \right)$$

$$= C_o \cdot \cdot \cdot \cdot C_n \frac{Y f}{\lambda_n} \quad \text{(E-14)}$$

in which

$$C_n = \frac{\lambda_n}{\lambda_n + \beta + \sigma_n g_n \bar{\Phi}_2 + I_n \bar{\Phi}_1^1} \quad . \quad \text{(E-15)}$$

By definition the poison fraction attributive to the n-th nuclide is

$$(pf)_n = \frac{\text{neutron absorptions in n-th nuclide}}{\text{neutron absorptions in fuel}}$$

$$= \frac{N_n (\sigma_n g_n \bar{\Phi}_2 + I_n \bar{\Phi}_1^1}{f(1 + \alpha)} \quad \text{(E-16)}$$

The value of N_n from Eq. E-14 may be substituted into Eq. E-16, and the result may be summed over all fission products to obtain the total poison fraction.

$$(pf)_{total} = \sum_{\substack{\text{all} \\ \text{fission} \\ \text{products}}} (\sigma_n g_n \bar{\phi}_2 + I_n \bar{\phi}_1^1) \frac{Y}{\lambda_n (1 + \alpha)} \prod_{j=0}^{n} C_j \qquad \text{(E-17)}$$

The terms in Eqs. E-10 to E-17 are identified as follows:

N = total number of atoms of a particular fission product isotope in the reactor fluid or blanket slurry under consideration,

λ = decay constant,

β = processing rate = processing flow rate/total system volume,

σ = thermal neutron cross section at 2200 m/sec,

g = temperature and non 1/v correction for thermal cross section,

I = resonance absorption integral,

$\bar{\phi}_2$ = thermal flux averaged over fluid or slurry,

$\bar{\phi}_1^1 = P_{02} (D_1/\tau)(1/\xi \sum_s) \bar{\phi}_1$,

Y = yield,

f = fission rate in reactor fluid or slurry under consideration,

P_{02} = resonance escape probability in thorium,

D_1 = resonance diffusion coefficient,

τ = neutron age,

$\xi \sum_s$ = slowing down power,

$\bar{\phi}_1$ = fast flux averaged over fluid or slurry,

α = capture cross section U-233/fissium cross section U-233.

Subscripts, except when applied to the term ϕ, refer to the member of the mass chain

$$A_o \longrightarrow A_1 \longrightarrow \cdots \longrightarrow A_n \ .$$

In Thomas's study only three-member chains were considered. If a chain split and if there were direct yield to a second or third nuclide, the chain yield was split accordingly between the two or three processes, and a calculation was made for each.

Sources of Data and Assumptions. - Yields for the various mass chains were taken from Walker (94). Since most of the fissions are from U-233, fission yields for U-233 were used. The chain split data of Blomeke (95), based on U-235 fission, were used since no data were available for U-233. Thermal neutron cross sections were corrected for non 1/v absorbers with g factors taken from Westcott (96).

The following assumptions were made in the poison fraction calculations:

(1) the mass chains 133 to 135 are removed from the core fluid as volatile fission products,

(2) Mo-99 is at equilibrium concentration with fission product Mo, in which the total concentration is 1 ppm,

(3) Zr in the core and blanket is fission product Zr,

(4) the solubility of Ru in Bi is 10 ppm,

(5) the solubility of Rh in Bi is 15 ppm.

Graphical Representations of Fuel Stream Fraction. - There are two groups of fission products that are affected by the chemical processing methods for the fuel solution. These are the FPS group and the FPN group. These groups are defined and their processing methods described in Appendix C. The different chemical behavior of these groups require different processes for their removal from the fuel solution, but their different nuclear properties allow different removal rates. The different rates affect the term β in the above equations. Solutions to the poison fraction equations obtained by Thomas (22) were used in this study after a slight modification to express poison fraction in terms of fuel exposure, viz., Mwt-days/ft^3. Curves for the FPS and FPN groups are presented in Figs. E-2-1 and E-2-2 respectively.

Fertile Stream Poison Fraction. - The fertile stream poison fraction was calculated using the ERC-5 code (86) for the IBM-704. This code calculated equilibrium concentrations utilizing reaction rate coefficients generated from GNU calculations (see Appendix H) plus other specifications such as process cycle times, volumes, volume fractions, etc. In this manner equilibrium concentrations were obtained for Xe-135, Sm-151, Sm-149,

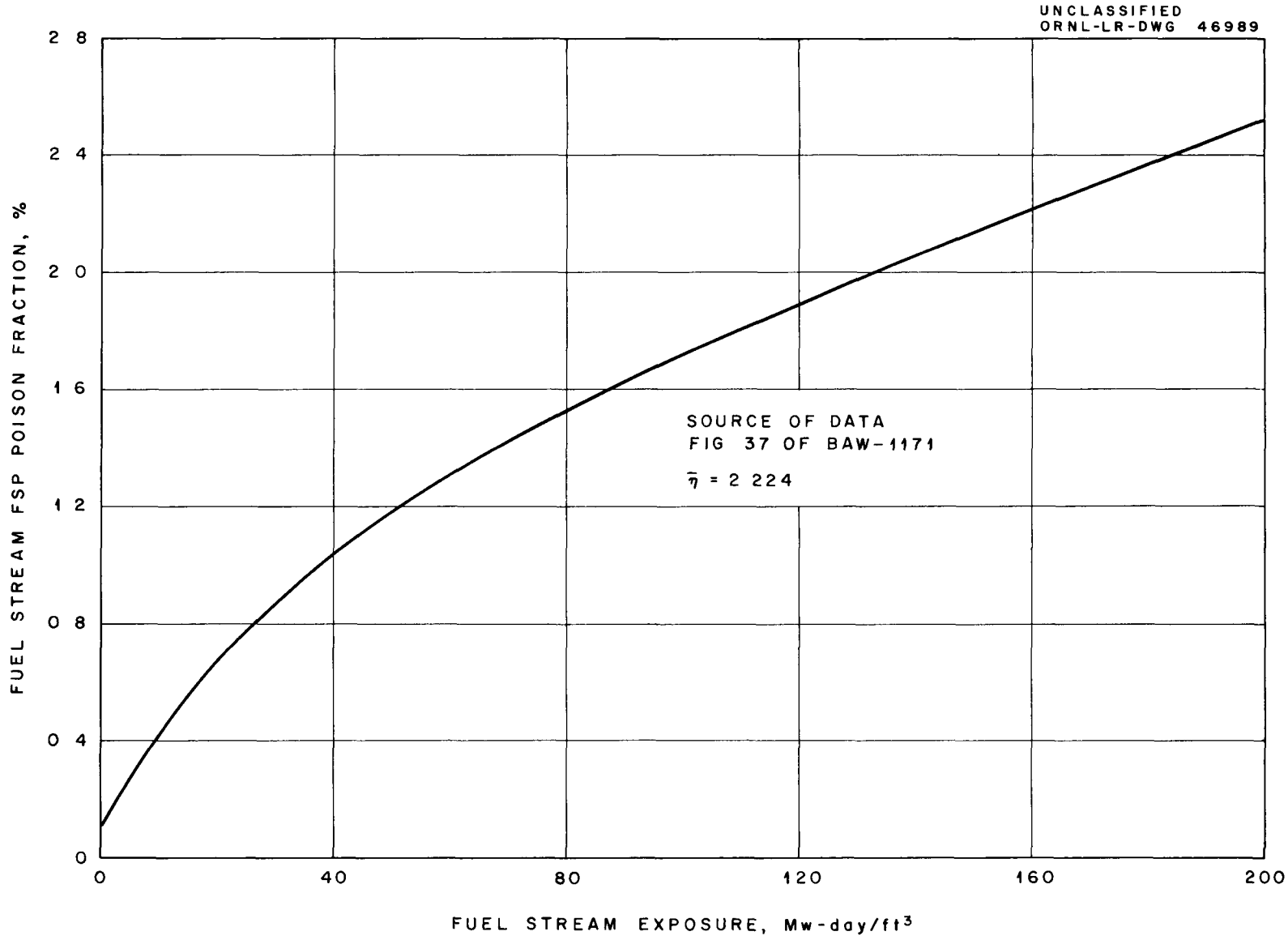

Fig E 2 1 Fuel Stream FSP Poison Fraction Vs Exposure - Liquid Bismuth Breeder Reactor

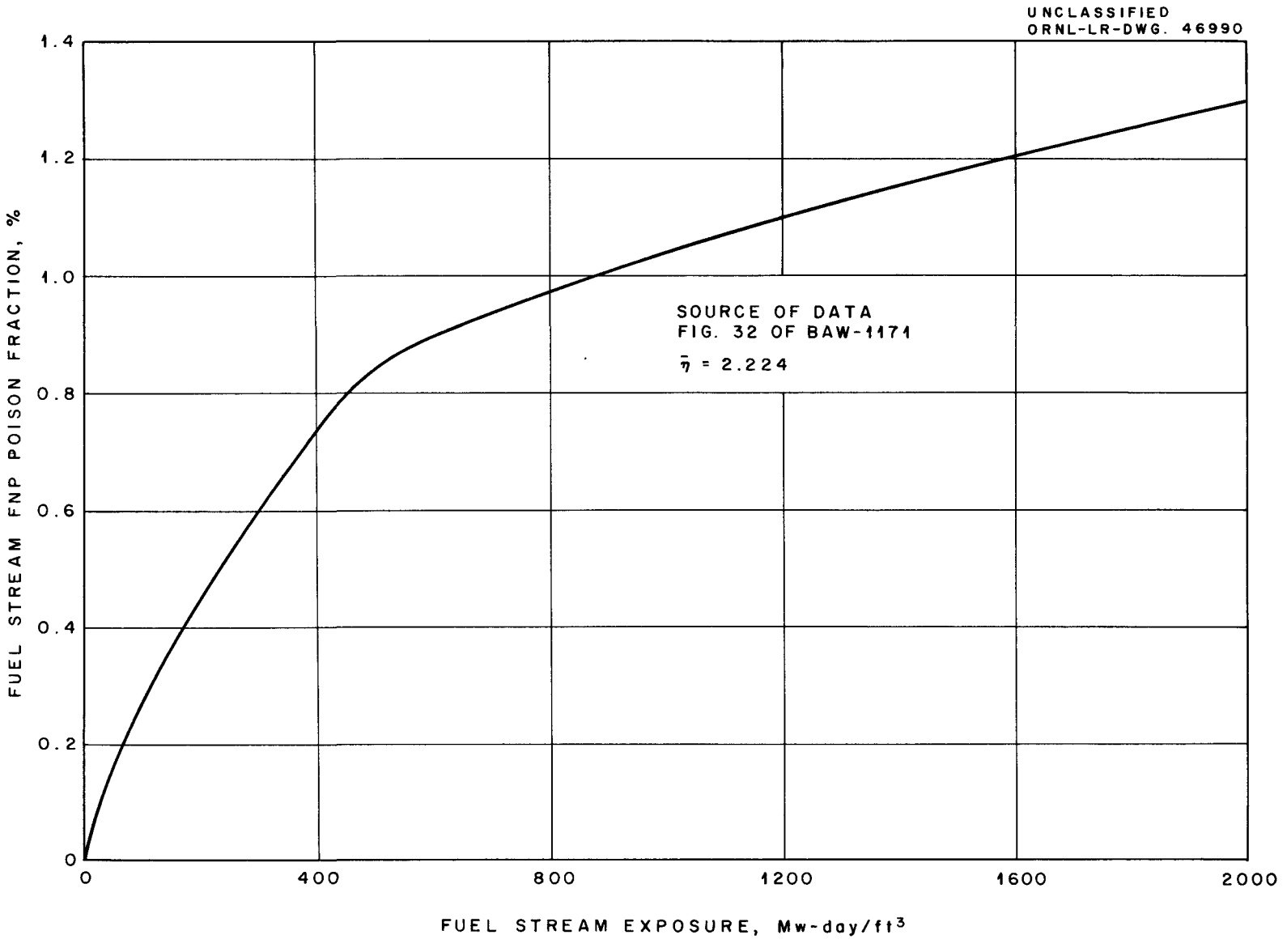

Fig. E.2.2. Fuel Stream FNP Poison Fraction Vs. Exposure – Liquid Bismuth Breeder Reactor.

and a composite of the remainder of the fission products identified as fissium and assigned an average cross section of 50 barns. ERC-5 code also computed the fraction of neutrons absorbed by each of these elements, making it a simple matter to obtain the respective contribution to the poison fraction by multiplying the fraction of absorptions by eta.

Xenon Poison Fraction. - The total xenon poison fraction is that attributive to fuel plus fertile stream Xe-135. It was assumed that in the fluid core Xe-135 could be controlled by gas sparging (see Appendix B) and that the technology is sufficiently advanced that a poison fraction as low as 0.005 could be maintained in the fuel stream.

In the fertile stream, which is composed of solid ThO_2 pellets, it was assumed that none of the fission product xenon escaped from the pellets during the irradiation period. The only mechanism by which xenon was lost was burnout. ERC-5 code computed this xenon concentration and fraction of neutrons lost to it. In the LBBR, Xe-135 poison fraction was about equally divided between the fuel and fertile stream.

3.0 Aqueous Homogeneous Breeder Reactor

In the AHBR, poison fractions associated with nuclides in the fuel stream are based upon experimental data from operation of the HRE-2 and from the laboratory. The chemical behavior of a large number of the important fission product poisons and some of the corrosion product poisons in a high-temperature, aqueous system permits the use of a relatively simple solid-liquid separation for poison control.

Poison Fraction from "Insoluble" Fission and Corrosion Products in Fuel Stream. - Fission products in the rare earth group are relatively insoluble in AHBR fuel solutions permitting removal by hydroclones. In addition these solids tend to settle out on heat exchanger walls and other metal surfaces of the system piping, locations in which they are ineffective as neutron poisons but undoubtedly can have a deleterious effect on heat transfer. In general, the solubility of individual elements increases with increasing atomic weight, and all tend to coprecipitate from mixtures with the effect of an apparent solubility much less than measured for individual elements. Also in HRE-2 operations it appears that solubilities are lower than those measured out of pile. The following tabulation of solubilities has been prepared by Burch (17) from laboratory and in-pile tests.

Table E.3.1. Solubilities of Selected Rare Earth Fission Products in AHBR Fuel

	Solubility (mg/liter)						
	La	Ce	Nd	Pr	Y	Sm	Pm
Individual solubility in 0.02 m UO_2SO_4, 0.005 m D_2SO_4 at 280°C	5	25	55	85	90	210	
In rare earth mixtures at 280°C		17	25				
Measured in HRE-2			~10		1		
Estimated concentration in large reactor	5	10	10	10	1	10	10

Most of the rare earths have absorption cross sections in the range 10-450 barns; however, several (Sm-149, Sm-151, Eu-155, Gd-155) have such large cross sections that practical processing rates are ineffective in removing these before they have captured a neutron. Hence in this study it has been assumed that each of these atoms formed disappeared by capturing a neutron. This contribution to the poison fraction is approximately 0.9%.

Other fission products that are important nuclearwise are Rh-103, Tc-99, and Mo-95. These, however, are extremely insoluble, in the range below 1 ppm. Another very insoluble group includes Zr, Te, and Ru; however, these are of little nuclear importance.

Iron and chromium from the corrosion of stainless steel has low solubility in AHBR fuel, being in the range 5-20 ppm. The poisoning effect of these nuclides in the AHBR is 0.1-0.3%, the large number being associated with the higher core power.

Data from HRE-2 operations show that the concentration of solids circulating in the reactor remains below a level significant from a nuclear standpoint, in the range 5-20 ppm. This concentration is apparently independent of the rate at which the solids are formed or removed and of the total inventory of the reactor. Processing rates in the range 3-10 fuel stream

volumes per hour are required to remove solids at the rate at which they are formed. Accordingly in this study it has been assumed that the fuel is processed through the hydroclone on a 15-minute cycle.

In calculating the poison fraction attributive to the rare earth group, a concentration of 10 ppm for each member was assumed. The corresponding fraction of neutron absorptions was a function of core power and was computed by GNU code using an average composite cross section equal to 50 barns.

Poison Fraction from Soluble Corrosion Products. - Nickel and manganese from stainless steel corrosion are quite soluble in AHBR fuel. In addition to its neutron poisoning effect it is mandatory that nickel concentration be controlled because of its adverse effect on fuel stability. The exact permissible nickel level is not known, but it is believed to be in the range 300-500 ppm. In these calculations the lower value was used requiring a cycle time of 150 days for the fuel volume through the peroxide precipitation process (see Appendix C). Manganese is also removed in this process, and this rate is more than sufficient to maintain manganese below the permissible level.

The poison fraction was calculated by entering this nickel concentration into a GNU calculation. A pseudo cross section composed from Ni and Mn cross sections was used so the neutron absorptions would be those corresponding to the total amount of soluble corrosion products.

Xenon Poison Fraction in Fuel Stream. - Methods of xenon control and xenon poisoning have been discussed in Appendix B. It has been assumed that the xenon poison fraction can be maintained at 0.005 in the fuel stream.

Fission Product Poison Fraction in Fertile Stream. - Fission products in the ThO_2 blanket of the AHBR cannot be removed by any known method except complete dissolution of the ThO_2 followed by aqueous solvent extraction in a Thorex process. In computing fission product poisoning it is assumed that all fission products remain in the ThO_2. Even if fissions near the pellet surface did eject the fission products, it is almost a certainty that they would be adsorbed on the surface of a nearby pellet.

The first step in calculating the fission product poison fraction is to determine the number of fissions occurring in the blanket. This in turn depends upon the U-233 concentration. Consequently the desired fertile stream loading, i.e., gm Pa-233 + U-233 per kg Th, is arbitrarily selected and the time-dependent equations are solved to determine the concentration of each. The integration also establishes the blanket cycle time. This concentration of U-233 is then entered as input for a GNU calculation from which the number of fertile stream fissions, fission product concentration, and the fraction of neutrons absorbed by fission products can be found. As in the calculation of fuel stream poison fraction, it was found that each Sm-149 and Sm-151 atom captures a neutron.

Xenon Poison Fraction in Fertile Stream. - A procedure analogous to that described above was employed to obtain the xenon poison fraction. It is assumed that all xenon is trapped inside the ThO_2 particles and is removed only by burnout or chemical processing. Xenon poisoning is discussed in Appendix B.

4.0 Graphite-Moderated, Gas-Cooled Breeder Reactor, and Deuterium-Moderated, Gas-Cooled Breeder Reactor

These two reactors are discussed together because their similarity in construction and methods of processing allows the use of identical methods for calculating poison fractions. It is assumed that all fission products formed in the graphite fuel elements or the ThO_2 pellets in the blanket are trapped until the fuel or pellet is removed for processing.

Fission Product Poison Fraction in Fuel. - The fission product poison fraction for the GGBR and DGBR was calculated from output data of equilibrium reactor calculations performed on ERC-5 code (86) for the IBM-704. This code uses reaction rate coefficients determined from a GNU calculation, cycle times, volumes, volume fractions, and other specifications to compute equilibrium concentrations for a number of elements. The corresponding fraction of neutrons absorbed by each element is also calculated. The poison fraction is then easily determined from the fraction of absorptions in fission products. As in the above reactors, these fission products (excluding Sm-149, Sm-151 and Xe-135) are a composite which has been assigned an average cross section of 50 barns. Samarium-149 and Sm-151 have such large cross sections that effectively their only mode of disappearance is burnout.

Xenon Poison Fraction in Fuel. - Xenon poison fraction in the fuel is computed from output of the ERC-5 code as described above.

Fission Product Poison Fraction in Fertile Stream. - This poison fraction was calculated from output of the ERC-5 code as described above. This value is a function of the blanket power and therefore increases as the blanket loading, gm Pa-233 + U-233 per kg Th, increases.

Xenon Poison Fraction in Fertile Stream. - ERC-5 output data was also used to calculate xenon poison fraction.

A P P E N D I X F

Multigroup Neutron Cross Sections For GNU Program

APPENDIX F

Multigroup Neutron Cross Sections for GNU Program

The cross sections used in this thorium breeder reactor study were those compiled by Nestor (24) especially for this study. This compilation represents the latest available data from published sources and from personal communications with persons directly concerned with measuring nuclear parameters. The principal source of data was that of Hughes and Schwartz (98). Elements for which all data were not taken from Hughes and Schwartz are U-233, Pa-233, Sm-151, and fissium. (Fissium is a mixture of fission products excluding Xe-135, Sm-151, and Sm-149.) The procedure followed in preparing the cross sections for these elements is discussed below.

A list of elements for which cross section were compiled is presented in Table F.1. The group structure for the GNU program is given in Table F.2.

Uranium-233. - The principal parameter of interest in nuclear calculations of a Th-U-233 breeder reactor is η, the number of neutrons produced per neutron absorbed in fuel. Experimental information on the energy dependence of η in the range 0 - 10 ev as measured at the Materials Testing Reactor was used to calculate group-averaged fission cross sections, using absorption cross sections calculated from total cross section data (99) and the scattering cross section as calculated by Vogt (100). The η-values used in preparation of the cross sections were normalized to a 2200 m/sec value of 2.28 (101).

In the energy range 0-0.8 ev, η was assumed to be constant at 2.28. In the range 0.8-10 ev group-averaged values of $\overline{\nu\sigma}_f = \overline{\eta\sigma}_a$ were calculated by numerical evaluation of the integrals in

$$\overline{\eta} = \frac{\int \eta(E)\, \sigma_a(E)\, dE/E}{\int \sigma_a(E)\, dE/E} \qquad \text{(F-1)}$$

$$\overline{\sigma}_a = \frac{1}{\Delta u} \int \sigma_a(E)\, dE/E \qquad \text{(F-2)}$$

where Δu denotes the lethargy width of the group.

Table F.1 Elements Used in GNU Program and Temperatures of "Thermal" Group

Element	GNU Identification Number	Temperature (°C) of "Thermal" Group for				
		AHBR	MSBR	LBBR	GGBR	DGBR
H	1	280				
Be	4	280		649		
B	5	280				
C	6	280		649		925
N	7	280				
O	8	280				925
F	9					925
Na	11	280				
Mg	12	280				
Al	13	280				
Li-6	15			649		925
S	16	280				
Li-7	17			649		
INOR-8	20			649		
MSBR Fuel Salt[a]	21			649		
MSBR Blanket Salt[b]	22			649		
Cr	24	280				
Mn	25	280				
Fe	26	280		649		925
Ni	28	280				
Cu	29	280				
Zr	40	280				
Corrosium-I[c]	52	280				
Corrosium-II[d]	53	280				
Xe-135	54	280		649		925
Sm-151	55	280		649		925
Sm-149	62	280		649		925
Th in MSBR Core[e]	68			649		
Th in MSBR Blanket[e]	69			649		
Th in AHBR Slurry[e]	70	280				
Th in Pebble Bed[e]	76	280				
Th (infinite dilution)[e]	77	280		649		
Th in LBBR Core[e]	78			649		
Bi	83			649		
U-233 Capture Cross Section	84	280		649		925
U-235 Capture Cross Section	85	280		649		925
Fissium	86	280		649		925
Np-237	87	280		649		925
D	88	280				925
Pa-233	91	280		649		925
Th (without resonance σ_a)	92	280		649		925
U-233	93	280		649		925
U-234	94	280		649		925
U-235	95	280		649		925
U-236	96	280		649		925

Footnotes for Table F.1

(a) Basic composition (mole %):

Li^7F - 63
Li^6F - 63 x 10^{-5}
BeF_2 - 37

(b) Basic composition (mole %):

Li^7F - 67
Li^6F - 67 x 10^{-5}
BeF_2 - 18
ThF_4 - 15

(c) Mixture of corrosion products (Fe, Cr, Zr) which precipitate as the oxides in the reactor.

(d) Mixture of corrosion products (approximately 87 mole % Ni and 13 mole % Mn) which are soluble in the fuel solution.

(e) Resonance σ_a only.

Table F.2 Group Structure for GNU Program

Group	Lethargy Width (Δu)	Energy Range (ev)
1	0.91629	$4 \times 10^6 - 10^7$
2	0.69315	$2 \times 10^6 - 4 \times 10^6$
3	0.69315	$1 \times 10^6 - 2 \times 10^6$
4	1.20400	$3 \times 10^5 - 1 \times 10^6$
5	1.09860	$1 \times 10^5 - 3 \times 10^5$
6	1.02400	$3 \times 10^4 - 1 \times 10^5$
7	1.09860	$1 \times 10^4 - 3 \times 10^4$
8	1.02400	$3 \times 10^3 - 1 \times 10^4$
9	1.09860	$1 \times 10^3 - 3 \times 10^3$
10	0.91629	400 - 1000
11	0.98083	150 - 400
12	0.40547	100 - 150
13	0.10536	90 - 100
14	0.11778	80 - 90
15	0.20764	65 - 80
16	0.26236	50 - 65
17	0.10536	45 - 50
18	0.19574	37 - 45
19	0.11441	33 - 37
20	0.09531	30 - 33
21	0.18232	25 - 30
22	0.22314	20 - 25
23	0.16252	17 - 20
24	0.23052	13.5 - 17
25	0.30010	10 - 13.5
26	0.28768	7.5 - 10
27	0.31015	5.5 - 7.5
28	0.31845	4 - 5.5
29	0.47000	2.5 - 4
30	0.57982	1.4 - 2.5
31	0.55962	0.8 - 1.4
32	0.28768	0.6 - 0.8
33		5.5 kT - 0.6
34		kT - 5.5 kT

In the range 10-30 ev, η was estimated to be 2.17; the data of Gaerttner and Yeater (80) indicate an average η in this range of about 0.95 times the 2200 m/sec value. From 30 ev to 30 kev, η was assumed to be 2.25; this is the value reported by Spivak (102) at 30 kev.

From 30-900 kev, measurements of η are available (102); fission cross sections are reported in BNL-325 (98) for the range 30 kev to 10 Mev. The total cross section in this range was taken equal to that of U-235 as suggested by Harvey (103). The value of ν was assumed to be linear in energy with a 2200 m/sec value of 2.50 (101) and a slope of 0.127 per Mev (104).

A plot of experimental values of η and group-averaged values for the energy range 0.01 ev to 1 kev is shown in Fig. F.1.1.

The group-averaged data on η-233 which were analyzed by Nestor (24) are given in Table F.3. Values (labeled MTR) from the Materials Testing Reactor (101) were the latest available values as of the Fall of 1959 and were used in the study; other values (labeled RPI) are taken from the work of Yeater, et al (130), which became available only after the calculations were nearly finished. The RPI values are not considered more reliable than the MTR data except in the energy range 30 ev to 1 kev where the RPI data represent the only measurements that have been made. The variation of eta in this range has only a small effect on the nuclear performance, as shown in Sec. 7.4.

Protactinium-233. - The 2200 m/sec cross section and the resonance integral were taken to be 70 b and 1200 b respectively as reported by Stoughton and Halperin (105). Multigroup absorption cross sections were prepared assuming a single Breit-Wigner resonance at 1 ev is responsible for the entire cross section. This assumption leads to a total width Γ for the resonance of about 55 ev. However, more recent data (139), obtained after this study had been started, indicate that the resonance integral might have a value as small as 900 barns.

FIG. F I.I GROUP VALUES OF $\eta^{23}(E)$ PRESENTLY BEING USED IN THORIUM BREEDER REACTOR STUDY

UNCLASSIFIED

ORNL-LR-DWG 46875 R

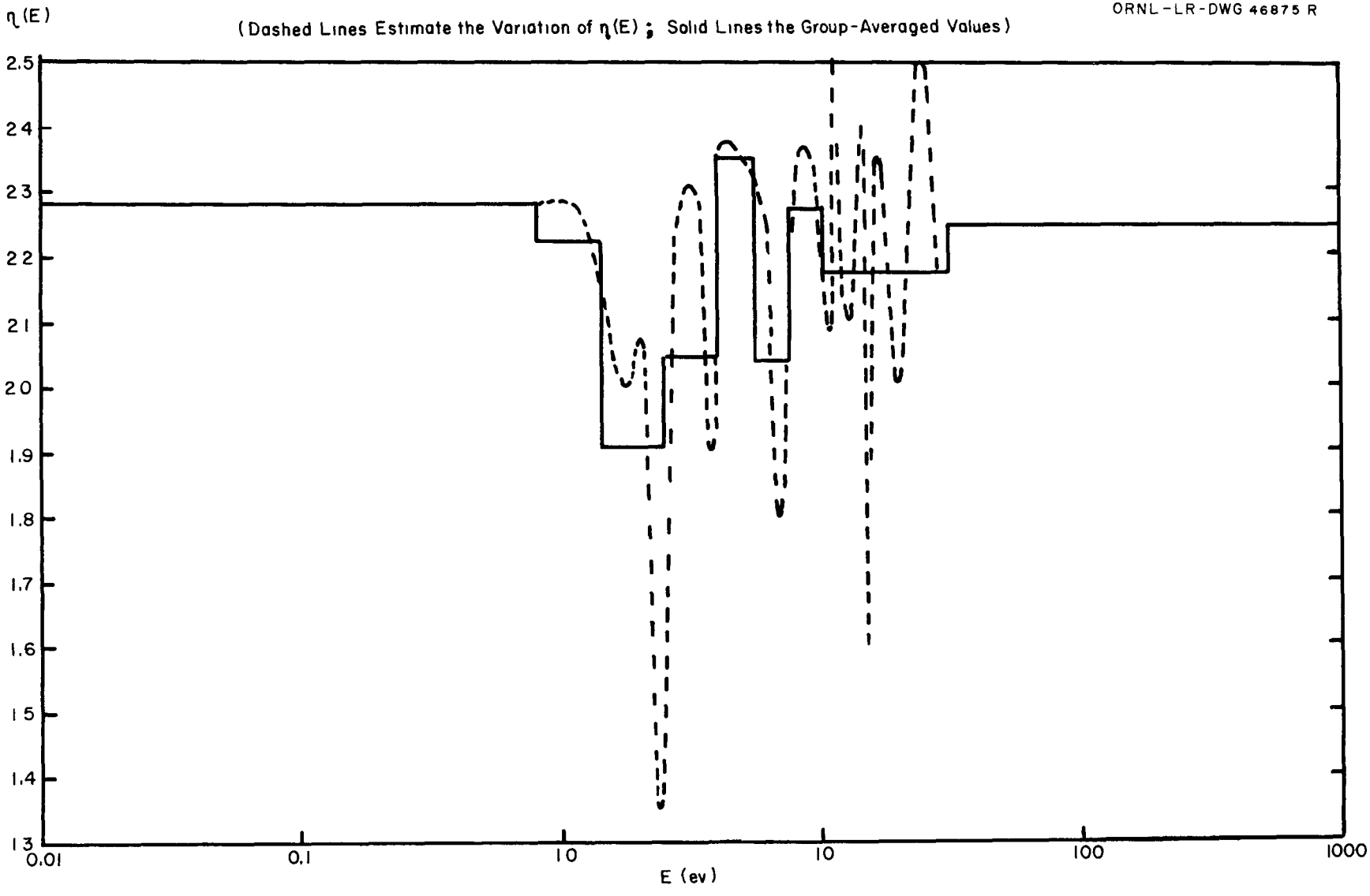

Table F.3 Group-Averaged Values of η-233

Group	Energy (ev)	η(MTR)	η(RPI)
1	$4x10^6$ - 10^7	3.39	3.39
2	$2x10^6$ - $4x10^6$	2.87	2.87
3	$1x10^6$ - $2x10^6$	2.69	2.69
4	$3x10^5$ - $1x10^6$	2.51	2.51
5	$1x10^5$ - $3x10^5$	2.37	2.37
6	$3x10^4$ - $1x10^5$	2.28	2.28
7	$1x10^4$ - $3x10^4$	2.25	2.25
8	$3x10^3$ - $1x10^4$	2.24	2.24
9	$1x10^3$ - $3x10^3$	2.25	2.25
10	$4x10^2$ - $1x10^3$	2.25	1.9
11	150 - 400	(2.25)	1.72
12	100 - 150	(2.25)	1.78
13	90 - 100	(2.25)	1.54
14	80 - 90	(2.25)	1.68
15	65 - 80	(2.25)	1.77
16	50 - 65	(2.25)	1.93
17	45 - 50	(2.25)	1.96
18	37 - 45	(2.25)	1.70
19	33 - 37	(2.25)	1.97
20	30 - 33	(2.25)	2.06
21	25 - 30	2.16	1.91
22	20 - 25	2.16	1.93
23	17 - 20	2.16	1.75
24	13.5 - 17	2.17	1.88
25	10 - 13.5	2.17	2.06
26	7.5 - 10	2.28	1.91
27	5.5 - 7.5	2.07	1.96
28	4 - 5.5	2.18	1.99
29	2.5 - 4	2.05	1.96
30	1.4 - 2.5	1.91	2.07
31	0.8 - 1.4	2.23	2.23
32	0.6 - 0.8	2.29	2.29
33	5.5 kT - 0.6	2.28	2.28
34	kT - 5.5 kT	2.28	2.28

( ) - Interpolated values

Samarium-151. - The preliminary measurements of Cocking (39) can be represented by two straight line segments on a log-log plot connecting the points

E,ev	σ(E), barns
0.01	25,000
0.10	5,000
1.00	500

This fit was used to calculate group-averaged cross sections for this isotope in the low energy groups.

Resonance parameters from BNL-325 (98) were used to calculate values of the infinite dilution resonance integral; in this calculation it was assumed that the entire contribution to the resonance integral of each resonance is concentrated in the group in which the resonance lies. Pertinent group-averaged cross sections and resonance integrals are given in Table F.4.

Table F.4 Group-Averaged Cross Sections and Infinite Resonance Integrals for Sm-151

Group	E_o(ev)	$g\Gamma_n$ (mv)	Γ_γ (mv)	I_∞ (barns)	$\bar{\sigma}_a$ (barns)
27	6.30	1.65	63	170	550
28					0
29	4.10	0.25	63	61	130
30	1.70	0.13	63	184	720
30	2.04	0.24	63	235	
31	1.10	0.30	63	1020	2300
32					725

Fissium. - Data on gross fission products as compiled by Pattenden (79) were used in preparing multigroup cross sections for the pseudo element fissium. The energy variations were assumed to be 1/v up to 0.6 ev with a 2200 m/sec value of the absorption cross section of 50 barns/fission. From 0.6-100 ev the curve computed by Gordeev and Pupko (reprinted in Ref. 79) for U-235 was used to calculate the group-averaged cross sections. This procedure gives a resonance integral of 150 barns/fission. If the fission product yields for U-233 fissions are substituted into Pattenden's table for U-235, a resonance

integral of 138 barns/fission is obtained. The Gordeev and Pupko curve is therefore a reasonable check on Pattenden's data. This curve and group-averaged values of the absorption cross section are shown in Fig. F.2.1.

Bismuth. - Neutron losses to the bismuth carrier in the LBBR were estimated using the method adopted previously by Thomas (22). A value of zero was assigned to the absorption cross section at all energies above thermal, and to account for resonance absorptions the thermal cross section was increased by 50%.

MSBR Fuel and Blanket Salts. - The fuel and fertile stream carriers were entered in the machine calculations as two single elements possessing pseudo cross sections. Cross sections were calculated for each energy group, by weighting the individual cross sections as shown in Eqs. F-3 and F-4 and summing the results over the atoms that make up the salt. The sum was then normalized to the basis of one particular atom in the salt so that the concentration of the salt could always be expressed in terms of the concentration of this atom. The fuel salt was normalized to the basis of the Li-7 concentration; the blanket salt to the basis of the Th concentration.

For the fuel salt, the group-wise cross sections are (see table below)

$$\sigma_i = \frac{\sum_j f_j \sigma_{ij}}{f_{Li^7}} \quad \text{(barns/atom } Li^7\text{)} \qquad \text{(F-3)}$$

and for the blanket salt

$$\sigma_i = \frac{N_{Li^7}}{N_{Th}} \sigma_{Li^7} + \frac{N_{Li^6}}{N_{Th}} \sigma_{Li^6} + \frac{N_{Be}}{N_{Th}} \sigma_{Be} + \frac{N_F}{N_{Th}} \sigma_F \,, \qquad \text{(F-4)}$$

in which σ_i is expressed in the units of barns/atom Th. The cross section of thorium is omitted in Eq. F-4 because thorium is treated as a separate element in the calculations.

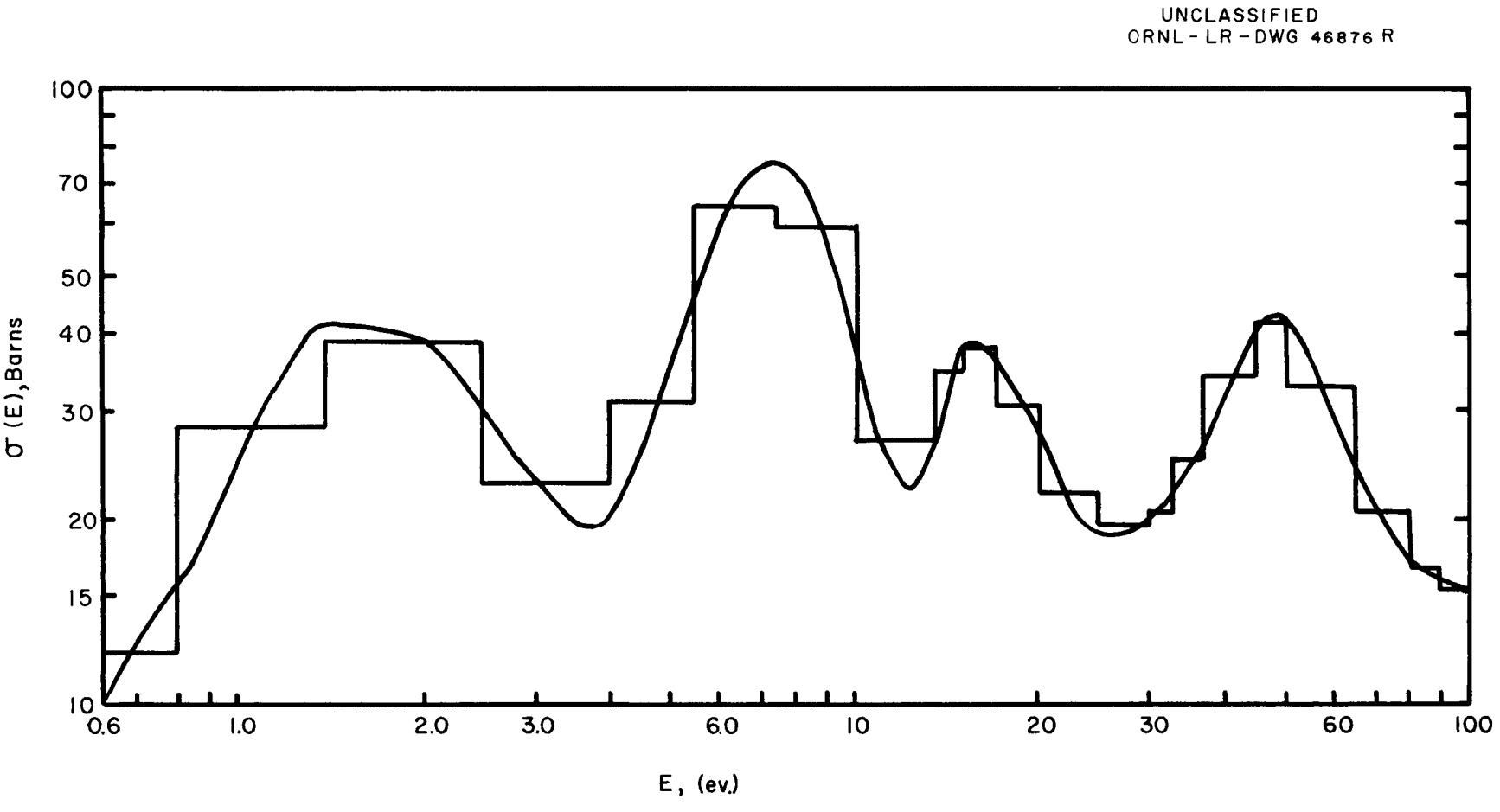

FIG. F.2.1. "FISSIUM" CROSS SECTIONS

In Eqs. F-3 and F-4,

σ_i = cross section for i-th energy group,
f_j = atom fraction of j-th atom,
σ_{ij} = cross section of j-th atom in the i-th energy group,
f_{Li7} = atom fraction Li-7,
N = atom density of indicated species.

In the MSBR studies it was assumed that the reactor would be charged with fuel and fertile salts in which the lithium component was 99.999 atom % Li-7. The salt compositions are given in the footnotes to Table F-1. Salts of low Li-6 content are highly desirable during the transient period of the reactor for a faster approach to equilibrium and better breeding performance during the period in which Li-6 is burning out. However, because of the preminium price for such high purity salt, it was further assumed that the equilibrium reactor would be supplied with replacement salts that are 99.99 atom % Li-7, and that the Li-6 concentration in the reactor would be the equilibrium concentration. The Li-6 concentration therefore becomes a function of the salt replacement rate. In all equilibrium reactor calculations (ERC-5 code) account was taken of the equilibrium Li-6 content, and neutron losses were computed for this condition.

Corrosium-I and Corrosium-II in AHBR. - These two pseudo elements were used to account for nuclear interactions with stainless steel and zirconium corrosium products in the AHBR. Corrosium-I represents the corrosion products which precipitate as oxides in AHBR fuel solution; these are iron, chromium, and zirconium. Corrosium-II represents the soluble fission products, viz., nickel and manganese. Cross sections for each energy group were calculated for these two pseudo elements by a procedure similar to that discussed above for the MSBR fuel and fertile stream salts. The cross sections of Corrosium-I were normalized on the basis of the number of chromium atoms; those of corrosium-II were normalized to the basis of the number of nickel atoms.

In computing the cross section for a particular energy group for corrosium-I, it was assumed that equal weights of the three atoms would be present in the fuel solution. Hence the expression for the cross section becomes

$$\sigma_I = \sigma_{Cr} + \frac{M_{Cr}}{M_{Fe}} \sigma_{Fe} + \frac{M_{Cr}}{M_{Zr}} \sigma_{Zr} \quad , \tag{F-5}$$

where M refers to the molecular weight of the indicated species, σ_I has the units barns per atom Cr.

Group-wise cross sections for corrosium-II were obtained from

$$\sigma_{II} = \sigma_{Ni} + \frac{f_{Mn}}{f_{Ni}} \sigma_{Mn} \quad , \tag{F-6}$$

where f refers to the atom fraction of the indicated species. In the AHBR the ratio f_{Mn}/f_{Ni} is 0.15. σ_{II} has the units barns per atom Ni.

A P P E N D I X G

Bi-Directional Loading in Solid Fuel Reactors

APPENDIX G

Bi-Directional Loading in Solid Fuel Reactors

1.0 Introduction

It seems certain that, in the long run, designers of solid fuel power reactors will be forced to provide for continuous loading of mobile fuel elements in order to achieve higher efficiencies in the use of the fuel and of the reactor. Current batch-loading techniques result in considerable downtime during which no power is produced. Further, the burnout proceeds at different rates in different parts of the reactors, and when the fuel is stationary, peripheral elements are scarcely used by the time central elements have reached the limit of their exposure. These and other advantages of continuous fueling have been reviewed by Foster, et al (106).

If the fueling is done continuously, then there are further advantages in fueling at both ends of the reactor so that fuel elements travel in opposite directions in adjacent channels. As shown below, concentrations of fissionable isotopes and fission products remain remarkably uniform when these are averaged over adjacent channels. Further, if the fueling rate in a channel is made proportional to the fission rate in that channel, the burnup in that channel can be made the same as in every other channel. That is to say, the fuel elements are charged seldom and move slowly in a peripheral channel, are charged often and move quickly in central channels. In this way the average concentration of fission products and fissionable isotopes can be made nearly uniform over a cross section of the core. Also, every fuel element may be given the maximum allowable exposure.

2.0 Theory

The change of concentration of fuel in an element with position of the element in a channel is

$$dN/dx = (dN/dt)\,(dt/dx) \qquad (G\text{-}1)$$

where N denotes concentration of fuel, x position of an element with respect to the entrance to the core, and t represents time. The rate of depletion is proportional to the concentration, the flux, and the cross section for neutron absorption.

$$dN/dt = \phi(x)\, N(x)\, \sigma_a \qquad (G\text{-}2)$$

Approximately, the flux will have a cosine distribution.

$$\phi(x) = K' \mathrm{Cos}\, (1 - \frac{2x}{\ell}) \frac{\pi}{2} \qquad (G\text{-}3)$$

where ℓ is the active length of the fuel channels, and K' is proportional to the reactor power.

The term, dt/dx, is the reciprocal of the velocity.

$$dt/dx = T/\ell \qquad (G\text{-}4)$$

where T is the residence time in the fuel channel. Combining these equations and integrating from a channel inlet to any arbitrary position, x, gives

$$N_x/N_o = \exp -K\, [(1 - \mathrm{Sin}(1 - \frac{2x}{\ell}) \frac{\pi}{2}\,] \qquad (G\text{-}5)$$

where N_o is the concentration in fresh fuel elements at the charging end, and

$$K = K'\sigma T/\ell\ . \qquad (G\text{-}6)$$

The constant K may be eliminated by relating it to the burnup. At the discharge end,

$$x = \ell$$

and

$$N_e/N_o = (1 - B) \qquad (G\text{-}7)$$

where B is the burnup fraction and N_e is the concentration at the end of the core. Substituting this into Eq. G-5 gives for K

$$K = -\frac{1}{2} \ln (1 - B)\ . \qquad (G\text{-}8)$$

Putting this back into Eq. G-5 gives

$$N_x/N_o = (1 - B)^{1/2}\, [1 - \mathrm{Sin}\, (1 - \frac{2x}{\ell}) \frac{\pi}{2}] \qquad (G\text{-}9)$$

At the midplane of the reactor

$$N_m/N_o = \bar{N}_m/N_o = (1 - B)^{1/2} \qquad \text{(G-10)}$$

where $\bar{N}_m$ is the concentration at the midplane averaged over adjacent channels. At the ends of the core, the discharge concentration, given by definition in Eq. G-7, is to be averaged with the concentration in a fresh element.

$$\bar{N}_e/N_o = 1/2\ [(1 - B) + N_o/N_o)] = 1 - B/2 \qquad \text{(G-11)}$$

Taking a ratio between Eqs. G-11 and G-10,

$$\bar{N}_m/\bar{N}_e = (1 - B)^{1/2}/(1 - \frac{B}{2}) \qquad \text{(G-12)}$$

By similar procedures, the concentration of fission products at the midplane is found to be related to the mean concentration at the core ends by

$$\bar{F}_m/\bar{F}_e = 2\ [1 - (1 - B)^{1/2}]/B \qquad \text{(G-13)}$$

where $\bar{F}_m$ is the mean concentration of fission products at the midplane and $\bar{F}_e$ is the concentration at the ends of the core averaged over adjacent channels.

3.0 Results

The values of the two ratios derived above are tabulated below for various burnups.

Concentration Ratios for Fuel and Fission Products in Bi-Directionally Loaded Reactors

Burnup Fraction	Fuel Ratio $\bar{N}_m/\bar{N}_e$	Fission Product Ratio $\bar{F}_m/\bar{F}_e$
0.1	0.999	1.02
0.2	0.995	1.05
0.3	0.985	1.09
0.4	0.986	1.13
0.5	0.943	1.17

4.0 Conclusions

From a consideration of the values of the ratios, it is inferred that the physics calculations for bi-directionally loaded solid fuel reactors can, to a first degree of approximation, be carried out with the assumption that the concentrations of fuel isotopes and fission products are nearly uniform over the core of the reactor, provided the burnup is not more than 40 or 50%.

APPENDIX H

Equilibrium Reactor Calculations: ERC-5 Program for the IBM-704

APPENDIX H

Equilibrium Reactor Calculations: ERC-5 Program for the IBM-704

1.0 Introduction

When a breeder reactor with on-site processing is operated a long time with steady feed and recycle rates under conditions that do not allow any substance to accumulate in the system without limit, the compositions of the various inventories and product streams approach equilibrium values asymptotically. Of particular importance in a thorium breeder reactor are the relative concentrations of higher isotopes of uranium in the fuel recycle stream at equilibrium. The rates of burnup relative to removal of fission products are also important. Here, the flux level, which is related to reactor power, also has an important bearing.

The ERC-5 program for the IBM-704 was developed primarily to compute the equilibrium states of the two-region, thermal-breeder reactors being studied by the Thermal Breeder Reactor Evaluation group at ORNL in 1959-60. These reactors originally comprised an aqueous homogeneous breeder reactor (AHBR), a graphite-moderated molten-salt reactor (MSBR), a graphite-moderated liquid-bismuth reactor (LBBR), a graphite-moderated gas-cooled reactor (GGBR), and a deuterium-moderated gas-cooled reactor (DGBR).

The AHBR had a solution core and a thorium oxide pellet blanket. The fuel stream penetrated one end-blanket. In the MSBR, the molten fuel carrier was passed through bayonet tubes inserted into holes in graphite moderator structure. The tubes were surrounded by thin annuli of molten salt containing dissolved ThF_4. This salt flowed through the annuli into the blanket region. The arrangement in the LBBR was similar except that fuel- and fertile-stream channels in the core were parallel rather than concentric. The GGBR employed fuel elements consisting of UO_2 dispersed in graphite fuel plates. These were loaded quasi-continusouly at power from both ends of the reactor with counter-current motion in alternate channels. The blanket consisted of thorium oxide pellet beds as in the AHBR. The DGBR was similar to the GGBR, except that the moderator, D_2O, was contained in a Zircaloy calandria. Also, some of the fertile stream (ThO_2 pellets) passed through the core region. The ERC-5 program was written as a generalized program capable of treating these diverse cases as well as others.

The equilibrium state of a nuclear reactor is here defined as the state resulting from steady operation for an indefinite period with quasi-continuous processing of fuel and fertile materials, and quasi-continuous loading and discharge of fuel and fertile materials at full power. The general case is treated wherein the fuel material may traverse the blanket region with an appreciable residence time and part of the fertile material may traverse the core region, as indicated schematically in Fig. H.1.1.

In circulating fuel reactors, the fuel stream passes through a pump and is recirculated rapidly. A small side-stream is withdrawn quasi-continuously and sent to processing. The concentration of any component in the side-stream is the same as that in the circulating stream. In solid fuel reactors, however, fuel elements are normally sent to processing after withdrawal and the discharge concentration of a given isotope may be appreciably different from the mean concentration in the core. Similar considerations apply to fluid versus solid fertile streams. Provision in ERC-5 was made for treating the various combinations that arise.

The philosophy of sales management affects the equilibrium state of a breeder. If pure U-233 should have a premium value sufficiently large, the reactor operator will sell bred material and recycle all of the spent fuel from the core. This causes U-234, U-235, and U-236 to accumulate to high levels since they disappear from the system only by neutron capture. As a result, the breeding ratio is low due to the large contribution to the fission rate of fissions in U-235 and due to large parasitic losses to U-236. If, on the other hand, spent fuel is nearly as valuable as U-233, the operator will recycle all of the bred material and sell spent fuel. This helps to remove U-234, etc., from the system and thereby improves the nuclear performance and increases income from sales. Again, if it is desired to compute a meaningful doubling time from the equilibrium nuclear performance, then it is necessary that the product sold shall be a mixture of spent fuel and freshly bred fuel such that the composition of the mixture is the same as the average composition of the entire reactor complex, including inventories in processing, in reserve, etc.

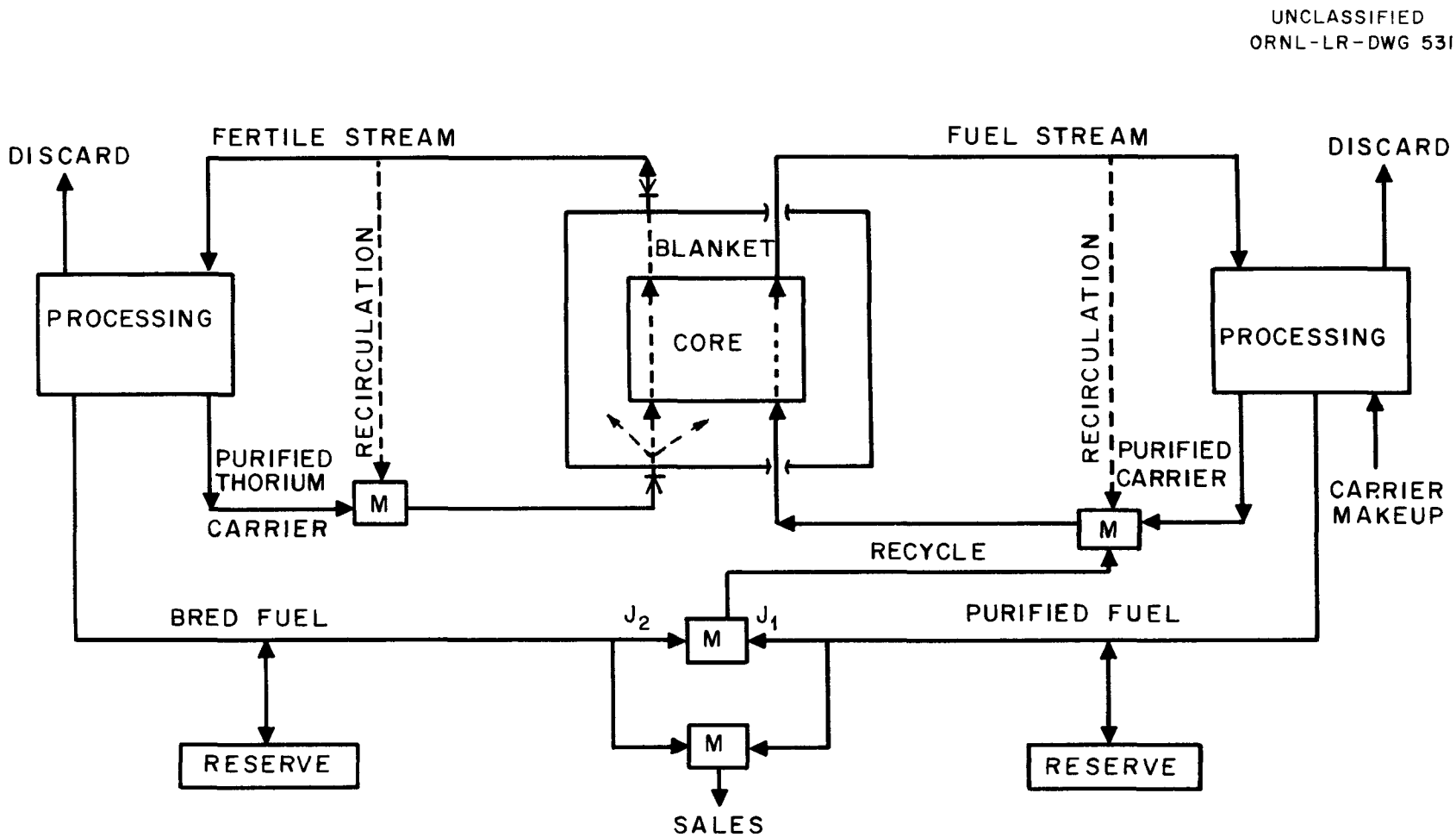

Fig. H.1.1. Generalized Two-Region Breeder.

Of lesser importance is the choice of composition of fuel held in reserve. This inventory can consist of spent fuel, of freshly bred fuel, or a mixture. In reactors operated so that the excess fuel sold has the same composition as the average of the complex, the performance of the reactor is favored by reserving spent fuel, as this increases slightly the amount of U-234, and higher isotopes in the sale-product.

For the purposes of economic evaluation, it is desirable to vary the processing cycle times widely.

The principal restraints imposed on the system of equilibrium equations are: (a) conservation of mass, (b) conservation of neutrons, and (c) criticality. The equations were programmed for the IBM-704; details of the derivations, input, and output formats are given in reference 86 . An extract concerning the most important features of the calculation is given in the following sections of this appendix.

2.0 Reactor Rate Coefficients

Of those elements whose concentrations vary in the approach to equilibrium, (excepting U-233, which is subject to a criticality condition), the governing equilibrium equations are adapted from a generalized isotope equation derived in Section 3.0. The sources of nuclides comprise feed, beta decay, fission yield, and neutron capture. Sinks comprise processing, beta decay, and neutron capture (both fission and n,γ). Of these sources and sinks, only those resulting from neutron capture are dependent upon distribution of the neutron population in space and energy. This dependency may be conveniently expressed by means of reactor rate coefficients defined as follows

$$C^{m}_{i,j,k} = \int_{V_k} \int_{u=0}^{u=\infty} \phi(u,\bar{r})\, \sigma^{m}_{i}\, du\, dV(\bar{r}) \qquad \text{(H-1)}$$

where i denotes the i-th isotope in stream j (fuel or fertile stream) passing through region k (core or blanket) of the reactor, m denotes the type of reaction (absorption, fission, or capture), V_k denotes the volume of the k-th region, ϕ is the neutron flux in neutron-cm per cc per neutron born in the reactor , and other symbols have their customary significance.

When an integral so defined is multiplied by the mean atomic concentration of the corresponding isotope, $f_{j,k}\ N_{i,j}$ (where $f_{i,j}$ is the fraction of the k-th region occupied by the j-th stream, and $N_{i,j}$ is the atomic concentration of the i-th isotope in the j-th stream) and by the birth rate of neutrons in the reactor NuF (where Nu is the neutron yield and F is the fission rate in fissions per second), the product, $\text{NuF}\ f_{j,k}\ N_{i,j}\ C^m_{i,j,k}$, is the neutron reaction rate in events per second in the reactor for reactions of the m-th kind with the i-th isotope in stream j in region k. The reaction rate is a source or a sink in an appropriate isotope equation.

The usefulness of the reaction rate coefficients C is that they are conveniently obtained from the results of a multigroup diffusion calculation performed by means of the GNU program for the IBM-704. Specifically

$$C^m_{i,j,k} = E^m_{i,j,k} / f_{j,k}\ N_{i,j} \tag{H-2}$$

where $E^m_{i,j,k}$ is the fraction of neutrons born in the reactor that disappear as a result of reactions of the m-th kind with atoms of the i-th kind in the j-th stream in region k. The denominator is part of the input data to the machine, and the numerator is obtained from the machine output.

Of course, the various isotope concentrations in a GNU calculation upon which an ERC calculation is based must not be too different from those of the equilibrium state, else the reaction coefficients C will not be valid. However, the coefficients C are determined principally by the spectrum and intensity of the neutron flux in a region. They are insensitive to minor changes in moderator-fuel ratio and distribution of fissions between core and blanket, and to major changes in concentration of secondary elements, such as fission products, Pa-233, etc.

In a GNU calculation, the neutron balance is computed from

$$b = \sum_i \int_u \int_v N_{i,j}\ f_{j,k}\ \sigma^a_i\ \phi(u,\bar{r})\ du\ dV(\bar{r}) \tag{H-3}$$

The fluxes generated by the solution of the group-diffusion calculation are such that the balance b is very close to unity. If now changes are made in the $N_{i,j}$, and the GNU calculation is repeated, a new balance will be obtained.

$$b + \Delta b = \sum_i \int_u \int_v (N_{i,j} + \Delta N_{i,j})\, f_{j,k}\, \sigma_i^a\, [\phi(u,\bar{r}) + \Delta\phi(u,\bar{r})]\, du\, dV(\bar{r})$$

However, the new fluxes generated will be such that the new balance is also near unity, and therefore Δb is approximately zero. By subtracting Eq. H-1 from Eq. H-2, one finds, to a first order approximation:

$$\sum_i \int_u \int_v \Delta N_{i,j}\, f_{j,k}\, \sigma_i^a\, \phi(u,\bar{r})\, du\, dV(\bar{r}) = -\sum_i \int_u \int_v N_{i,j}\, f_{j,k}\, \sigma_i^a$$

$$[\phi(u,\bar{r}) + \Delta\phi(u,\bar{r})]\, du\, dV(\bar{r}) \quad .$$

Or, making use of the definition of C in Eq. H-1

$$\sum_{i,j,k} \Delta N_{i,j}\, f_{j,k}\, C^a_{i,j,k} = -\sum_{i,j,k} N_{i,j,k}\, f_{j,k}\, \Delta C^a_{i,j,k} \quad . \tag{H-4}$$

The approximation that

$$\Delta C^a_{i,j,k} = B\, C^a_{i,j,k} \tag{H-5}$$

is now introduced, where B is the same for all i.

Substituting into Eq. H-4 and solving for B gives

$$B = \frac{-\sum_{i,j,k} \Delta N_{i,j}\, f_{j,k}\, C^a_{i,j,k}}{\sum_{i,j,k} N_{i,j}\, f_{j,k}\, C_{i,j,k}} = -\sum_{i,j,k} \Delta N_{i,j}\, f_{j,k}\, C^a_{i,j,k} \tag{H-6}$$

Since the denominator is unity, by Eq. H-3.

If the input to ERC-5 is correctly composed, the initial value of B will equal the neutron balance b (~ unity) of the basic GNU case. The equilibrium equations will then operate on these concentrations, changing them, and thereby changing B.

$$\Delta B_n = \sum_{i,j,k} (N^n_{i,j,k} - N^1_{i,j,k}) f_{j,k} C^a_{i,j,k} \qquad \text{(H-7)}$$

Substituting this into Eq. H-6, and making use of Eq. H-5, one finds

$$(C^a_{i,j,k})_n = C^a_{i,j,k} (1 - \Delta B_n) \qquad \text{(H-8)}$$

But

$$1 - \Delta B_n \cong 1/(1 + \Delta B_n); \text{ if } \Delta B_n \leqslant 0.05 \qquad \text{(H-9)}$$

and B_1 is approximately unity. Therefore,

$$(C^a_{i,j,k})_n \cong \frac{C^a_{i,j,k}}{B_n} \qquad \text{(H-10)}$$

very closely.

Thus, to a first degree of approximation, the reaction rate coefficients are given by the quotient of the initial coefficients and the flux factor. Therefore, in all equations where rate coefficients appear, except in Eq. H-1, they are divided by B_n.

3.0 General Isotope Equation

Let the volume of a circulating stream (fuel or fertile, and including any portion external to the reactor in pumps, etc.) be denoted by V_j, where j denotes the stream, and let $N_{i,j}$ be the concentration in atoms per unit volume of an isotope of the i-th kind. The rate of change of the number of atoms of the i-th kind in stream j, symbolized by $V_j (dN_{i,j}/dt)$, where t is time, may be equated to the sum of the sources and sinks, in stream j, of atoms of the i-th kind.

Beta decay of atoms of the i'-th kind may be a source. The rate of formations is equal to $V_j N_{i',j} \lambda_{i'}$, where $\lambda_{i'}$ is the decay constant of the precursor atom. Again, atoms of the i-th kind may be formed by capture of a neutron in an atom of the i"-th kind; the source being equal to the sum $N_{i",j} \sum_k f_{j,k} C^c_{i",j,k}$. Atoms of the i-th kind may be brought in from the other stream (the j'-th), the rate being given by $\delta_{i,j'} N_{i,j,d} V_{j'} E_{i,j'} \epsilon_{i,j'} J_{j'} / t_{j'}$, where $\delta_{i,j'}$ is either 1.0 or 0.0, depending on whether the isotope is removed from the j-th stream by processing or not, $N_{i,j',d}$ is the reactor <u>discharge</u> concentration in the j'-th stream which is different from the mean concentration, $N_{i,j}$, if the stream makes only one pass through the reactor before being processed, as in reactors having solid fuel or blanket elements. The relation between $N_{i,j}$ and $N_{i,j,d}$ for several specific isotopes is derived in reference 86. $E_{i,j}$ is the efficiency of removal in the process plant of the i-th isotope from the j-th stream expressed as a fraction per pass through the process plant. The quantity $\epsilon_{i,j}$ is the efficiency with which the i-th isotope is recovered from the processing plant, the fraction $1 - \epsilon_{i,j}$ being lost in various ways. J_j is the fraction of the fissile atoms removed from the j-th stream that are <u>recycled</u>, the fraction $1 - J_j$ being sold.

Finally, atoms of the i-th kind may be formed by the fission reaction; the rate is $F f_j Y_i$, where F is the fission rate, fissions per second, f_j is the fraction of all fissions taking place in the j-th stream, and Y_i is the fission yield of atoms of the i-th kind, atoms per fission.

Atoms of the i-th kind may be removed from the j-th stream by decay, neutron absorption, and processing and the terms are similar in form to the source terms. One has

$$\frac{V_j dN_{i,j}}{dt} = N_{i',j} V_j \lambda_{i'} + N_{i",j} \sum_k f_{j,k} C^c_{i",j,k} + \delta_{i,j'} N_{i,j'} V_{j'} E_{i,j'} \epsilon_{i,j'} J_{j'} / t_{j'}$$

$$- N_{i,j} V_j \lambda_i - N_{i,j} \sum_k f_{j,k} C^c_{i,j,k} - \delta_{i,j} N_{i,j} V_j E_{i,j} \epsilon_{i,j} J_j / t_j$$

$$+ f f_j Y_i \qquad \text{(H-11)}$$

In the steady state, the derivative is zero. $N_{i,j,d}$ may be replaced by the appropriate function of $N_{i,j}$ and the equation solved for $N_{i,j}$.

In circulating fuel reactors, the concentration of any isotope in the side stream sent to processing is, for all practical purposes, equal to the mean concentration in the circulating stream which also differs negligibly from the mean reactor concentration. In reactors in which the fuel or fertile stream makes only one pass through the reactor, or, if recycled, is not mixed with fresh feed, the discharge concentration, $N_{i,j,d}$, may differ appreciably from the mean reactor concentration, e.g., the discharge concentration of U-233 in the fertile stream of such a reactor will be approximately twice the mean concentration (for long exposure times). The derivations of the various equations, which are straightforward but rather tedious, will be found in reference 86.

4.0 Criticality Conditions and U-233 in Fuel Stream

The concentration of U-233 in the fuel stream was made subject to the criticality requirements, viz:

$$k = \frac{1}{B} \sum_{i,j,k} f_{j,k} N_{i,j,k} Nu_i C^f_{i,j,k} = 1.0000 \pm \delta_c \qquad \text{(H-12)}$$

Since the concentration of U-235 ($N_{5,1}$) is linked to that of U-233 by equilibrium equations, it is necessary to iterate an inner loop involving U-233, U-234, and U-235 in order to satisfy criticality and equilibrium conditions simultaneously.

By perturbation of the critical equation,

$$N^{n,s}_{3,1} = \frac{B_n - \sum_{i,j,k} f_{j,k} Nu_i N^n_{i,j} C^f_{i,j,k}}{Nu_3 \sum_k f_{1,1} C^f_{3,1,k}} + N^{n,s-1}_{3,1} \qquad \text{(H-13)}$$

where s is the inner loop iteration index. When the quantity $\left| N^{n,s}_{3,1} - N^{n,s-1}_{3,1} \right| \div N^{n,s}_{3,1}$ is less than δ_c, the calculation is terminated.

In circulating fuel reactors, the discharge concentration is equal to the time-mean concentration (W = 0.0); in station fuel reactors, the U-233 burns out exponentially (W = 1.0).

$$N^n_{3,1,d} = N^n_{3,1}\,(1-W) + \frac{W N^n_{3,1}\,\alpha T_1\, e^{-\alpha T_1}}{1 - e^{-\alpha T_1}} \qquad \text{(H-14)}$$

$$\alpha = \frac{F\,\overline{Nu}}{B_n V_1}\, f_{1,1}\, C^a_{3,1,1} \qquad \text{(H-15)}$$

5.0 Sales Ratio and Recycle Fractions

In this study, it was desired that the recycle fractions J_j in Eq. H-11 should have values such that the product sold would have the same average composition as the mixture of isotopes in the entire system, including processing plants, etc. As shown in reference 86, this condition is satisfied when the ratio of the sales fractions, $1-J_j$, is made equal to the ratio of the sum of the holdup times in the fuel and fertile stream processing cycles (including residence time in the reactor); i.e.,

$$\frac{1 - J_1}{1 - J_2} = \frac{\sum_e t_{e,1}}{\sum_e t_{e,2}} = R \qquad \text{(H-16)}$$

where the t_e's are the holdup times for fuel isotopes in the various steps of the process or exposure in the reactor, subscript 1 refers to fuel stream, and 2 to the fertile stream, and R is the sales ratio.

Since the J's must also satisfy a material balance, they are uniquely determined as soon as a value of R is assigned.

6.0 Input

P (Station Power). - The total thermal power in Mw is entered here.

W (Fuel-Stream Option). - For circulating fuel reactors, set W = 0.0; for stationary fuel reactors, set W = 1.0.

R_o (Sales Option). - Setting R_o = 0.0 causes the code to compute a ratio for mixing fuel and fertile streams such that the composition of the mixture equals that of the reactor complex.

S (Fertile Stream Option). - If the fresh fertile material is added continuously and is well mixed with irradiated material, S = 0.0. If, on the other hand, fertile material is added batchwise and the batches are segregated and not mixed with prior or subsequent batches (though a batch may be stirred or "self-mixed" to maintain uniformity of concentration within the batch), S = 1.0.

By setting S equal to zero, the concentrations of any isotope in the discharge to the process plant is made equal to the time-mean concentration in the fertile stream in the reactor. With S equal to one, the concentrations of Pa-233 and U-233 are computed from equations which average over the residence time and account for exponential decay and neutron capture rates.

T (Criticality Option). - To achieve criticality by adjusting the concentration of U-233 in the fuel stream, T = 1.0; by adjusting the volume fraction of fertile stream in core (see definition of $f_{2,1}$ below), T = 2.0.

$f_{1,1}$ (Volume Fraction of Fuel Stream in Core). - This number is the fraction of the core volume occupied by the fuel stream, whether fluid or solid, homogeneous or heterogeneous. It excludes moderator not mixed with the fuel, coolant not mixed with fuel, structural materials, etc.

$f_{1,2}$ (Volume Fraction of Fuel Stream in Blanket). - In fluid fuel reactors the fuel is sometimes passed through the end-blankets in tubes of reduced cross section, and the fuel present in these regions may give rise to an appreciable number of fissions.

$f_{2,1}$ (Volume Fraction of Fertile Stream in Core). - In some reactors, notably a version of the liquid metal fuel reactor and a molten salt breeder, part of the fertile stream is passed through the core region in separate channels. One computes $f_{2,1}$ by dividing the volume of fertile stream in the core by the volume of the core region, including structure, moderator, etc.

$f_{2,2}$ (Volume Fraction of Fertile Stream in Blanket). - This fraction is computed by dividing the volume of fertile stream in the blanket by the total volume of the blanket region.

p (Poison Override). - In operating a breeder reactor plant, it may by desirable or necessary to stop operations in the processing plant without stopping reactor and electric plant operations. The amount of fuel reserve required to override poisons is computed by the code from p, the expected decrease in the multiplication k due to accumulation of poisons in the fuel stream during the period of processing plant shutdown.

t_1 (Fuel Stream Cycle Time, days). - This number is computed by dividing the entire fuel-stream volume by the rate at which fuel is withdrawn for chemical processing.

t_2 (Fertile Stream Cycle Time, days). - This number is computed by dividing the entire fertile-stream volume by the rate at which fertile material is withdrawn for chemical processing.

t_3 (Reserve Time, days). - This is the number of days that it is desired to operate the reactor with chemical processing facilities shutdown.

t_4 (Fuel Stream Processing Time, days). - This is the time required for an atom of fuel to pass through the processing plant.

t_5 (Fertile Stream Processing Time, days). - This is the average time required for an atom of bred material to pass through the processing plant. Since Pa-233 is counted as fissionable material, t_5 must include a properly weighted time period assigned for Pa-233 decay.

U (Reserve Option). - The operator of a breeder reactor may reserve fuel having any composition ranging from that of blanket product (nearly pure U-233) to that of spent fuel. Setting U equal to 0.0 reserves spent fuel, while a U of 1.0 reserves bred material. If it is desired to reserve normal feed, set U equal to J_2/J_1.

δ_B (Convergence Criterion). - When the absolute value of the difference between successive flux factors divided by the last flux factor is less than δ_B, the calculation is stopped, and the output is edited.

δ_c (Criticality Criterion). - When the absolute difference between successive values of the concentration of U-233 divided by the concentration of U-233 becomes less than δ_c, the iteration on the inner loop is terminated.

v_1 (Volume of Fuel Stream, ft^3 per Station). - In stationary, solid fuel reactors, this volume comprises the volume of the fuel elements in the reactor only, and excludes those in the reserve and in the holdup for cooling. In fluid fuel reactors the fuel stream volume includes that in piping, pumps, heat exchangers, dump tanks, etc., external to the reactors, but again excludes fuel in reserve or being held for cooling.

v_2 (Volume of Fertile Stream, ft^3 per station). - This number includes any portion of the fertile stream exterior to the reactor, e.g., in solid blanket reactors, any fertile material that is stored outside the reactor to allow Pa to decay before being recycled for further irradiation is excluded.

$N^o_{i,j}$ (Atomic Concentration). - The concentration of i-th element in j-th stream is given in atoms per cc of stream (fluid or solid) scaled by 10^{-24}.

The initial (input) concentrations and reaction rate coefficients (see below) if correctly composed, will produce an initial balance (see Output) very close to unity. The code will then operate on concentrations of Pa-233, U-233, U-234, Np-237, fissium, Xe-135, Sm-151, and Sm-149 in both the fuel and fertile stream, and U-234, U-236, and Np-237 in the fuel stream until they satisfy the equilibrium condition.

$N_{13,2}$ provides for neutron absorptions by structure in the blanket, delayed neutrons, leakage, and any other miscellaneous losses not accounted for by prior entries. The most convenient procedure is to set $N_{13,2}$ equal to 1.0, and to enter a fictitious coefficient as discussed below under $C_{i,j}$.

$E_{i,j}$ (Processing Purge Factor). - This number is the fraction of the atoms of the i-th element in the j-th stream removed from the process stream per pass through the processing plant.

$\epsilon_{i,j}$ (Processing Recovery Factor). - This number is the probability that an atom of the i-th element from the j-th stream will not be lost in the waste from the processing plant but will be recovered. Thus ϵ should be near 1.0 for uranium isotopes, and as near 0.0 as possible for fission products. It is also desirable that ϵ for Np-237 should be low.

$C^a_{i,j,k}$ (Absorption Rate Coefficient). - This number, when multiplied by the "homogenized" atomic concentration (atoms x 10^{-24}/cc) of the i-th species of the j-th stream in the k-th region, gives the fraction of all neutrons born in the reactor that are absorbed by those atoms (see Eqs. H-1 and H-2).

$C^f_{i,j,k}$ (Fission Rate Coefficient). - This number is the corresponding fission rate coefficient, and is computed in the same way as $C^a_{i,j,k}$ from GNU output.

Permanent Constants. - Constants which are not part of the normal input:

(1) λ_1 (Decay constants, sec^{-1}).

(2) Y_i (Fission yield of i-th element): These are listed as atoms per fission. One atom of fissium corresponds to two atoms of fission products less xenon, and its precursors, and samarium.

(3) Nu_i (Neutron yield of i-th element):

M_i (Atomic mass x 10^{-3} of i-th element, AMU): For elements 9 through 13, this number is not used.

7.0 Output

Initial Balance, B_1. - If the input is correctly composed, this number should differ from 1.0000 by less than 0.005.

Final Flux Factor, B_n. - If this number differs from 1.000 by more than 0.05, the output concentrations, $N_{i,j}$, should be used to prepare a new GNU case to obtain new coefficients for a second ERC-5 calculation. Discrepancies of this magnitude indicate that the equilibrium equations have altered the concentration of fuels and heavy absorbers appreciably.

Fraction of Fissions in Fertile Stream, f_n. - This includes any fissions in thorium or other nominally "non-fissile" isotope.

Fuel Stream Recycle Fraction, J_1. - This is the fraction of the uranium atoms in the process fuel stream that are returned to the reactor after processing to remove fission products, etc. The fraction $1-J_1$ is excess and available for sale.

Fertile Stream Recycle Fraction, J_2. - This number is the fraction of the bred material (U-233 and Pa-233) leaving the blanket that is fed into the fuel stream after reprocessing. The fraction $1-J_2$ is excess fuel and available for sale.

Iteration Number, n. - This number shows the number of times the computer has calculated the flux factor B before the convergence criterion δ_B was satisfied.

Final Volume Fraction of Fertile Stream in Core, $f_{2,1}$. - The code will bring the reactor to criticality by adjusting the amount of fertile material in the core. See criticality option above.

Production Ratio, R. - This value is different from the input value R_o only when the latter is zero. This value of R_o instructs the program to compute a production ratio R such that the composition of the excess fuel sold is the same as the average composition of the entire system.

Mean Value of Neutron Yield, Nu. - This is the average neutron yield from all fissions in the reactor.

Discharge Concentration of U-233 in Fuel Stream, $N_{3,1,d}$. - In a fluid-fuel reactor this number is equal to the mean core concentration; in a solid-fuel reactor it will be appreciably different from the average core concentration.

Stream Concentrations, $N_{i,j}$. - The isotopic components of the fuel and fertile streams are listed in the left-hand column of the table. The corresponding atomic concentrations, scaled down by a factor of 10^{-24} are listed in the column under N, and are to be identified with the $N_{i,j}$'s of the input and the equilibrium equations.

Absorptions, $A_{i,j}$ - The fraction of neutrons absorbed by each element is each stream is computed. The sum is 1.0000, plus or minus a small round-off error.

Inventories, $I_{i,j}$ - The inventories in kilograms of the several species are listed.

Processing Rates, $Q_{i,j}$ - The processing rates of the several species of interest in kg/day are listed.

Fuel Stream Reserve Inventory, $I_{1,R}$ - This is the kilograms of spent fuel held up in the fuel reserve.

Fertile Stream Reserve Inventory, $I_{2,R}$ - This is the kilograms of U-233 from the fertile stream held up in fuel reserve.

A P P E N D I X I

Fuel Yield and Breeding Credit Equations

A P P E N D I X I

Fuel Yield and Breeding Credit Equations

1.0 Fuel Yield

The fuel yield, Y, of each reactor was related directly to the thermal power, breeding gain, and inventory by the following equation:

$$Y = \frac{K\ G\ R\ P_e\ F}{E\ I} \times 100$$

$$= \frac{37.8\ G\ R\ P_e\ F}{E\ I} \qquad \text{(I-1)}$$

where

- Y = fuel yield (%/ yr),
- K = conversion factor (kg/yr-mw),
- G = breeding gain, i.e., the number of excess atoms of fuel produced per atom consumed in the nuclear chain reaction,
- R = $\nu/\bar{\eta}\epsilon$,
- P_e = station power (Mwe). In this study P_e = 1000,
- F = plant factor, i.e., the fraction of time that the plant is at full power operation; taken as 0.8 in this study,
- E = thermodynamic efficiency,
- I = station inventory of fissionable material including U-233, U-235, and Pa-233 (kg).

The quantity K has the value 0.378 and is calculated as follows:

$$K = \frac{(0.233)(3.1 \times 10^{16})(3600)(24)(365)}{0.6023 \times 10^{24}} \quad \text{kg/yr-Mw}$$

The breeding gain, G, is computed from output data of equilibrium reactor calculations (86) discussed in Appendix H. It is the net neutron production, $\bar{\eta}\epsilon$, minus the sum of all parasitic neutron absorptions and losses as well as minus the single neutron required to perpetuate the chain reaction. A typical calculation is shown in Table 6.1.1.

The term, R, is the ratio of fuel atoms destroyed to fuel atoms fissioned, and in this study had a value in the range 1.11-1.14. The thermodynamic efficiency, E, is the overall efficiency of the plant; in this study the values ranged from 27.5% for the AHBR to 42.3% for the MSBR.

2.0 Breeding Credit

The breeding credit associated with the equilibrium reactor is the credit that can be taken for bred fuel in excess of that required to maintain operation at the specified power level. The net production of fissionable material is given by

$$\text{Production} = \frac{(3.1 \times 10^{16})(24)(3600)(365)(0.233)\ P_e\ G\ R\ F}{(E)(0.6023 \times 10^{24})}$$

$$= 0.378\ \frac{P_e\ G\ R\ F}{E}\ ,\ \frac{kg}{year} \qquad \text{(I-2)}$$

The terms of this equation are defined exactly as given above for Eq. I-1. The constant term is a combination of factors which gives the production rate in kg/year-Mw.

When Eq. I-2 is multiplied by the unit value of fissionable material and an appropriate conversion factor, the breeding credit in mills per kwhr is obtained. In this study a value of $15,000/kg has been assigned to bred U-233. The conversion factor is

$$\frac{1000}{(1000)(365)(24)\ P_e\ F}\ ,\ \frac{\text{mills/kwhr}}{\$/\text{year}} \qquad \text{(I-3)}$$

Combining Eq. I-2 with Eq. I-3 and the unit value of U-233, there obtains

$$\text{Breeding credit} = 0.6476\ \frac{G\ R}{E}\ ,\ \frac{\text{mills}}{\text{kwhr}} \qquad \text{(I-4)}$$

The result obtained by solving Eq. I-4 is subtracted from the gross fuel cycle cost to obtain the net fuel cycle cost.

A P P E N D I X J

Canadian Deuterium Uranium Reactor

APPENDIX J

Canadian Deuterium Uranium Reactor

5.6.1 Introduction

In order to place the calculated thermal breeder fuel cycle costs in perspective with what appear to be the lowest fuel costs claimed for any of the current nonbreeder reactor types, the CANDU reactor concept was selected for a limited study to be included in this report.

CANDU is the letter-designation (CANadian-Deuterium-Uranium) that refers to full-scale nuclear power reactors (200 Mwe) fueled with natural-uranium dioxide clad in a Zircaloy alloy, moderated with low temperature D_2O, and cooled with heavy water in pressure tubes. The CANDU design is a scale-up of its 82.5 Mwt (20 Mwe) prototype, NPD-2, which is under construction at Rolphton, Ontario about 16 miles upstream from Chalk River on the Ottawa River. NPD-2 was scheduled to be in full-power operation by mid-1961, but because of delays in equipment delivery may not start up till late this year. It will be used to test the fuel charging machines that are being considered for the first CANDU plant.

The first CANDU reactor will be constructed at Douglas Point, Ontario on the eastern shore of Lake Horon, about 110 miles west-northwest of Toronto. Construction is scheduled to be completed by mid-1964.

The CANDU approach to economical nuclear power appears to be on a sound basis because it is based on achieving fuel costs, from the burning of low-priced (at this time) natural uranium, that are sufficiently lower than those obtained from burning fossile fuel to compensate for the higher capital costs required for the nuclear power plant. The increment of higher capital cost is penalized less in Ontario because their financial and tax structure permits a lower annual fixed charge on capital investment - about 7-8%, compared to about 14% in the U.S.

5.6.2 CANDU Reactor Concept

CANDU (and NPD-2) designs utilize horizontal, thin aluminum or Zircaloy calandria tubes in large tanks containing heavy water at about 80°C. Zircaloy pressure tubes, 3.25 in. ID x 0.157 in. (or 0.164 in.) wall thickness, are

contained inside the calandria tubes. The gas gap between the calandria tubes and the pressure tubes minimizes the transfer of heat from the pressure tubes to the low temperature moderator.

A typical 200-Mwe reactor has a calandria tank about 16 ft long by 19 ft in diameter penetrated by about 300 pressure tubes spaced on 9-in. centers in a square lattice array. The diameter of the reactor tank is about 4 to 5 ft greater than the diameter of the active core to provide a 2- to 2½-ft-thick D_2O reflector that is integral with the moderator contained between the calandria tubes of the active core.

Reactivity is controlled by varying the level of moderator in the reactor tank; moderator is kept from draining to the dump tanks through the large gooseneck drain ports by means of gas pressure in the dump tank which is maintained by constantly pumping helium from the gas space of the reactor tank to the dump tank and allowing it to bleed back to the reactor tank. This differential pressure, which is varied by adjusting the gas bleed rate, is used to control the moderator level in the reactor tank. To scram the reactor, a fast dump of the moderator may be accomplished by equalizing the pressure between the reactor and the dump tank by opening the valves in the large gas pressure-equalizing lines connecting the reactor and the dump tanks.

Xenon over-ride after short shut-downs may be accomplished using a few enriched separately-cooled and slowly movable rods.

There is no end-reflector and the ends of the Zircaloy pressure tubes are provided with stainless steel fittings to allow a refueling machine to be clamped to the pressure tube, remove the end plug and either insert a new fuel element or remove a spent fuel element from the fuel channel while the reactor is operating at full power.

Heat is removed from the fuel elements by circulating a stream of high temperature, high velocity (~ 25-30 ft/sec) heavy water through the pressure tubes penetrating the reactor. About 5-7% of the heat associated with fission is absorbed and wasted in the low temperature moderator. D_2O coolant which has been heated in the reactor then passes through shell and tube heat exchangers where it gives up its heat to generate steam. Cooled D_2O from the steam generators is returned to the inlet headers of the reactor. Coolant

flows in opposite directions in adjacent pressure tubes to avoid uneven temperature distributions in the reactor. Orifices in individual flow channels are used to throttle the flow of coolant in proportion to the heat release so as to provide approximately equal outlet temperatures at each tube.

The reactor is contained in a vapor-tight vault which is provided with special ventilation and D_2O-recovery systems to recover, without downgrading, the D_2O that is expected to leak from the reactor, fuel-charging machines and circulating pumps.

5.6.3 CANDU Fuel System

The fuel fed to the CANDU reactors is natural uranium dioxide in the form of high density (10.4 g/cc, or 95% theoretical) sintered pellets canned in 0.6 in. O.D. x 0.015 in. wall thickness Zircaloy-2 tubing and assembled into 19-rod bundles $19\frac{1}{2}$ in. in length. It is expected that fuel charging and discharging will be accomplished while the reactor is at full power using fuel charge-discharge machines mounted at each end of the horizontal calandria tank. By using semicontinuous, bidirectional refueling (adding fresh fuel bundles to adjacent fuel channels from opposite ends), and exposing each fuel element that is discharged from the reactor to approximately equal nvt, axial neutron flux symmetry and radial flattening are achieved, and high burnups, the order of 8000-10,000 Mwd/T of contained uranium, are calculated. At present-day costs of uranium and fabrication, it is believed by W. B. Lewis[1] that the value of this spent fuel would not warrant the costs required to recover the contained plutonium, hence spent fuel from CANDU will be stored for an indefinitely long time with no further treatment after being discharged from the reactor.

The steps in the fabrication of CANDU fuel are:

1. Buy U_3O_8 (yellow cake, mine concentrates) from supplier.
2. Convert U_3O_8 to ADU (ammonium diuranate).
3. Convert ADU to UO_2.
4. Form UO_2 pellets.
5. Sinter pellets at high temperature in hydrogen atmosphere to achieve 95% theoretical density.
6. Grind pellets to required dimensional tolerances.

7. Place pellets in thin-wall Zircaloy tubing and weld end shut.
8. Assemble fuel rods into 19-element bundles.

Some of the advantages UO_2 offers over uranium metal alloys are:

1. good corrosion resistance in water,
2. good resistance in radiation damage (no swelling after long burnup),
3. high melting point,
4. good retention of fission products, including gases, and
5. no neutron absorbing additives.

UO_2 has had demonstrated success in reactor use. The PWR Core I blanket, consisting of sintered pellets of UO_2 sheathed in Zr-2 has achieved ~ 10,000 Mwd/TU burnup in peak regions with only one or two suspected failures among 95,000 rods. Dresden also uses sintered pellets. Test data indicate that sintered pellets will withstand exposures of at least 25,000 to 30,000 Mwd/TU.

The melting point of UO_2 is ~2800°C, and its relatively low thermal conductivity decreases with temperature so that it is easy to run up to the melting point at relatively low heat generation rates in massive UO_2 bodies. UO_2 tends to become plastic at about 2000°C, so that problems of thermal expansion and required strength of cladding material do not appear to be as binding as first thought.

The permissible heat rating appears to be $\int_{\text{Surface}}^{\text{Maximum}} k(\theta)\, d\theta = 50$ watts/cm, if surface temperature = ~ 300°C. It is at this rate of heat generation that the center temperature approaches the melting point, and the release of fission gases from the UO_2 lattice might become a serious problem. The melting point is reached at $\int k d\theta = 75$ watts/cm.

Although a rating of $\int k d\theta = 50$ w/cm may be satisfactory, and the release of fission gases increases notably above $\int k d\theta = 30$, a value of $\int k d\theta = 40$ has generally been accepted as a nominal design maximum heat generation limit that can be used with confidence on the basis of demonstrated technology. For solid, round rods it may be shown that the heat output is approximately $4 \pi \int k d\theta$ watts per cm of length, independent of its diameter. Placing the design limit at $\int k d\theta = 40$ gives a value of

about 15 kw per ft of rod for the heat output of fuel elements in regions of maximum neutron flux. In a given reactor design, the average fuel element would be operating at slightly less than half this value when the reactor was at full power.

5.6.4 CANDU Power System (Douglas Point Reactor)

Heavy water coolant circulating at a rate of 2.41×10^7 lb/hr and having reactor inlet and outlet temperatures of 480°F and 560°F transfers its heat to preheated boiler feedwater (340°F) in 8 boilers, each consisting of 10 vertical U-shell-and-tube heat exchangers and one steam drum, producing 2,562,000 lb/hr of steam at 583.7 psia and containing 0.25% moisture. The D_2O coolant is circulated by eight 7000-gpm, shaft-sealed, centrifugal pumps operating at 200 psi head. The heat exchangers use $\frac{1}{2}$ in. OD monel tubes and their total surface area include 74,500 ft^2 boiling area and 11,050 ft^2 preheating area.

The power plant will have one 220 Mw tandem compound turbine-generator with moisture separators and reheaters. Its steam cycle efficiency of 33.34% as guaranteed by the contractor, Associated Electrical Industries, Ltd., Manchester, England is based on the following conditions:

Throttle steam pressure	597.7 psia
Throttle temperature	482°F
Reheat conditions: Pressure	67.9 psia
Temperature	430°F
Condenser back pressure	1 in. Hg
Number of stages of feed heating	3 low pressure heaters
	1 direct-contact deaerator
	2 high-pressure heaters
Final feedwater temperature	340°F
Cycle efficiency	33.34%
Condenser	
Type and number	1 horizontal single-pass surface condenser
Surface area	158,000 ft^2

After allowing for about 5½% of fission heat absorption in the moderator, and for station self-consumption of power for pumps, etc., a net station efficiency of 29.1% results.

5.6.5 Status of CANDU Development

A prototype power reactor of 82.5 Mwt capacity, NPD-2, is under construction at Rolphton, Ontario. It is scheduled to begin operations in 1961. NPD-2 will be used to test the refueling schemes proposed for CANDU, as well as to obtain operating experience pertaining to the problems of maintaining D_2O purity and minimizing D_2O losses; the corrosion and erosion problems associated with the Zircaloy pressure tubes and thin-walled fuel elements; the radiation stability of UO_2 fuels operating at high rates of heat release with central temperatures close to the melting point.

The cooperative effort between USAEC and AECL on the development of heavy water power reactors will include development of a refueling machine for Douglas Point, and components such as valves and pumps where leakage of heavy water is a problem.

Fuel Cycle Optimization

6.6.1 Special Assumptions

Estimation of Heavy Water Inventory. - Coolant circuit: As in the AHBR study,[11] the D_2O volume in the heat removal system (exclusive of the flow distribution headers at the ends of the reactors) was assumed to be 18.9 liters/Mwt.

Distribution headers: It was assumed that the D_2O volume in the headers would be approximately proportional to the volume of the calandria tank as well as to the thermal power

$$D_2O \text{ vol. in headers} = \sim 0.2 \times \text{Reactor Volume} \times \frac{P}{P_o}$$

where,

P_o = 700 Mwt

P = Reactor power, Mwt

In the reactor: D_2O volume in the reactor is equal to the volume of the calandria tank minus the volume of the calandria tubes.

Total D_2O inventory was taken as the sum of these three volumes times 1.1 (the assumed density of D_2O).

The volume of the calandria tank may be calculated from:

$$\text{Tank Volume} = \left[\text{Pitch}\sqrt{\frac{\text{Reactor Power}}{\text{Power per cell-cm}}} + \text{Reflector Thickness}\sqrt{\pi \times \text{Cell Length}}\right]^2 \times 10^{-6}$$

where,

Volume	=	cubic meters
Pitch	=	square lattice spacing, cm
Reactor power	=	thermal kilowatts
Power per cell-cm	=	kilowatts per cm of cell length
Reflector thickness	=	cm of D_2O surrounding active core
Cell length	=	length of reactor tank, cm

A method of determining average power per cell cm is outlined below.

Calculation of UO_2 Loading

The UO_2 loading in the active core is generally established by the heat removal limitation of the oxide rods, which is based upon the design value assigned to the quantity $\int kd\theta$.

$$\text{Average power per cell cm} = \frac{4\pi \int kd\theta \times n \times 0.96 \times 10^{-3}}{(1 - f_m) \times k_\phi}$$

where,

Power per cell cm = kwt/cell-cm

$\int kd\theta$	=	fuel maximum heat rating, watts/cm
n	=	number of rods in fuel cluster; e.g., in the fuel cell
0.96	=	factor to allow for inactive zone between fuel bundles
f_m	=	fraction of reactor power absorbed in the moderator; e.g., fraction of fission heat that is not transferred to the coolant
k_ϕ	=	peak-mean power ratio over the reactor. k_ϕ is the product of peak/mean power ratios in the axial and radial directions and across the fuel cluster itself. k_ϕ is a function of the flatness of power distribution, and for large reactors is ~ 2.1 to ~2.3. For Douglas Point

$$k_{\phi} = \left(\frac{\text{Peak}}{\text{Mean}}\right)_{\text{Axial}} \times \left(\frac{\text{Peak}}{\text{Mean}}\right)_{\text{Radial}} \times \left(\frac{\text{Peak}}{\text{Mean}}\right)_{\text{Fuel Cluster}}$$

$$k_{\phi} = \left(\frac{1}{0.649}\right)\left(\frac{1}{0.7885}\right)(1.099)$$

$$k_{\phi} = 2.1475.$$

Thus, the UO_2 loading in the active zone of the reactor is given by

$$UO_2 \text{ loading, tonnes} = \frac{\text{Reactor Thermal Power} \times \frac{\text{grams } UO_2}{\text{cell-cm}} \times 10^{-6}}{\text{average power per cell cm}}$$

$$\text{grams/cell-cm} = 0.96\, n\, r^2\, \rho(UO_2)$$

where,

r = pellet radius, cm
n = number of rods/cluster

For CANDU reactors such as Douglas Point utilizing on-power fueling machines the actual fuel loading in the pressure tubes will be greater than that calculated above because one fuel bundle at each end of the pressure tube will be outside the active zone which is defined by the length of the calandria tank containing heavy water moderator. For Douglas Point there will be 10 fuel bundles in the active zone of a fuel channel and 12 bundles in the pressure tube, so the total reactor fuel loading will be 20% greater than the active zone loading.

$$\text{Thus, } UO_2 \text{ loading} = \frac{1.2\, r^2\, \rho(UO_2)\,(1 - f_m)\, k_{\phi}\, P}{4 \int k d\phi}$$

where,

UO_2 loading = tonnes UO_2
r = pellet radius, cm
$\rho\ UO_2$ = pellet density, g/cm^3
k_{ϕ} = peak/mean power ratio over the reactor
P = reactor total power, Mwt
f_m = fraction of reactor power absorbed by moderator
$\int k d\phi$ = fuel heat rating, watts/cm.

Reactor Calculations

EXPIRE[2] input requires masses and nuclear properties for all materials in six regions of a unit cell, which is assumed to have a homogenized inner region of fuel (U-235, U-238, Pu, Np, etc.), diluent (oxygen in UO_2), cladding and extras (Zircaloy), and coolant (D_2O) whose radius is the same as that of the inner radius of the pressure tube. Region 2 is composed of material in the wall of pressure tube and the calandria tube and the insulating gas gap between the calandria tube and the pressure tube. For nuclear calculations, the gas gap is assumed to be a void, and the radius of Region 2 is the same as the outside radius of the calandria tube. Regions 3, 4, 5, and 6 are composed of moderator (D_2O at 80°C was assumed). The radius of Region 6 is the same as the radius of the unit cell which is calculated from the lattice spacing of the fuel channels. The radii of Regions 3, 4, and 5 are arbitrary values intermediate between R_2 and R_6.

Disadvantage factors, defined as the ratio of the average flux in any region to the average flux in the central fuel region, for the various regions 2 through 6 as a function of total macroscopic cross-section of the fuel region are calculated using the I-2 code in the IBM-704, which uses a P_3 expansion of the single-energy Boltzmann equation. The thermal-flux disadvantage factors are then expressed as a quadratic function of the absorption cross-section, with coefficients of the quadratic determined using a least squares fitting routine. The moderator temperature and the disadvantage factor coefficients are then used in NTC program[3] to calculate the effective neutron temperature, which was 89.5°C for a moderator temperature of 80°C in the Douglas Point cell geometry. This neutron temperature was used to specify various cross-sections required for EXPIRE input.

The value for $(\sqrt{S/M})_{eff}$ was determined by a method described by Hellstrand.[4]

In the EXPIRE code the average power density and neutron flux are calculated from the average power and volume per unit length of cell assuming that 3.38×10^{13} fissions per second are equivalent to 1 kw.

Some volumes and nuclear constants used for the lattice assumed for Douglas Point are shown in Table J-1.

Table J-1. Parameter Values for Douglas Point Reactor

		Douglas Point
V_{UO_2}	Volume of UO_2, cm^3/cm	29.644
V_{S+E}	Volume, cm^3/cm	3.735
V_C	Volume, cm^3/cm	20.141
V_{PT}	Volume, cm^3/cm	10.841
V_{GG}	Volume, cm^3/cm	25.021
V_{CT}	Volume, cm^3/cm	4.307
V_M	Volume, cm^3/cm	428.889
$(\sqrt{S/M})_{eff}$		0.32914
Neutron temperature, °C		89.5
τ_{R1}	Neutron age, cm^2	122.4
τ_{R2}	Neutron age, cm^2	129.2
τ_{R3}	Neutron age, cm^2	136.0
Γ	Volume of region 1/volume UO_2	1.8054
ϵ	Fast fission factor	1.0173
ρ_{UO_2}	UO_2 density, g/cm^3	10.4

Subscripts

S+E = sheath + extras
C = coolant
PT = pressure tube
GG = gas gap
CT = calandria tube
M = moderator
R1 = resonance energy region 1
R2 = resonance energy region 2
R3 = resonance energy region 3

6.6.2 Key Variables

The key variables that influence fuel cycle cost for CANDU are:

Attainable exposure, MwD/TU

Price of UO_2

Price of fuel fabrication

Price of D_2O

Thermodynamic efficiency

UO_2 specific power, kwt/kg UO_2

D_2O specific power, kwt/kg D_2O

Plant factor

Annual fixed charge on D_2O inventory

Annual fixed charge on fuel inventory

D_2O loss rate

Of these variables, those that can be fixed by edict (for cost studies) are:

Price of UO_2: $8.32/lb (based on current AEC purchase price)

Price of D_2O: $28/lb

Plant factor: 80% (7000 full-power hr/yr)

Annual fixed charges:

	United States Bases	Canadian Bases
Fabricated fuel or fertile material	12.7	8
Heavy water	12.7	8

Annual D_2O loss rate: 2% of total inventory (based on performance assumed by Lewis).

D_2O Specific Power as discussed in Section 6.6.1 will be determined by the heat rating of the fuel, the flatness of the power distribution, the lattice spacing and the reflector thickness, and the efficiency of the heat removal system.

UO_2 Specific Power, as discussed in Section 6.6.1, will be determined by the heat rating of the fuel, the flatness of the power distribution, and the density and diameter of the fuel pellets.

Thermodynamic efficiency will be determined by the inlet and outlet temperatures of the coolant, (which are set by stress and pressure limitations of the pressure tubes), the condenser back pressure, and the loss of heat to the moderator. The Douglas Point value of 29.1% was adopted even though it assumes 1 in. Hg condenser pressure, whereas U.S. conditions usually produce at least $1\frac{1}{2}$ in. Hg back pressure.

Price of fuel fabrication will be determined by labor costs and cost of Zircaloy, and will be influenced by the fuel rod diameter and length.

For estimating U.S. fabrication costs of Zircaloy-clad natural UO_2 fuel the formula

$$\text{Fabrication Cost, \$/lb } UO_2 = 20/D$$

was adopted, where D is the pellet diameter in inches. This relationship fits fairly well, at the lower limit, the plot of fabrication cost range vs diameter as shown in the AEC Nuclear Power Plant Cost Evaluation Handbook,[5] and includes the cost of converting yellow cake to UO_2 powder, forming, sintering, pellet grinding, fabrication of the Zircaloy sheath, and assembly, inspection and testing of the fuel rod clusters.

Published estimates of fabrication costs[6] for NPD-2 and CANDU range from \$21/lb UO_2 for ~ 0.565 in. diameter pellets for CANDU in 1964 to \$28.50/lb UO_2 for NPD-2 fuel (pellet diameter = ~ 0.937 in.). Based on these estimates, the Canadian fabrication cost estimate would appear to be given by

$$\text{Fabrication Cost, \$/lb } UO_2 = 12.2/D$$

Attainable exposure will vary with the lattice pitch of the fuel channels, the fuel loading (oxide density and enrichment), reflector thickness, amount of structural material (poisons) in the cladding, pressure tubes and calandria, moderator and coolant temperature, and reactor size and geometry.

Technical and financial requirements conflict. For instance, increasing the lattice spacing (up to a point) or increasing the reflector thickness, will increase reactivity lifetime; yet each of these changes increases the volume and D_2O hold-up in the reactor, which decreases specific power relative to D_2O. Optimum lattice spacing and reflector thickness are

determined by the price of both D_2O and fabricated fuel, and practical lattice arrangements will be those as close to the optimum which engineering considerations permit.

Recognizing that Lewis et al have been working intensively for a long time on determining the characteristics of an optimum power reactor utilizing natural uranium and heavy water, the Canadian ideas and specifications have been used where ever possible; but, since a machine code (EXPIRE) for calculating reactivity lifetime of an average fuel element under conditions that approximate the Canadian bidirectional fueling scheme was available, independent calculations have been made of the effects in fuel cycle costs of varying the lattice spacing, the reflector thickness, reactor size (varying the net electrical capability from 200 Mw to 333 Mw) and fuel rod diameter using the assumptions of cost and heat capabilities listed above.

An attempt was made to compare EXPIRE results (of attainable burn-up) with those from AECL as reported in DM-57 (ref. 7) by using the same geometries and masses (obtained from the published descriptions). The following table illustrates the agreement (or in some cases lack of agreement) between the calculated exposures (as limited by reactivity lifetime). It is notable that, whereas with the AECL results the attainable exposure passed through a maximum at a lattice spacing of about $9\frac{1}{2}$ inches, with EXPIRE the attainable exposure increases with the lattice spacing and had not yet gone through a maximum at the greatest pitch considered (10.78 inches). Furthermore, in one case (A-3, with a pitch of 7.06 inches) which was initially subcritical, according to EXPIRE, an attainable exposure of 7650 MwD/T was obtained by the AECL calculation.

The agreement between the two calculations, though not good for the tighter lattices, was considered good enough for the optimum and practical lattice pitches greater than $8\frac{1}{2}$ inches to permit use of the EXPIRE code for further studies involving optimization of reflector thickness, reactor size, and fuel rod diameter.

The effect of changing the reflector thickness of 203 Mwe reactors utilizing a Douglas Point core was studied in Cases E-1, F-1, and G-1. Reflector thicknesses 60, 68, and 75 cm were chosen. Minimum costs were obtained with the 60-cm reflector because of reduced D_2O inventory; therefore,

a 60-cm reflector was adopted for the subsequent cases investigating the effects of varying reactor size and/or fuel rod diameter.

Cases E-1, E-2, and E-3 were reactors having capabilities of 203, 250, and 333 Mwe (giving multiples of 5, 4, and 3 reactors per 1000 Mwe stations) using the same fuel (0.6 in. rods) and pressure tube arrangements (length and spacing) as the Douglas Point core, but with more tubes, and hence larger diameter cores, for the larger heat output reactors. The largest core gave the greatest attainable fuel exposure, and had the minimum fuel cycle costs.

Since the assumed fuel fabrication cost varies inversely with the diameter, it was postulated that there might be an optimum fuel rod diameter in the range 0.6 to 1.0 in. Six additional reactor cases were studied: H-1, H-2, and H-3; J-1, J-2, and J-3 in which 200, 250, and 333 Mwe reactors utilized 1-in. fuel rods in a 7-element cluster and 0.82-in. diameter fuel rods in a 19-element cluster. Some significant design characteristics and calculated fuel exposures are shown in Table J-4.

Table J-2. Effect of Lattice Spacing on Attainable Exposure

AECL Case Number*	Equivalent Pitch (Square Lattice) (in.)	Reactor Tank Diameter (ft)	Active Core Length (ft)	Attainable Exposure by EXPIRE (MwD/T)	Attainable Exposure by AECL (MwD/T)
A-3	7.06	16.47	14.20	0	7650
A-2	7.34	16.47	15.25	4370	8440
B-4	7.75	17.72	14.20	6175	9250
B-2	8.36	17.72	16.40	7696	9770
C-4	8.83	19.03	15.25	8266	10,080
C-2	9.51	19.03	17.62	8931	10,180
D-4	10.02	20.44	16.40	9216	10,100
D-2	10.78	20.44	18.90	9500	9960
Douglas Point**	9	19.7	16.4	8754	9750

* As reported in DM-57, using 60-cm reflector thickness.

** As reported in reference 154; 75-cm reflector thickness.

Table J-3. Effect of Varying Core Size and Reflector Thickness on Attainable Burn-up, Fuel Inventory, and D_2O Inventory

Reactor Identification	E-1	F-1	G-1*	E-2	E-3
Power (net), Mwe	203	203	203	250	333
Power, Mwt	698	698	698	859	1144
Efficiency, %	29.1	29.1	29.1	29.1	29.1
Throttle temperature, °F	482	482	482	482	482
Throttle pressure, psig	579.7	579.7	579.7	579.7	579.7
Condenser pressure, psig	1.0	1.0	1.0	1.0	1.0
Reactor Core					
Tank diameter, ft	18.7	19.2	19.7	20.5	23.0
Active diameter, ft	14.80	14.80	14.80	16.6	19.0
Active length, ft	16.4	16.4	16.4	16.4	16.4
Reflector thickness, in.	23.6	26.8	29.5	23.6	23.6
Square lattice pitch, in.	9	9	9	9	9
No. fuel channels	306	306	306	383	505
Tank volume, m^3	127.6	134.8	141.1	153	192.4
Fuel					
UO_2 in active core, tonnes	47.2	47.2	47.2	59.1	77.9
UO_2 in reactor, tonnes	56.6	56.6	56.6	70.8	93.4
Est. burn-up (by EXPIRE), $\frac{MwD}{TU}$	8586	8670	8754	8840	10,100
Est. burn-up (by AECL), $\frac{MwD}{TU}$	-	-	9750	-	-
D_2O Inventory, tonnes					
Active core moderator	72.2	72.2	72.2	90.2	120.2
Reflector	52.5	60.4	67.2	53.0	59.4
External system	48.9	48.9	48.9	61.1	81.4
Total	173.6	181.5	188.3	204.3	261.0

*Douglas Point Geometry

Table J-4. Effect of Fuel Rod Diameter on Fuel and D_2O Inventories and on Fuel Burn-up

Reactor Identification	H-1	H-2	H-3	J-1	J-2	J-3	E-1	E-2	E-3
Reactor capability, Mwe	203	250	333	203	250	333	203	250	333
Fuel rod diameter, in.	1	1	1	0.82	0.82	0.82	0.60	0.60	0.60
Rods per cluster	7	7	7	19	19	19	19	19	19
Reactor Core									
Tank diameter, ft	23.1	25.4	28.7	20.5	22.5	25.4	18.7	20.5	23.0
Active diameter, ft	19.2	21.4	24.7	16.6	18.6	21.4	14.8	16.6	19.0
Active length, ft	25.6	25.6	25.6	19.5	19.5	19.5	16.4	16.4	16.4
Square lattice pitch, in.	9	9	9	11.24	11.24	11.24	9	9	9
No. fuel channels	513	641	854	247	310	412	306	383	505
Tank volume, m^3	304	367	468	183	220	280	127.6	153	192.4
Fuel									
UO_2 in active core, tonnes	127.8	159.8	212.8	88.5	110.6	147.3	47.2	59.1	77.9
UO_2 in reactor, tonnes	143.8	179.8	239.4	103.2	129.0	171.8	56.6	70.8	93.4
Est. burnup, MWD/TU	10,230	10,417	10,573	9460	9640	9865	8586	8840	10,100
D_2O Inventory, tonnes									
Active core (moderator)	188.8	235.8	314.2	107.9	135.4	179.9	72.2	90.2	120.2
Reflector	104.4	116.3	131.9	69.8	77.0	89.8	52.5	53.0	59.4
External system	86.0	104.0	134.0	57.6	70.0	90.0	48.9	61.1	81.4
Total	279.2	456.1	580.1	235.3	282.4	359.7	173.6	204.3	261.0

Reflector thickness 23.6 in.
Station efficiency 29.1%
UO_2 density 10.4 g/cc

Table J-5. Summary of Fuel and D_2O Costs for Reactors Described in Tables J-3 and J-4

	E-1	F-1	G-1	E-2	E-3	H-1	H-2	H-3	J-1	J-2	J-3
Power, Mwe	203	203	203	250	333	203	250	333	203	250	333
UO_2 inventory, tonnes	56.6	56.6	56.6	70.8	93.4	143.8	179.8	239.4	103.2	129.0	171.8
D_2O inventory, tonnes	173.6	181.5	188.3	204.3	26.0	379.2	456.1	580.1	235.3	282.4	359.7
Exposure, MWD/TU	8586	8670	8754	8840	10,100	10,230	10,417	10,573	9460	9640	9865
						U.S. BASES					
Fuel Price, $/kg UO_2											
UO_2 purchase	18.35	18.35	18.35	18.35	18.35	18.35	18.35	18.35	18.35	18.35	18.35
Fabrication	77.40	77.40	77.40	77.40	77.40	46.25	46.25	46.25	55.80	55.80	55.80
Total	95.75	95.75	95.75	95.75	95.75	64.60	64.60	64.60	74.15	74.15	74.15
Fuel Costs, mills/kwhr											
UO_2 purchase	0.347	0.344	0.340	0.337	0.295	0.291	0.286	0.282	0.315	0.309	0.302
Fabrication	1.463	1.450	1.436	1.422	1.244	0.734	0.721	0.710	0.958	0.940	0.918
Total burn-up	1.810	1.794	1.776	1.759	1.539	1.025	1.007	0.992	1.273	1.249	1.220
Reactor inventory	0.242	0.242	0.242	0.246	0.243	0.415	0.419	0.420	0.342	0.347	0.347
30-day supply inventory	0.024	0.024	0.024	0.024	0.020	0.013	0.013	0.013	0.017	0.016	0.016
Total fuel supply cost	2.076	2.060	2.042	2.029	1.802	1.453	1.439	1.425	1.632	1.612	1.583
D_2O Costs, mills/kwhr											
Inventory @ 12.7%/yr	0.948	1.001	1.039	0.915	0.877	2.092	2.043	1.949	1.298	1.265	1.276
Loss @ 2%/yr	0.149	0.158	0.164	0.144	0.138	0.330	0.322	0.307	0.204	0.199	0.200
Total	1.097	1.159	1.203	1.059	1.015	2.422	2.365	2.356	1.502	1.464	1.476
Total Fuel + D_2O Cost, Mills/kwhr	3.173	3.219	3.245	3.088	2.817	3.875	3.804	3.781	3.134	3.076	3.059
						CANADIAN BASES					
Fuel Price, $/kg UO_2											
UO_2 purchase	13.75	13.75	13.75	13.75	13.75	13.75	13.75	13.75	13.75	13.75	13.75
Fabrication	47.20	47.20	47.20	47.20	47.20	28.20	28.20	28.20	34.00	34.00	34.00
Total	60.95	60.95	60.95	60.95	60.95	41.95	41.95	41.95	47.75	47.75	47.75
Fuel Costs, mills/kwhr											
UO_2 purchase	0.260	0.257	0.255	0.252	0.221	0.218	0.214	0.211	0.236	0.232	0.226
Fabrication	0.892	0.884	0.876	0.867	0.759	0.448	0.440	0.433	0.584	0.573	0.560
Total burn-up	1.152	1.141	1.131	1.119	1.080	0.666	0.654	0.644	0.820	0.805	0.786
Reactor inventory	0.097	0.097	0.097	0.098	0.098	0.170	0.171	0.172	0.139	0.141	0.140
30-day supply inventory	0.010	0.010	0.010	0.009	0.008	0.006	0.005	0.005	0.007	0.007	0.007
Total fuel supply cost	1.259	1.248	1.238	1.266	1.186	0.842	0.830	0.821	0.966	0.953	0.933
D_2O Costs, mills/kwhr											
Inventory @ 8%/yr	0.598	0.631	0.654	0.577	0.552	1.318	1.287	1.228	0.818	0.797	0.804
Loss @ 2%/yr	0.149	0.158	0.164	0.144	0.138	0.330	0.322	0.307	0.204	0.199	0.200
Total	0.747	0.789	0.818	0.721	0.690	1.648	1.609	1.535	1.022	0.996	1.004
Total Fuel + D_2O Cost, mills/kwhr	2.006	2.037	2.056	1.947	1.876	2.490	2.439	2.356	1.988	1.949	1.937

6.6.3 Results

The over-all fuel cycle costs, and the various components that comprise the total fuel-cycle cost, calculated for the cases listed in Tables J-3 and J-4, are shown in Table J-5. The fuel-cycle cost for all cases when computed in the assumed U.S. bases was more than 0.94 mills/kwhr greater than when calculated on the assumed AECL bases. U.S. costs (for 0.60 in. diameter fuel) were in the range 2.82 to 3.24 mills/kwhr, and the AECL costs were in the range 1.88 to 2.06 mills/kwhr. The results for the same fuel in 200 Mwe reactors also show that a reflector thickness of 60 cm gives lower total fuel-cycle costs than reflectors 68 and 75 cm thick. Going from a 60-cm reflector to a 75-cm reflector increases the costs by 0.05 mill/kwhr (AECL bases) and 0.07 mill/kwhr (U.S. bases).

Minimum total fuel-cycle costs of 2.82 mills/kwhr (U.S. bases) and 1.88 mills/kwhr (AECL bases) were obtained for the assumed 333 Mwe reactor with 0.6-in.-diameter fuel because of the higher calculated attainable exposure and higher D_2O specific power.

The assumption of lower fuel fabrication cost associated with larger diameter fuel rods resulted in slightly lower fuel costs for the 0.82-in.-diameter fuel in the 200- and 250-Mwe reactors than for the 0.60-in.-diameter fuel. Differences of 0.090 mill/kwhr (U.S. bases) and 0.018 mill/kwhr (AECL bases) were found for the 200-Mwe reactors; however, the larger diameter fuel has two very distinct and real disadvantages because of its lower specific power, namely: (1) for a given heat output, the reactor using 0.82-in. rods is much larger, hence would cost more to build; (2) the fuel cladding in the reactors fueled with 0.82-in. rods would have to remain intact almost twice as long as the 0.6-in. rods. Taking these considerations into account, the minor savings in fuel cycle costs of < 0.1 mill/kwhr made possible by the use of the larger diameter rods would probably be more than offset by higher capital costs and more frequent fuel element failures.

There may be a fuel rod size intermediate between 0.60 in. and 0.82 in. diameter that would be optimum for all considerations, but no attempt was made to determine this.

It should be noted that fuel cost estimates published by W. B. Lewis[1] do not include inventory charges on fuel or D_2O, nor D_2O replacement costs; e.g., the Canadian estimates of fuel costs correspond exactly with those

listed in Table J-5 under the heading "Total Burn-up Costs." In computing CANDU costs, Lewis takes a figure of \$30/lb UO_2 for the fabricated fuel, a burn-up of 9750 MwD/tonne, a station efficiency of 29.1% and no credit for value of spent fuel. These numbers lead to an estimated Canadian burn-up cost of 1.1 mills/kwhr, (and a future cost of 0.88 mill/kwhr when the fabricated fuel price drops to \$24/lb UO_2). For comparison it may be seen that the burn-up costs for the cases shown in Table J-5 vary from 0.99 to 1.81 mills/kwhr (U.S. bases), or from 0.64 to 1.15 (AECL bases).

7. Comparison to AHBR

Case E-3, a 333-Mwe reactor, was selected from Table J-5 as representing the best CANDU-reactor from the standpoint of minimum total fuel cycle costs calculated on U.S. bases to compare with similar fuel cycle costs of AHBR (also on the U.S. bases) and with estimated costs of CANDU - Douglas Point (calculated on Canadian bases). These costs are listed in Table J-6.

For the purposes of comparison, the inventory charge on the 30-day supply of fuel was combined with the charge on fuel in the reactor. Also, the costs were adjusted downward corresponding to a slightly more optimistic estimate of station net efficiency of 30% instead of 29.1% as assumed in Table J-5.

In Case E-3, 1.1% of the U-238 and 86% of the U-235 in the natural uranium fed are consumed and the spent fuel contains about 3.2 kg of fissionable plutonium per tonne which would be available for use at a future time when it might be economic to recover and recycle the plutonium.

Although this comparison shows a fuel cycle cost advantage of at least 1 mill/kwhr for the AHBR, when compared on the basis of development status, the CANDU system is very much closer to the fruition of its hopes. Its one-tenth scale prototype will be in operation in a few months, and construction of a full-scale plant has begun. In-pile studies of its fuel elements have increased confidence in the ability of the UO_2 fuel to withstand the exposure to the high attainable burn-ups predicted by reactivity calculations, and experience in the fabrication of the initial loadings for NPD-2 and Douglas Point will show the way to decreasing fuel fabrication costs. Two significant uncertainties remain: (a) the demonstration of the on-power, bidirectional

fueling (and the reliability and service-life of the fueling machines); and (b) the demonstration that D_2O losses can be kept within economic limits. It has been pointed out that on-power refueling is not an economic requirement, hence D_2O conservation is really the only major uncertainty (the problem of D_2O conservation also exists in the AHBR).

Table J-6. Fuel Cycle Costs for CANDU and AHBR Systems

Cost Bases	Douglas Point[a] Can.	E-3[a] CANDU U.S.	AHBR U.S.
Inventory charges		mills/kwhr	
Enriched fuel (at 4%/yr)	-	-	0.12
Thorium or natural uranium[b]	0.10	0.25	0.07
D_2O	0.63	0.87	0.26
Replacement charges			
Th[c] or natural uranium	0.32	0.28	0.01
D_2O[d]	0.17	0.14	0.06
Fuel fabrication or reprocessing	0.75	1.20	0.61
Credit for excess fuel[e]	-	-	-0.20
Net fuel cycle cost, mills/kwhr	1.97	2.74	0.93

a. Station net efficiency, 30%

b. Based on value of fabricated material

c. At $12.25/lb Th as pellets of ThO_2

d. At 3%/yr for AHBR, 2%/yr for CANDU

e. At $15/gm for AHBR product

REFERENCES

1. W. B. Lewis, "Competitive Nuclear Power for Canada," Nucleonics, Vol. 18, No. 10, Oct. 1960, p 54.

2. S. Jaye, EXPIRE - A Reactivity Lifetime Calculation, ORNL-CF-60-10-138, (Oct. 13, 1960).

3. R. R. Coveyou, R. R. Bate, and R. K. Osborne, Effect of Moderator Temperature upon Neutron Flux in an Infinite Capturing Medium, ORNL-1958, (Oct. 1955).

4. E. Hellstrand, "Measurements of the Effective Resonance Integral in Uranium Metal and Oxide in Different Geometries," Journal of Applied Physics, Vol. 28, No. 12, Dec. 1957.

5. USAEC, Evaluation and Planning Branch Civilian Reactors, Division of Reactor Development, Nuclear Power Plant Cost Evaluation Handbook, Vol. 4, Nuclear Fuel Cycle Costs, Oct. 1, 1960.

6. A. J. Mooradian, J. A. L. Robertson, "CANDU Fueling Costs," Nucleonics, Vol. 18, No. 10, Oct. 1960, p 60.

7. W. B. Lewis, Basic Considerations in the Design of the Full-Scale Heavy Water and Natural Uranium Power Reactor, DM-57, (AECL-785), Mar. 28, 1959.